UNIVERSITÀ DEGLI STUDI DI PADOVA

DIPARTIMENTO DI BIOLOGIA

Corso di Laurea magistrale in Molecular Biology

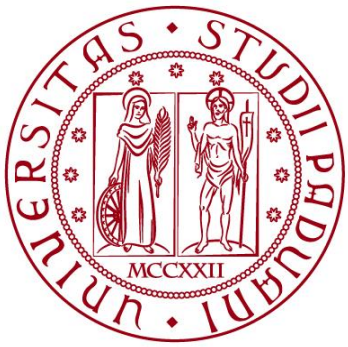

TESI DI LAUREA

INVESTIGATION OF MOLECULAR MECHANISMS BEHIND THE NEURODEVELOPMENTAL DISORDER PURA SYNDROME USING CRISPR/Cas9-GENERATED CELL MODELS

Relatore: Prof.ssa Chiara Rampazzo
Dipartimento di Biologia

Correlatore: Prof. Dierk Niessing
University of Ulm

Supervisore: Carolin Ketteler
Helmholtz Zentrum München

Laureanda: Silvia Marcato

ANNO ACCADEMICO 2023/2024

ABSTRACT

The *purine-rich element-binding protein A* (PURA), is a small DNA and RNA binding protein, located in the cytoplasm and involved in multiple cellular molecular pathways, albeit the actual molecular function is still unclear. *De novo* heterozygous mutations on *PURA*, cause the rare neurodevelopmental disorder PURA syndrome, characterized by moderate to severe intellectual disability, hypotonia, epilepsy, feeding difficulties, next to many other symptoms that vary between patients. Dissecting PURA's molecular function in a cellular context is fundamental to understand its role in PURA syndrome and so to develop potential treatments. In this study, an isogenic control (isoCTRL) cell line was successfully generated from patient induced Pluripotent Stem Cells (iPSC) carrying the most common mutation F233del using the CRISPR/Cas9 technology. Subsequent differentiation of both isoCTRL and patient iPSC into Neural Progenitor Cells (NPCs) revealed that the F233del does not impair early neural differentiation based on NPC morphology and expression of neuronal markers like PAX6, MAP2 and FOXG1. Furthermore, it was shown that PURA and FMRP colocalize in NPCs and that this colocalization was not disrupted in the patient cells. In addition, a PURA overexpressing cell line for BioID analysis to investigate PURA's interactome and a PURA Knock Out (KO) cell line were generated from Human Neural Stem Cells (HNSCs), which are fundamental to explore potential neural markers interacting with PURA or regulated by PURA, respectively. This comprehensive approach provides the cellular bases and molecular insights to further study PURA's molecular mechanism and its implications in PURA syndrome.

ACKNOWLEDGEMENTS

I am extremely grateful to my supervisor, Carolin Ketteler, for the constant support and guidance, for believing in me, for the motivation and constructive suggestions while planning and developing this project, for her incredible patient and feedback, and for her help writing this thesis.

I would also like to thank Prof. Dierk Niessing who gave me the opportunity to join his research group and to take part to the PURA project. I would like to thank all members of the Niessing lab for the great atmosphere during my time there. Special thanks go to Avina, David, Rob, Sabrina, Simi and Vera for their great help and for sharing with me their passion for research. Many thanks also to the PURA group, Sandra and Estera, who always helped with advice and to the former members Lena and Marcel who provided the bases to develop this project.

I would like to thank my internal supervisor, Prof. Chiara Rampazzo and my co-examiner Prof. Paola Costantini for their valuable feedback in this work.

I want to thank Ejona Rusha for her help when performing FACS experiments.

Big thanks to my family, especially my parents Federico and Franca, my brother Claudio and my sister Emma for their emotional support and for believing in me and in my career every single day. Special thanks to Giulio for being so patient and supportive through this path. Thanks to my friends, in Italy and around the world, and to the Majorettes Nove group who were always close to me.

I would like to extend my heartfelt gratitude to all individuals who provided support and assistance throughout this project, even if not mentioned explicitly.

Without all of you, this would not have been possible.

TABLE OF CONTENTS

GLOSSARY

APBB1	amyloid beta precursor protein binding family B member 1
ASCL1	achaete-scute family bHLH transcription factor 1
BMP	Bone morphogenetic Protein
cDNA	complementary DNA
CNS	Central Nervous System
CRISPR	Clustered Regularly Interspaced Short Palindromic Repeats
CYSTM1	cysteine rich transmembrane module containing 1
DBS	Double-Streanded DNA Breaks
DCP1A	Decapping mRNA 1A
DDX6	DEAD Box Protein 6
DOX	Doxycyclin
EB	Embryonic body
EGF	Epidermal Growth Factor
EMSA	Electrophoretic Mobility Shift Assay
F233del	delition of phenylalanin 233
FACS	Fluorescence-activated Cell Sorting
FGF-β	Fibroblast growth Factor 2
FMRP	X mental retardation protein
FOXG1	forkhead box G1
FSC-A	Forward Scattering Area
FSC-W	Forward scattering width
FXR1	FMR1 autosomal homolog 1
FXR2	FMR1 autosomal homolog 2
G3BP1	G3BP stress granule assembly factor 1
GFP	Green Fluorescence Protein
gRNA	guide RNA
GT	Gel trex
HDR	Homology-Directed Repair

HES5	Hairy And Enhancer of Split 5
hnRNPU	heterogeneous nuclear ribonucleoprotein U
HNSC	Human Neural Stem Cells
hPSC	human Pluripotent Stem Cells
iCLIP	individual-nucleotide resolution UV crosslinking and immunoprecipitation
ID	Intellectual Disability
IF	Immunofluorescence
IGIP	IgA inducing protein
iPSC	induced Pluripotent Stem Cells
KD	Knock Down
KO	Knock Out
MALAT1	metastasis associated lung adenocarcinoma transcript 1
MAP2	dendritic microtubule associated protein 2
MBP	Myelin basin protien
Mhc	major histocompatibility complex, class I, C
nAch	neuronal nicotinic acetylcholine
NEAT1	nuclear paraspeckle assembly transcript 1
NPC	Neural Progenitor Cells
NRG2	Neuregulin 2
P62 or SQSTM1	Sequestome 1
PAM sequence	Protospacer adjacent motif
PAX6	paired box 6
PB	PiggyBac
PCDHA	clustered protocadherin A
PCDHB	clustered protocadherin B
PCDHC	clustered protocadherin C
PCR	polymerase chain reaction
PDL	Poly-D-Lysine
PMA	Purmorphamine
PURA	purine-rich element-binding protein alpha

PURB	purine-rich element-binding protein beta
PURG	purine-rich element-binding protein gamma
qPCR	quantitive polymerase chain reaction
RI	Rock-inhibitor
RNP	Ribonuceloprotein
SOX1	SRY-Box Transcription Factor 1
SOX2	SRY-Box Transcription Factor 2
SRO	Shortes region of overlap
SSC-A	Side Scattering Area
Stau1	staufen double-stranded RNA binding protein 1
TGF-β	Transforming growth factor-β
TNF-α	Tumor necrosis factor alpha
TOPO cloning	Topoisomerase-based cloning
tracrRNA	trans-activating CRISPR RNA
WB	Western Blot
WT	Wild type
YBX1	Y-Box Binding Protein 1
ZO1	tight junction protein 1

1 INTRODUCTION

1.1 PURA SYNDROME

PURA syndrome is a rare neurodevelopmental disorder caused by *de novo* heterozygous mutation in the *purine-rich element-binding protein A* (*PURA*) gene. It is characterized by Intellectual Disability (ID) and other related symptoms (Shimojima K, 2011; Hosoki K., 2012).

1.1.1 HISTORY OF PURA SYNDROME

Prior to PURA being identified as the cause of PURA syndrome, patients with symptoms like those of PURA syndrome were classified as affected by 5q31.3 microdeletion syndrome, as the disease was not precisely linked to the *PURA* locus. The main difference between the two conditions is that 5q31.3 microdeletion syndrome is caused by a non-recurrent genomic 5q31.3 deletion, which may partially or completely include the *PURA* locus (Lalani S. R., 2014), while PURA syndrome is caused by gene variants in the *PURA* locus. The shortest region of overlap (SRO) in the 5q31.3 microdeletion syndrome was first considered of 2.6 to 5.0 Mb which includes, besides PURA, several other like, *clustered protocadherin A, B, and G* (*PCDHA, PCDHB,* and *PCDHG*) genes, and *Neuregulin 2* (*NRG2*). These were all candidates for the observed neurodevelopmental disorder (Shimojima K, 2011; Hosoki K., 2012). A subsequent study on other patients narrowed the SRO to 101 kb (Brown N., 2013) which includes only three genes, namely *PURA*, *IgA inducing protein* (*IGIP*) gene, and *cysteine rich transmembrane module containing 1* (*CYSTM1*) gene, highlighting PURA as the primary candidate for the neurodevelopmental disorder (Brown N., 2013).

In 2014, the whole exome sequencing was performed on 11 patients sharing symptoms with those affected by 5q21.3 microdeletion syndrome, identifying 11 different mutations laying on *PURA* (Lalani S. R., 2014; Hunt D., 2014). To date, around 620 individuals have been diagnosed with PURA syndrome worldwide (Personal communication, PURA Syndrome Foundation, **Figure 1.1**). Diagnosis is made via next generation sequencing, such as whole exome sequencing or whole genome sequencing. Alternatively, panel testing can be performed focusing on genes linked to neurodevelopmental disorders or genetic epilepsies (Reijnders MRF, 2018). Since these techniques are more accessible nowadays, an increasing number of cases is expected.

Figure 1.1: individuals with PURA syndrome. Taken from (Reijnders M. R. F., 2018)

1.1.2 MUTATIONS CAUSING PURA SYNDROME

Around 270 different pathogenic mutations causing PURA Syndrome are known. They are distributed along the entire *PURA* sequence, including missense variants, in-frame deletions, and protein-truncating variants caused by point mutations, nonsense mutations, frameshift mutations, and indels (**Figure 1.2**) (Reijnders MRF, 2018; Johannesen K. M., 2021). Only those mutations located at unstructured N- and C-terminal regions, as well as those in which conservative amino acids exchanges, do not result in PURA syndrome. Almost all the disease-causing mutations located in folded domains result in the whole spectrum of symptoms (Reijnders MRF, 2018).

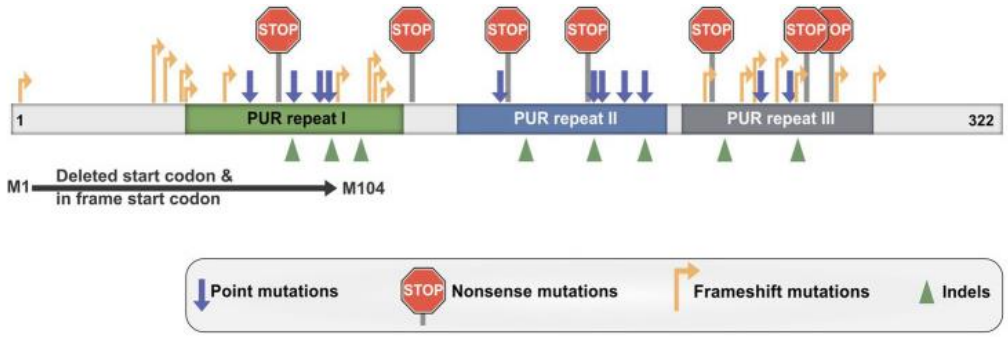

Figure 1.2: PURA syndrome causing mutations. *De novo* mutations within PURA gene. Figure taken from *(Molitor L. B. S., 2021)*

1.1.3 CLINICAL SPECTRUM OF PURA SYNDROME

Reported PURA syndrome's symptoms affecting all patients are mild to moderate developmental delay and ID. Nearly all individuals suffer from hypotonia, feeding difficulties, and remain non-verbal. Around half of the patients also exhibit gastrointestinal problems such as constipation and drooling as well as breathing problems, hypersomnolence, ophthalmological abnormality, and epilepsy. Additional reported symptoms are skeletal and respiratory issues as well as endocrine abnormalities like Vitamin-D deficiency. Other reported symptoms are chorea, interspersed with dystonic and uncoordinated movements, nystagmus, feeding difficulties, craniofacial dysmorphisms (Molitor L. B. S., 2021) (**Figure 1.3**).

When PURA syndrome was first characterized, it was suggested that sequence variations disrupting *PURA* may correlate with clinical severity (Lalani S. R., 2014; Hunt D., 2014). However, with increasing number of cases the phenotypic spectrum expanded, and no correlation was found between symptoms and mutation type (Lee B. H., 2018).

Up to now, PURA syndrome treatment is solely symptomatic. As the disease manifests in many tissues, treatment needs to be executed by an

interdisciplinary team of doctors. In addition, some symptoms might be secondary consequences of others, further complicating the search of causal origin.

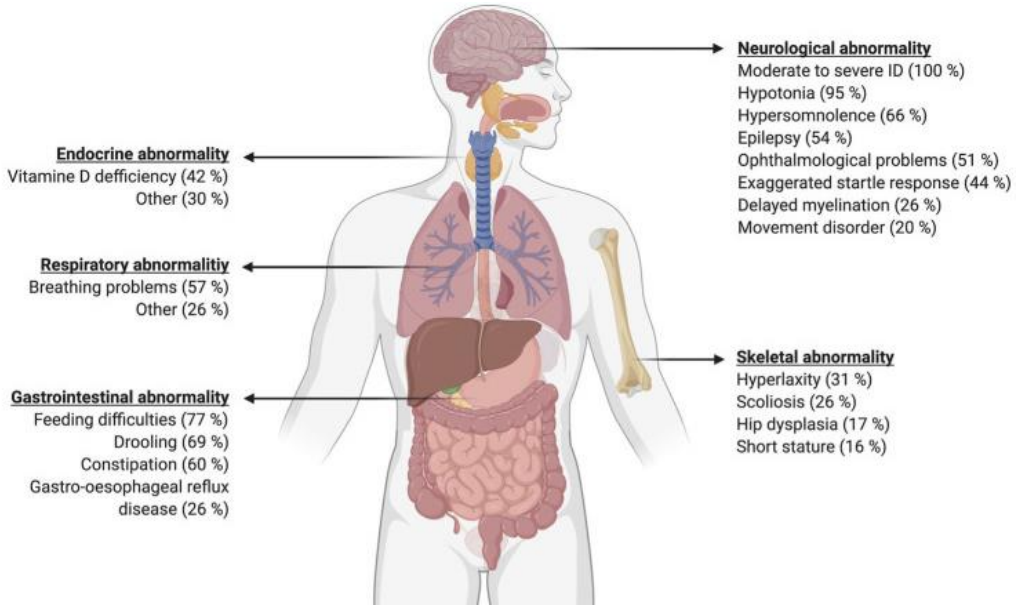

Figure 1.3: Overview of PURA syndrome symptoms. Schematic representation of described PURA syndrome patients (Figure taken from *(Molitor L. B. S., 2021)*, symptoms taken from *(Reijnders M. R. F., 2018)*. In brackets are reported the percentages of clinical features among the analyzed 32 patients *(Reijnders M. R. F., 2018)*.

1.2 PURINE-RICH ELEMENT BINDING PROTEIN PURA

1.2.1 *PURA* GENE AND PURA PROTEIN

PURA is a 322 amino acid long protein coded by the *PURA* gene (Bergemann A. D. M. Z., 1992). The mono-exon structure of the gene suggests a high conservation. Indeed, PURA homologs have been found in metazoans, plants, and bacteria, however, it is lacking in fungi and viruses. Concurrently, the mono-exon structure of *PURA*, suggests an evolutionary pressure to prevent alternative splicing of this gene. In vertebrates, two PURA paralogs exist, namely PURB and two isoforms of PURG (PURG A, PURG B) which share 70% and 48% of their sequence with PURA, respectively (Graebsch A. R. S., 2009).

Crystal structure of PURA from *Drosophila melanogaster* (dmPURA) defined three PUR repeats with conserved four antiparallel β-sheet, followed by a single α-helix (β-β-β-β-*α*) topology (Graebsch A. R. S., 2009; Graebsch A. R. S., 2010). PURI and PURII repeats interact with each other to form an intramolecular N-terminal PUR domain (also known as type I PC4-like domain) built from a single peptide chain with a β-β-β-β-α-linker-β-β-β-β-α topology (Janowski R., 2020)). Although PURI and PURII share only ~30% of sequence identity, they have identical binding motif and they adopt the same fold. Crystal structure of PURI and PURII of human PURA (hsPURA), resembles the dmPURA topology, with a higher flexibility at loop regions (**Figure 1.4-A**) (Proske M, 2024). The β-sheets and the linker on repeat I and II, are responsible for single stranded nucleic acid binding as shown in a co-structure of single-stranded DNA and dmPURA (**Figure 1.4-B**) (Weber J, 2016). Besides, the strong conservation of the amino acids involved in

nucleic acidic binding, NMR chemical shift perturbation experiments and electrophoretic mobility shift assay showed that PURA binds DNA and RNA with same affinity (Weber J, 2016).

PURIII repeat has the typical four antiparallel β-strands and one α-helix motif, like PURI and PURII in both dmPURA and hsPURA (Graebsch A. R. S., 2009; Graebsch A. R. S., 2010; Proske M, 2024). Its main function is to interact with another PURIII (**Figure 1.4-C**), forming the so-called type II PC4-like domain (formed by two identical peptides with β-β-β-β-α fold). This acts as an inter-molecular homodimer if interacting with a PURIII of another PURA or an inter-molecular heterodimer if interacting with a PURIII of the known PUR paralogs. Although PURIII main function is the interaction with another PURIII repeat, the PC4-like domain they form when interacting with each other, suggests a nucleic binding function (Janowski R., 2020), which is also confirmed from a recent study (Proske M, 2024).

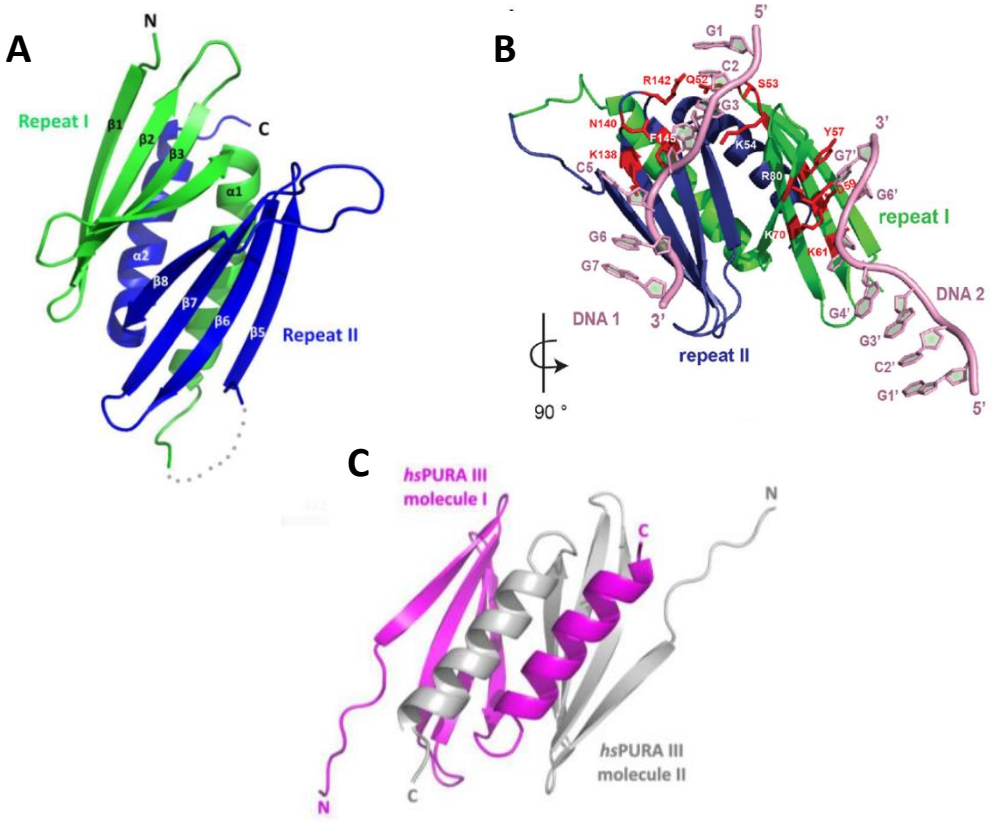

Figure 1.4: hsPURA has three PUR repeats, binds nucleic acids and form dimers. (A) Crystal structure of wild-type hsPURA repeat I (green) and repeat II (blue), adapted from *(Proske M., 2024)*. **(B)** Crystal structure of dmPURA PURI (green) and PURII (blue) with two single-stranded DNA molecules (pink), important amino acids involved in DNA interaction are depicted in red, adapted from *(Weber J., 2016)*. **(C)** Crystal structure of repeat III from two hsPURA molecules (magenta and grey), adapted from *(Proske M., 2024)*

1.2.2 PATIENT-RELATED MUTATION F233del

Based on wild type hsPURIII crystal structure, protein folding defects caused by mutation at C-terminal PUR domain were predicted. Of note, protein having patient-related mutation affecting repeat III were not crystallizable, due to

PURA being soluble only in dimer form (Graebsch A. R. S., 2009), suggesting altered PURA dimerization if mutations affect PURIII. Of high interest for this thesis is the effect of deletion of phenylalanine 233 (F233del) which is one of the most common mutations causing PURA syndrome. F233 interacts with T222 to form the typical β-sheet hydrogen bonds between C=O and N-H groups. F233 also interacts with three different amino acids of the α-fold of the other PURIII, meaning that it is involved in the PURIII dimerization (**Figure 1.5**). F233del leads to a change in the orientation of all subsequent side chains within the β-sheet. The following hydrophilic residue (D234) enters a hydrophobic core region, which likely destroys the interaction network required for protein folding and for the PURIII dimerization (Proske M, 2024).

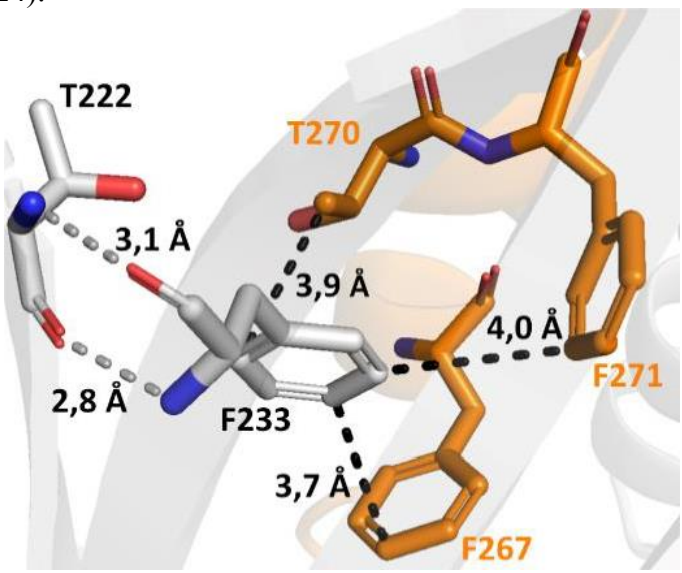

Figure 1.5: F233 residue interaction in wt hsPURA. Shown are the interacting amino acid residues of F233. The two dashed lines in grey are representing the two typical β-sheet H-bonds between the C=O and N-H groups of F233 and T222. The three dashed lines in black are representing the interaction between F233 and three residues in the α -fold of the other PURA molecule. The coloring is element where the carbon backbone is white (molecule I) or orange (molecule II), nitrogen groups are blue and oxygen groups are red.

1.2.3 LOCALIZATION AND MOLECULAR FUNCTION OF PURA

PURA was first discovered due to its binding to purine-rich sequences upstream of the human *c-myc* gene (Bergemann A. D., 1992), therefore it was initially considered a transcription factor. PURA was also discovered to be involved in transcription of *myelin basic protein (MBP)* gene (Haas S., 1995) or in the activation of promoters of the *Tumor necrosis factor alpha (TNF-α)* gene (Darbinian N., 2001), the *neuronal nicotinic acetylcholine (nAch)* gene (Du Q., 1997), or the *amyloid beta precursor protein binding family B member 1 (APBB1)* gene (Zambrano N, 1997). Furthermore, PURA was described to interact with RNA and to be dependent on it for its folding (Herault Y., 1995; Gallia G. L., 1999). The similar DNA and RNA binding affinity of PURA, suggests that RNA and DNA are competing in binding PURA and thus their competition is a way of gene expression regulation (Molitor L. B. S., 2021). For instance, the RNA circSamd4 forms a complex with PURA proteins, thus preventing PURA proteins from repressing the *major histocompatibility complex, class I, C* (*Mhc*) gene transcription in the nucleus (Pandey PR, 2020).

This finding is consistent with previous studies showing that PURA and PURB regulate alpha- and beta-myosin heavy chains (Gupta M., 2003; Hariharan S., 2014). Another study showed that PURA and PURB localized to the so-called paraspeckles, which are nuclear membrane-less compartments. There, PURA was detected in the interactome of *nuclear paraspeckle assembly transcript 1* (*NEAT1*) and *metastasis associated lung adenocarcinoma transcript 1* (*MALAT1)* RNAs (West JA, 2014) (**Figure 1.6**).

Studies in mice (Khalili K., 2003; Hokkanen S., 2012) and a recent study in HeLa cells (Molitor L., 2023) show PURA mainly localizing in the cytoplasm, more precisely in membrane less compartments. PURA localizes in stress granules where it has been reported to be responsible for their formation (Daigle J. G., 2016) and neuronal transport granules where it co-localizes with other neuronal RNA-binding proteins, such as PURB, staufen double-stranded RNA binding protein 1 (Stau1), heterogeneous nuclear ribonucleoprotein U (hnRNPU), and fragile X mental retardation protein (FMRP; (Mitsumori K., 2017; Ohashi S, 2002; Johnson E. M., 2006)). Furthermore, it was shown that PURA can associate with MAP2 mRNA in mouse brains and is suggested to be involved in its transport (Johnson E. M., 2006). This observation is in line with results from *PURA*-/- mice, where a significant overall reduction of MAP2 protein in whole brain lysates was reported (Hokkanen S., 2012). Recently, a multi-omics approach to study PURA targets using HeLa cells has been performed. The identified PURA targets suggested PURA's role in immune responses, mitochondrial function, autophagy, and processing body (P-body) activity (Molitor L., 2023). Interestingly, P-bodies association was impaired in HeLa cells when downregulating PURA (Molitor L., 2023) or overexpressing PURA with patient-derived mutations (Proske M, 2024).

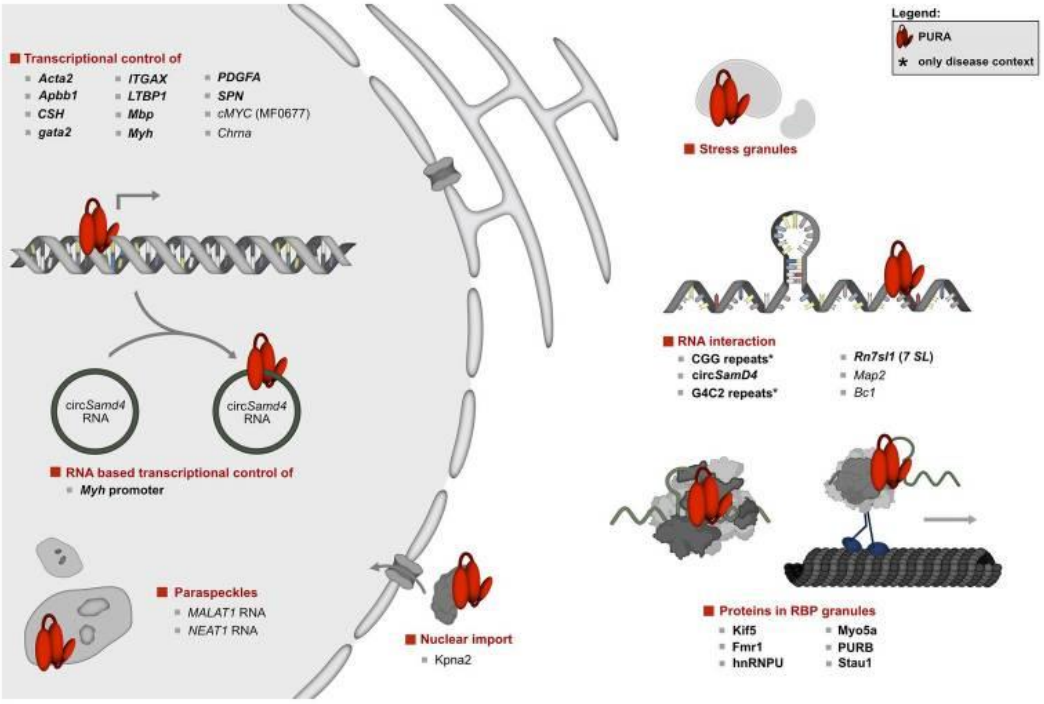

Figure 1.6: Overview of PURA molecular interaction and cellular pathway. Figure from *(Molitor L. B. S., 2021).*

1.3 EXPERIMENTAL MODELS

Since PURA was first characterized, PURA function have been explored using *in vivo* and *in vitro* models. Two independent PURA Knock Out mice have been generated and PURA KD in HeLa cells have been performed for multi omics approach. Although research in HeLa upon PURA KD provided multiple molecular pathways in which PURA might be involved, a gap remains in understanding its impact on the neurodevelopmental disorder PURA syndrome, due to the absence of a neural cellular model.

1.3.1 *In vivo* MODELS

In 2003 a first *PURA*-/- mouse model was reported (Khalili K., 2003). Later, in 2012 a second *PURA*-/- mouse model was independently created which confirmed the phenotype of the first mouse model (Hokkanen S., 2012). Indeed, both homozygous mouse models seemed normal at birth but at postnatal day 14 they had increased tremor upon motion, infrequent mobility, spontaneous seizures, and flaccid tail (Khalili K., 2003; Hokkanen S., 2012). *PURA* -/- mice have a lifespan of ~ 4 weeks (Khalili K., 2003), which can be prolonged to 5-6 months upon glucose injection (Hokkanen S., 2012).

Histologically, *PURA*-/- mice had 20 to 80% less proliferative cells depending on the tissue as well as an overall lower quantity of neurons (Khalili K., 2003). Both mice models had impaired neurogenesis and neural differentiation based on altered cytoskeleton of neurons, as well as altered Purkinje cell morphology and compromised synapse formation with significant reduction of dendritic microtubule associated protein 2 (MAP2) level during brain development. A further study confirmed PURA's role in dendrite development, in particular by associating with non-coding dendritic RNA species and with mRNA targeted to dendrites (Johnson E. M., 2006).

A heterozygous mouse model was also characterized (Khalili K., 2003) which allows findings more related to the patients as they have heterozygous mutations. *PURA*+/- mice showed intermediate phenotype between *PURA*+/+ and *PURA*-/- mouse models with a reduced number of neurons, memory deficiency, decreased tone and gait abnormalities (Khalili K., 2003; Barbe M. F., 2016).

1.3.2 *In vitro* MODELS

The symptoms variety, the increasing number of patients and the need for a specific therapy, require to first understand PURA's molecular role and PURA's mutation effect into the cells. In addition, given that PURA syndrome is a neurodevelopmental disorder, neural cellular model is of high interest to study PURA function and PURA syndrome.

Two types of neural cellular model have been used in this project: Neural Progenitor Cells (NPCs) derived from induced pluripotent stem cells (iPSC) and Human Neural Stem Cells (HNSC).

iPSC are self-renewal pluripotent cells expressing the pluripotency markers OCT4, SOX2 and NANOG. These transcription factors suppress the genes that lead

to differentiation and thus maintain the pluripotency of the cells. Given their pluripotency, iPSCs can differentiate towards any type of cell, which in the case of this project are neural progenitor cells. The NPCs differentiation protocol (Reinhardt P, 2013), is based on dual-SMAD inhibition (SMAD are central mediator of TGF-β signaling pathway), generating a population of multipotent, SOX1, SOX2, NESTIN, FORSE-1 and PAX6 positive NPCs (Reinhardt P, 2013). This protocol relies on Dorsomorphin and on SB431542. The first one acts on the Bone Morphogenetic Protein (BMP) type I receptors, inhibiting its activity, while the second one acts on the Lefty–Activin–Transforming growth factor-β (TGF-β) pathway by blocking the ALK receptor signaling, reproducing the Lefty inhibition of Nodal during neuroectodermal formation. The self-renew capability of these cells is maintained by Sonic hedgehog (SHH) and WNT signaling which are activated by Purmorphamine (PMA) and CHIR99021, respectively. In addition, supplemented Ascorbic Acid and Fibroblast growth factor 2 (FGF-β) induce Embryonic Body (EBs) to form neural rosettes-like structures, which have been associated with the developmental stage of neural plate formation (Conti L., 2010). Besides the self-renew advantage, the NPCs can be efficiently specified into neural tube as well as into neural crest lineages (Reinhardt P, 2013). isoCTRL and patient NPCs were tested for neural progenitor marker PAX6 (mRNA and protein), for MAP2 mRNA, a neural dendritic marker and for FOXG1 mRNA, involved in the telencephalon formation. Other neural progenitor protein markers that can be validated are SOX1, SOX2, NESTIN, FORSE-1, HES5 and ASCL1 whose signal should increase with higher passages. In addition, immunostaining of CADHERIN and ZO-1 marks the apical surface of the rosettes.

The other neural cellular model used in this project is the Human Neural Stem Cell (HSNC) which is a nestin-positive, immortalized, multipotent stem cell line. It derived from human embryonic brain cells and it is capable of differentiate towards the three major lines of the Central Nervous System (CNS), namely neurons, astrocytes and oligodendrocytes (Villa A., 2000). The immortalized capability was given by the p110 gag-myc fusion protein derived from the avian retroviral genome (v-myc). The undifferentiated status is maintained by the presence of mitogens (FGFβ and EGF) in the culture medium and for survival, N2 supplement is required. HNSCs present a flattened unipolar morphology when grown on Poly-D-Lysine coated plates.

1.4 AIM AND OBJECTIVES

To study PURA syndrome, patient derived iPSCs can be used, however a proper isogenic control with the same genetic background is lacking. For this reason, a first aim of this thesis is to generate and validate an isogenic control iPSC cell line from three independent patients carrying the F233del mutation using the CRISPR/Cas9 technology.

Since PURA syndrome is a neurodevelopmental disorder, a second aim of this thesis is to differentiate one of the patient's derived iPSC and the relative isogenic control to Neural Progenitor Cells (NPCs). Patient NPCs are used to verify one of the identified PURA interacting protein, FMRP, by performing a colocalization analysis on immunofluorescence (IF) images.

Although several PURA targets have been identified in the past, these studies were not performed in neural-like cells. For this reason, this thesis' third aim is to generate a PURA overexpressing Human Neural Stem Cell line (HNSC) and a PURA Knock Out (KO) HNSC line. The first cell line is needed to perform proximity-dependent biotin identification (BioID) expanding the already available datasets and thus, identify potential neural protein interacting with PURA which may cooperate with PURA as RNA-binding protein. The PURA KO HNSC line can be used to perform transcriptomic and shotgun proteomic studies, which may identify potential neural targets that are directly or indirectly regulated by PURA, enlarging the available dataset from Hela cells.

2 MATERIALS

Generally stock solutions, standard reagents, agar plats containing antibiotic, LB media for bacterial culture and competent DH5-α were provided by Vera Roman (Niessing lab, STB, HMGU).

2.1 LARGE EQUIPMENT

Table 2-1: Large Equipment

Name	Type	Cat No	Manufacturer
Automated Cell Counter	LUNA Automated cell Counter	L10001	Logos Biosystem
Automated Cell Counter	Countess II FL	AMQAF1000	ThermoFisher Scientific
Protein Concentration measurement device	BioPhotometer plus	6132	Eppendorf
Bright-field microscopy cell imaging system	OLYMPUS cellSens Entry 1.18	-	Olympus Corporation
Cell Culture Safety Cabinet S2	Biological safety cabinet class II	S2020 1.2	ThermoFisher Scientific
Centrifuge	Heraeus Pico 17	75002414	ThermoFisher Scientific
Centrifuge	EBA 20	Z601020	Andreas Hettich GmbH
Centrifuge	Centrifuge 5415 R	4354	Eppendorf
Table centrifuge	Rotina 420R	-	Hettich
Centrifuge 96- well plate	Universal 320	-	Andreas Hettich GmbH & Co KG
CO_2 Incubator	C170	-	Binder GmbH
4D-Nucleofector	4D-Nucleofector Core Unit	AAF-1003B	Lonza
4D-Nucleofector	4D-Nucleofector X Unit	AAF-1003X	Lonza
Freezer (-80°C)	Ultra Low Temperature Freezer	Innova U535	Eppendorf
Cell Imaging System	EVOS FL Cell Imaging System	AMF4300	ThermoFisher Scientific
DNA gel and Western Blot Imaging system	FusionCat Advance SL4	-	Villber Lourmat
Incubator	Thermomixer comfort	5355	Eppendorf
Bacteria Incubator	HeraTherm Incubator	-	ThermoFisher Scientific

Bacteria Inbucator and shaker	Innova44 Incubator Shaker Seires	-	New brunswick scientific
Inverted Fluorescence microscope	Axio Observer.Z1	-	Carl Zeiss AG
Fluorescent microscope	Evos FL Fluorescent	AMF4300	Life technologies
Bright-field microscope	Olympus CKX53	CKX53SF	Olympus
NanoDrop	Spectrophotometer	ND-100	NanoDrop
NanoDrop software	ND-100 V3.8.1	-	-
PCR Thermocycler	T100 ThermoCycler	T100 ThermoCycler	BIO-RAD
Power supply	check isabella	PowerPac Basic	BIO-RAD
Power supply	PeqPOWER	E0203	peqlab
qPCR Thermocycler	LightCycler 480 Ral-Time PCR instrument	05015278001	Roche
qPCR software	LightCycler 480 SW 1.5.1.62 SP3	.	Roche
Refrigerator (-20°C, 4°C)	T 1700 Comfort	-	Liebherr Group
Rotator	Roto-Shaker Genie	SI-1102	Scientific Industries
Rotator	Reax 2 inlc. universal adaptor	541-21009-00	Heidolph
Analytical Balance	Analytical Balance	XS105DU	Mettler Toledo
Ultrasonic Cleaner	Ultrasonic Cleaner	142-6044	VWR
Heated Magnetic Stirrer	-	-	Ikamag RCT
Vortex	Vortex Genie 2	G560E	Scientific Industries
Water Purification System	MilliQ	-	Millipore

2.2 CONSUMABLES

Table 2-2: Consumables

Name	Type	Cat. No	Manufacturer
10 cm Petri Dish	Tissue Culture dish (10 cm)	353003	Corning

12-well plate	Multiwell 12 well	353043	Corning
24-well plate	Multiwell 24 well	353047	Corning
6-well plate	Multiwell 6 well	353046	Corning
96-well	Multiwell 96 well	167008	ThermoFisher Scientific
Black tubes	Rotilabo reaction vials, 1.5 mL, black, non-sterile	71027013	Carl Roth GmbH & Co
Cell scraper	Cell scraper/Lifter 25cm, sterile	7696760/761	LABsolute
Centrifuge tubes	15 mL	322095	Corning
Centrifuge tubes	50 mL	352070	Corning
Counting slides	LUNA Cell Counting Slides	L12001	logos biosystem
Counting slides	Countess cell counting chamber slide	C10283	Invitrogen
Cover Slips	Cover Slips	CB00120RA120MNZ0	Epredia
Cryo tube	CYO.S 2mL sterile	122263	Greiner
Gloves	EcoSHIELD Eco Nitrile PF 250	625123	ecoSHIELD Scientific
Gloves	Nitril NextGen	1283M	Meditrade GmbH
Low attachement plate	Costar 6 well Plate, Ultra - Low Attachment Surface	3471	Corning
Microscope slides	Microscope Slides	631-1553	Avantor by VWR
Parafilm	Parafilm, M Laboratory Film	PM999	-
Pipette tips	Pipette tips, 10 µL, 200 µL, 1250 µL	-	Sarstedt AG & Co KG
Plastic Film for WB	Polypropylen Disposal Bags	E706.1	Carl Roth GmbH
Protein Bis-Tris Gel	NuPAGE 4-12% Bis-Tris Gel	NP0323BOX	ThermoFisher Scientific
PVDF Transfer membrane	Western Blot PVDF transfer membrane	88518	ThermoFisher Scientific
PVDF Transfer Membrane	PVDF Transfer Membrane	YA3805092	ThermoFisher Scientific
qPCR reaction plates	FrameStar 96 well Semi-Skirted PCR Plate, Roche style	4TI-0952	Azenta Life Sciences

RNAse free tubes	Non-stick RNAse-free 1.5 mL tubes	616-201	Greiner bio-one
Sterile Pipette tips 10 µL	Sterile Pipette tips 10 µL	VT0200	SurPhob
Sterile Pipette tips 1250 µL	Sterile Pipette tips 1250 µL	VT0270	SurPhob
Sterile Pipette tips 20 µL	Sterile Pipette tips 20 µL	70.760.211	Biosphere plus
Whatman paper	Chromatography paper (3 MM CHR)	3030-392	GE Healthcare

2.3 CHEMICALS

Table 2-3: Chemicals

Name	Type	Cat. No	Manufacturer
1 kb DNA Marker	Gene ruler 1kb + DNA ladder	SM0311	ThermoFisher Scientific
100 bp DNA Marker	Gene Ruler 100bp + DNA Ladder	SM0323	ThermoFisher Scientific
Agarose	DNA Agarose Biozym	870055	Biozym Scientific GmbH???
Antioxidant	NuPage Antioxidant	NP0005	ThermoFisher Scientific
BCA Reagent A	Pierce BCA Protein Assay Reagent A	23221	ThermoFisher Scientific
BCA Reagent B	Pierce TM BCA Protein Assay Reagent B	23224	ThermoFisher Scientific
Casein	Casein powder	22.544.292	VWR BDH Chemicals
Chloroform	Trichlorometan/Chloroform	6340.4	Carl ROTH GmbH
DAPI	DAPI stain (5mg/mL)	10236276001	Roche Diagnostics
DNA loading dye	6x DNA Loadying dye	R0611	Fermentas
Donkey serum	Donkey serum	D9663	Merck, Sigma-Aldrich
ECL Solution	ECL Prime Western Blotting Detection Reagent	RPN 2232	Cytiva
ECL Solution	Pierce ECL Western Blotting Substrate	32106	ThermoFisher Scientific
Electroporation enhancer	Alt-R Cas9 electroporation Enhancer	1075915	IDT
Ethanol	Ethanol absolute	1.009.831.000	-

Formaldehyde	37% formaldehyde solution	A0823,0500	PanReac Appli-Chem
GelRed	GelStain Red	0984.1	Carl Roth GmbH
Glycogen	Glycogen, RNA grade	R0551	ThermoFisher Scientific
Isopropanol 100%	Propan-2-ol	P/7490/15	Fisher Chemical
Kanamycin	Kanamycinsulphate	T832.2	Carl Roth GmbH & Co KG
LDS	NuPage (4x) LDS Sample Buffer	NP0007	invitrogen
Methanol	Methanol 100%	1.060.092.500	Signma Aldricht
Mounting medium	ProLong Diamond Antifae Mountant	P36961	invitrogen
Protein Marker prestained	FastGene BlueStar Plus Pre-stained Protein Marker	MWP04	NIPPON Genetics EUROPE GmbH
Reducing Agent	NuPage (10x) Sample Reduc-ing Agent	NP0009	invitrogen
Rnase away	Decontamination reagent	10666421	ThermoFisher Scientific
Running Buffer 20x	NuPAGE MOPS Running Buffer (20x)	NP0001-02	invitrogen
tracrRNA	Alt-R CRISPR-Cas9 tracrRNA	1073190	IDT
Transfer Buffer 20x	NuPAGE (20x) Transfer Buf-fer	NP00061	invitrogen
Triton X - 100	Triton X -100	A16046	ThermoFisher Scientific
Trizol	TRIzol Reagen	15596026	ambion by life technologies
Trypan Blue	Trypan Blue solution, 0.4%	T8154	Sigma Aldricht
Tween 20	Tween-20	786-517	Biosciences

2.4 ENZYMES

Table 2-4: Enzymes

Name	Type	Cat. No	Manufactu-rer
Cas9 endonuclease	Alt-R S.p. Cas9 Nuclease V3	1081058	IDT
PCR polymerase	CloneAmp HiFi PCR Premix	639298	TaKaRa

Reverse Transcriptase	5x PrimeScript RT Master Mix	RR036A	TaKaRa
SYBR Green for qPCR	Power SYBR Green PCR Master Mix	4367659	appliedbiosystem

2.5 KITS

Table 2-5. Kits

Name	Type	Cat. No	Manufacturer
DNA extraction kit	Dneasy Blood & Tissue kit (50)	69504	Qiagen
Lipotransfection kit	Lipofectamine 3000 Transfection kit	L3000-008	invitrogen
Nucleofection kit	Amaxa P3 Primery Cell 4D-Nucleofector X Kit L (24 RCT)	V4XP-3024	Lonza
PCR purification	NucleoSpin Gel and PCR Clean-up	740609.50	Macherey-Nagel
Plasmid purification	NucleoSpin Plasmid	740588.50	Macherey-Nagel
Reverse Transcription Kit	5x PrimerScript RT Master Mix	RR036A.1	TaKaRa
TURBO DNA free kit	TURBO DNA-free Kit	AM1907	invitrogen
Zero Blunt TOPO PCR Cloning Kit	pCR - Blunt II - TOPO vector	45-0245	invitrogen

2.6 BUFFER AND SOLUTIONS

Table 2-6: Buffer and Solutions

Name	Composition	Application
NuPAGE 20x SDS Running Buffer	1x SDS MOPS Running	Western Blot
NuPAGE 20x Transfer Buffer	1x Transfer Buffer, (v/v) 20% Methanol	Western Blot
PBS-T	1x PBS, (v/v) 0.1% Tweeen 20	Western Blot and IF
Ponceau red stain	0.5% Ponceau S in 1% aceti acid	Western Blot
RIPA buffer	50 mM Tris-HCl pH7.5-8, 150 mM NaCl, (v/v) 1% Triton X -100, (v/v) 0.5% Sodiumdeoxycholate, (v/v) 0.1% SDS	Western Blot
TAE buffer	40 mM Tris base, 20 mM acetic acid, 1mM EDTA	Agarose Gel

Western Blot blocking buffer	PBS-T, (v/v) 1% casein	Western Blot

2.7 CELL CULTURE

Table 2-7: Cell Culture Media and Supplements

Name	Type	Cat. No	Manufacturer
Accutase	Accutase solution	A6964	Sigma-Aldrich, Merck KGaA
Activin A	Recombinant Activin A	338-AC	TOCRIS/R&D
Ascorbic Acid	L Ascorbic Acid	3525.1	roth
B27 w/o	B-27 Supplement (50X) without Vitamin A	12587-010	gibco
B27 with	B-27 Plus Supplement (50x)	A3582801	gibco
BSA	Bovine Serum Albumin	SLCP9751	Sigma-Aldrich, Merck KGaA
CHIR99021	CHIR99021 Trihydrochloride	4953	TOCRIS/R&D
DMEM/F12	DMEM/F12	11320-033	Gibco
DMSO	Dimethyl sulfoxide (DMSO) Cell culture grade	A3672,0100	PanReac AppliChem
DMSO	DMSO anhydrous	90082	Biotium, Inc
Dorsomorphin	Dorsomorphin Dihydrochloride	3093	TOCRIS/R&D
DOX	Doxycyclin	631311	TaKaRa
EDTA	Ethylendiaminetetraacetic acid	A5097	PanReac AppiChem iTW Reagents
EGF	-	Internally produced	-
FBS	Fetal Bovin Serum	-	gibco
FGF	-	Internally produced	-
FGF-β	rhFGF basic/FGF2/bFGF	AFL3718	R&D systems
Freezing medium	Cryopreservation medium CryoStor S10	210102	BioLife Solutions
Geltrex	Reduced Growth Factor Basement Membrane Matrix without Phenol red	A14132-02	gibco

GlutaMAX	GltaMAX -I	35050-038	gibco
HEPES	HEPES solution	H0887	SIGMA Life Science
Hygromycin B	Hygromycin B	10687010	invitrogen
Insulin	Insulin	12585014	Life Technologies Corporation
KSR	Knockout Serum Replacement	-	invitrogen
N2	N-2 Supplement	17502-048	gibco
NEAA	MEM NEAA	11140-050	gibco
Neurobasal	Neurobasal -A medium	10888-022	gibco
OptiMEM	optiMEM	31985062	Gibco
PBS (10x)	Sterile PBS	14190744	Gibco
PDL	Poly-D-Lysine	-	-
Penicillin/Streptomycin	Antibiotic	15140122	Gibco
PMA	Purmorphamine	-	-
ROCK inhibitor	ROCK inhibitor	1254	Sigma-Aldrich, Merck KGaA
RPMI	RPMI medium 1640	21875-042	gibco
SB431542	StemMACS SB431542	130-106-275	Miltenyi Biotec
Sodium Butyrate	Sodyum Butyrate	B5887	Sigma-Aldrich, Merck KGaA
StemMACS iPS-Brew	StemMACS iPSC_Brew XF	130-104-368	MACS Media
StemMACS supplement	StemMACS iPSC_Brew XF 50x Supplement	130-104-368	MACS Media
Trypsin-EDTA	Trypsin-EDTA	L215.**3**	Merck KGaA
β-ME	β-mercaptoethanol	31350-010	gibco
β-ME	2-Mercaptoethanol	31350-010	gibco

2.8 CELL MEDIUM

Table 2-8: Cell Medium

Medium	Composition	Application
HNSC proliferation medium	(v/v) DMEM/F12, (m/v) 10% BSA, (v/v) 10% FBS, (v/v) 10% P/S, (v/v) 10% HEPES, (v/v) 5% N2, 20 ng/mL EGF, 20 ng/mL FGF	Cell culture HNSC
iPSC brew	iPSC brew supplemented with 50x ???	Cell culture iPSC
KSR	(v/v) 80% DMEM/F12, (v/v) 20% KSR, (v/v) 1% NEAA, (v/v) 1% GlutaMAX, (v/v) 0.2% ß-ME	Cell culture NPC
N2B27	(v/v) 50% DMEM/F12, (v/v) 50% Neurobasal, (v/v) 10% B27 without Vitamin A, (v/v) 5% N2, (v/v) 10% GlutaMAX	Cell culture NPC

2.9 PRIMARY ANTIBODY

Table 2-9: Primary Antibody. WB, Western Blot. IF, Immunofluorescence.

Type	Cat. No	Manufacturer	Clone-Species	Dilution and Application	ECL (for WB)
DDX6	HPA024201	Sigma Aldrich	Polyclonal/Rabbit	WB: 1:1,000	Low
FLAG	F3165	SIGMA	Mouse	WB: 1:2,000	Low
FMRP	AB17722 or 1033987-1	Abcam	Rabbit	IF: 1:200	-
GAPDH	HPA040067	Atlas Antibodies	Rabbit	WB: 1:2,000	Low
Igg	14-4301-82	Invitrogen	Rat	IF	-
Igg	02-6102	-	Rabbit	IF	ThermoFisher Scientific
NANOG	D73G4 XP	Cell Signaling Technology	Rabbit	IF: 1:1,000	-
OCT-4A	C30A3	Cell Signaling Technology	Rabbit	IF: 1:1,000	-
P62	610832	BD Biosciences	Monoclonal/mouse	WB: 1:1,000	Low
PAX6	42-6600	Invitrogen	Rabbit	IF: 1:100	-

PURA	Anti-PURA^{12D11}	-	Monoclo-nal/rat	WB: 1:10 IF: undiluted	High
SOX2	AB5603	EMD Millipore Corp	Rabbit	1:1,000 (IF)	-

2.10 SECONDARY ANTIBODY

Table 2-10: Secondary Antibody

Name	Clone	Cat. No	Dilution
Donkey anti-rabbit AlexaFluor 555	Polyclonal	A-31572	IF: 1:1,000
Donkey anti-rat AlexaFluor 488	Polyclonal	A-21208	IF: 1:1,000
Goat anti-rabbit AlexaFluor 647	Polyclonal	A212445	IF: 1:1,000
Goat anti-rabbit HRP	Polyclonal	Ab6721	WB: 1:10,000
Mouse anti-rat AlexaFluor 647	Polyclonal	A-21235	IF: 1:1,000
Mouse anti-rat HRP	Polyclonal	31470	WB: 1:20,000
Rabbit anti-mouse HRP	Polyclonal	AP160P	WB: 1:10,000

2.11 OLIGONUCLEOTIDES

2.11.1 PRIMERS FOR POLY CHAIN REACTION (PCR)

Table 2-11 Primers for PCR

Name	Sequence	Primer No
BTBD2_for	TCTTCCTGCACTTCACCGTC	CK82
BTBD2_rev	TCCTTGAACATGACGCGGAA	CK83
C8A_for	TGCTGGATGAAGGAATGCTGCAG	CK101
C8A_rev	ACCATGACCTGGTGTCTGTGTTG	CK102
DNAH1_for	TGCTTCTCCATCTACCCCTCCAG	CK107
DNAH1_rev	GAAAGACTCCAGAATCCCGCCTG	CK108
FAM43A_for	AAGGTCTTCGCCTGGGTGTAC	CK111
FAM43A_rev	GCCGCTTGAGGCGTTTAAATTCC	CK112
LAMB3_for	TCCTCTACACATGCTACCTCCAG	CK113
LAMB3_rev	CCATTGATGTGGTCACGGATCTG	CK114
LPXN_for	GGCCCTGAGAATCCAAGCAT	CK84
LPXN_rev	CAGGGCTGAGGACAGGAAAG	CK85

MINDY3_for/FAM188A_for	CAGCCTGCTGTGTGTATCTTGTG	CK103
MINDY3_rev/FAM188A_rev	AAAGTGGCAATGTGTCCACAGAG	CK104
PLEKHG4_for	AGAGGGTGCAGTTTGGGATG	CK86
PLEKHG4_rev	ACCAAGGTCTGCCATCTGTG	CK87
POLE2_for	GCCTGAGTCGATGTGGTGTT	CK88
POLE2_rev	ACAGGCCCTATGGAGAGAGA	CK89
PURA_for	GATCTCAAGGAGAACCAGCGC	CK9
PURA_for	CTTAGGCCCACTCTCTGTGCTT	LM30
PURA_rev	ACTTGCAGAAGGTGTGTCCGA	LM22
PURB_for	TGCGTGAGAACCGCAAGTAC	CK99
PURB_rev	GAAGGGTACGGTGATGGCATTG	CK100
SON_for	AGAGCCTTCAGAAACCCTTGTGG	CK105
SON_rev	ATGGTACGTCTACAGGCTGCTC	CK106
STRIP1_for	ACATTGACCCTGGCTCTGCTTC	CK109
STRIP1_rev	AGGCTGCTCTCATGTTGCGAATC	CK110
SYNGR4_for	CTGCCCCTTTTCTCTCCCTG	CK90
SYNGR4_rev	GACTTTGGAGCGGTCAGACA	CK91
U2SURP_for	AGGATGTTCCAGATGACCTTGA	CK92
U2SURP_rev	TTCTCTGCATCTGAGGGCAA	CK93

2.11.2 PRIMERS FOR QUANTITATIVE PCR (qPCR)

Table 2-12: Primers for qPCR

Name	Sequence	Primer No
CXCR4_for	CACCGCATCTGGAGAACC	SB138
CXCR4_rev	GCCCATTTCCTCGGTGTAGTT	SB139
FOXA2_for	CCACGACTTGCCCAGCAT	SB136
FOXA2_rev	GGGAGCGGTGAAGATGGA	SB137
FOXG1_for	GCTGGACATGGGAGATAGG	SB25
FOXG1_rev	GTTGATGCTGAACGAGGAC	SB26
GAPDH_for	GCTCATTTCCTGGTATGACAACG	SB1
GAPDH_rev	GAGATTCAGTGTGGTGGGGG	SB2
MAP2_for	CAGGTGGCGGACGTGTGAAAATTGAGAGTG	SB142
MAP2_rev	CACGCTGGATCTGCCTGGGGACTGTG	SB143
MESP_for	CTGCCTGAGGAGCCCAAGT	SB9

MESP_rev	GCAGTCTGCCAAGGAACCA	SB10
MIXL_for	CCGAGTCCAGGATCCAGGTA	SB13
MIXL_rev	CTCTGACGCCGAGACTTGG	SB14
NANOG_for	CCTTCCTCCATGGATCTGCTT	SB7
NANOG_rev	CTTGACCGGGACCTTGTCTTC	SB8
NCAD_for	CCCACACCCTGGAGACATTG	SB17
NCAD_rev	GCCGCTTTAAGGCCCTCA	SB18
OCT4_for	CAATTTGCCAAGCTCCTGAAG	SB3
OCT4_rev	AAAGCGGCAGATGGTCGTT	SB4
PAX6_for	TCCGTTGGAACTGATGGAGT	SB138
PAX6_rev	TAAGGATGTTGAACGGGCAG	SB139
PURA_del_for	GTGGACAACAAGCGCTTCTTCG	CK67
PURA_for	CGTGTTTATGCGAGTGAGCG	CK76
PURA_rev	CTTGTAGGGCACGGTGATG	CK2
PURA_rev	AACTTGGCCCACACCTTGTAG	CK4
PURA_rev	AGTTGCGATAGGTGGGCTTC	CK69
PURA_rev	ACTTGGCCCACACCTTGTAG	CK77
PURA_wt_for	AGCGCTTCTTCTTCGATGTG	CK1
PURA_wt_for	TGGACAACAAGCGCTTCTTCTTC	CK70
RPL32_for	AAATTAAGCGTAACTGGCGG	LM154
RPL32_rev	GTTGGGCATCAAGATCTGG	LM155
SOX17_for	GCCCATTTCCTCGGTGTAGTT	SB134
SOX17_rev	GGCGCAGCAGAATCCAGA	SB135
SOX2_for	CCTCCGGGACATGATCAGCATGTA	SB5
SOX2_rev	GCAGTGTGCCGTTAATGGCCGTG	SB6
T_for	CAACCTCACTGACGGTGAAAAA	SB11
T_rev	ACAAATTCTGGTGTGCCAAAGTT	SB12
TUBA_for	GGC AGT GTT TGT AGA CTT GGA ACC C	CK32
TUBA_rev	TGT GAT AAG TTG CTC AGG GTG GAA G	CK33

2.11.3 PRIMERS FOR SEQUENCING

Table 2-13: Primers for sequencing

Name	Sequence	Primer No
BTBD2_rev	TCCTTGAACATGACGCGGAA	CK83
DNAH1_rev	GAAAGACTCCAGAATCCCGCCTG	CK108
PLEKH4_rev	ACCAAGGTCTGCCATCTGTG	CK87
POLE2_for	GCCTGAGTCGATGTGGTGTT	CK88
PURA_rev	ACTTGCAGAAGGTGTGTCCGA	LM22
SYNGR4_rev	GACTTTGGAGCGGTCAGACA	CK91
U2SURP_rev	TTCTCTGCATCTGAGGGCAA	CK93

2.11.4 OLIGONUCLEOTIDES FOR CRISPR/Cas9

Table 2-14: Oligonucleotides for CRISPR/Cas9

Name	Sequence	Manufacturer	Application
F3	GGCAGCGGAGCGCAG-CATCA	IDT	PURA KO
Hs.Cas9.PURA.1.AB	GCCAAGCTCATCGACGACTA	IDT	PURA KO
CD.HC9.GFYR2118.AU	AACAAGCGCTTCTTCGATGT	IDT	F233del correction
CD.HC9.QLLN1936	CGAGGGCAC-CTCCTGACTGTG GACAACAGCGCTTCTTCTTC GATGTGGGCTCCAACAAGTA GGCGTGTTTATGCGAG-TGAGC	IDT	F233 del correction

2.12 PLASMIDS

Table 2-15: Plasmids

Name	Application	Insert	Resistance	Source
MP6	BioID	Flag-BirA	Hygromycin B	Proske M.
MP4	BioID	Flag-PURA_BirA	Hygromycin B	Proske M.

2.13 CELL LINES

Table 2-16: Cell Lines

Cell line	Media composition	Detaching agent	Coating agent	Passaging dilution	Source
HNSC CTRL	HNSC proliferation media	Trypsin	PDL	1:10	Internally produced
HNSC Flag-BirA	HNSC proliferation media	Trypsin	PDL	1:10	Internally produced
HNSC Flag-PURAwt-BirA	HNSC proliferation media	Trypsin	PDL	1:10	Internally produced
HNSC KO	HNSC proliferation media	Trypsin	PDL	1:10	Internally produced
HNSC WT	HNSC proliferation media	Trypsin	PDL	1:10	Brack-Werner lab (VIRO, HMGU)
isoCTRL (iPSC) #1	iPS brew XF (Miltenyi)	Accutase	Geltrex (1% in DMEM:F12)	1:10	Internally produced
isoCTRL (iPSC) #3	iPS brew XF (Miltenyi)	Accutase	Geltrex (1% in DMEM:F12)	1:10	Internally produced
isoCTRL (NPC) #1	N2B27 media	Accutase	Geltrex (1% in DMEM:F12)	1:10	Differentiated from iPSC
patient (iPSC) #1[1]	iPS brew XF (Miltenyi)	Accutase	Geltrex (1% in DMEM:F12)	1:10	Internally produced
patient (iPSC) #3[2]	iPS brew XF (Miltenyi)	Accutase	Geltrex (1% in DMEM:F12)	1:10	Internally produced
patient (NPC) #1	N2B27 media	Accutase	Geltrex (1% in DMEM:F12)	1:10	Differentiated from iPSC

[1] Patient samples have been handled under the ethics approval AZ 668/21 S-SR from 2.12.2021 of the Ethics Commission of the Technical University Munich to Prof. Dr. Dierk Niessing.
[2] Patient samples have been handled under the ethics approval AZ 668/21 S-SR from 2.12.2021 of the Ethics Commission of the Technical University Munich to Prof. Dr. Dierk Niessing.

3 METHODS

3.1 CELL CULTURE

All cell lines were cultured in the indicated media and passaged using the specified detaching agent (**Table 2-16**). All cell culture work was performed in a biosafety cabinet and generally reagents were sterile. The prepared culture media was stored at 4 °C. All cell lines were cultivated at 37 °C in a humidified incubator with 5 % CO_2.

3.1.1 CULTIVATING AND PASSAGING CELLS

Cells were grown to around 80% confluency and passaged subsequently. Briefly, media was removed, and cells were washed once using PBS. Then, the detaching agent was added (according to **Table 2-16**) and cells were incubated at 37 °C for 3-5 min in the incubator. Culturing media was added to the detached cells to dilute the detaching agent, cell suspension was transferred to a falcon tube and centrifuged at 300-500 x g for 5 min. The supernatant was aspirated, and the cell pellet was resuspended in culturing media and plated as indicated in the passaging dilutions column in **Table 2-16**. Medium was changed every 2-3 days. iPSCs were plated with 1:1000 Rock Inhibitor (RI) which was removed after 24 h.

3.1.2 CRYOPRESERVATION OF CELLS

For cryopreservation, cells were detached as described in Section 3.1.1. After centrifugation, the cell pellet was resuspended in 1 ml of cryopreservation medium for iPSCs and NPCS or culturing medium with 10 % DMSO for HNSCs. The cell suspension in was then transferred to a cool container and stored overnight at -80 °C. Subsequently, the frozen cells were stored in liquid nitrogen until further use.

3.1.3 THAWING CELLS

Cells were thawed by addition of warm culture media to the frozen cell suspension under the laminar flow work bench. The suspension was mixed by gently pipetting up and down until the entire suspension was thawed and then the mix was centrifuged at 300-500 x g for 5 min. The supernatant was discarded, and fresh culture medium was added. The resulting cell suspension was spread on a culture dish and finally incubated at 37 °C with 5 % CO_2.

3.1.4 CELL COUNTING

For counting, cells were detached and centrifuged as described in section 3.1.1. After resuspension with medium, 10 µL were taken and mixed with 10 µL of trypan blue. Of this mix, 10 µL were pipetted into a counting chamber and placed in the cell counter (LUNA Automated cell Counter) which automatically computed the total number of cells and the percentage of viable cells. When performing the gene editing with CRISPR/Cas9, cells were counted with Invitrogen Countless automated cell counter.

3.1.5 CELL HARVEST

Cells were harvested by removing the medium and washing once with PBS. PBS was added and cells were scrapped off with a cell scraper. Scrapped cells were transferred to 1.5 mL tubes and centrifugated at 300-500 x g for 5 min. Supernatant was discarded and cell pellet was either used directly with required lysis buffer for different application or conserved at -80 °C until further use.

3.2 GENERATION OF CELL LINE WITH CRISPR/CAS9

PURA KO in HNSC and correction of F233del mutation from PURA patient iPSC were performed by CRISPR/Cas9 ribonucleoprotein (RNP) which contained the Cas9 endonuclease, the trans-activating CRISPR RNA (tracrRNA) and the guide RNA (gRNA). The Cas9 protein and the tracrRNA are standard products whereas the gRNAs were designed and optimized to target PURA sequence (unpublished data, Molitor L. and Bacher S.) and the PURA mutated site (unpublished data, Ketteler C.). **Table 3-1** contains the list of the gRNAs for KO and F233del mutation correction.

Table 3-1: CRISPR/Cas9 gRNAs for PURA KO (gRNA_1 and gRNA_2) and for F233del correction (gRNA_3).

gRNA No	gRNA name	Sequence (5´-3´)	Application
gRNA_1	F3	GGCAGCGGAGCGCAG-CATCA	PURA KO
gRNA_2	Hs.Cas9.PURA.1.AB	GCCAAGCTCATCGAC-GACTA	PURA KO
gRNA_3	CD.HC9.GFYR2118.AU	AACAA-GCGCTTCTTCGATGT	F233del correction

RNPs were generated before nucleofection. Briefly, a gRNA/tracrRNA duplex was generated by mixing 1.5 µL of each RNA (100 µM). The mix was heated up to 95°C for 5 min and cooled down to room temperature for at least 10 min, the resulting duplex stock (50 µM) can be stored at -20°C up to 3 months. To prepare the RNP, the duplex stock was mixed with PBS. Lastly, Cas9 protein was added slowly (**Table 3-2**). The reaction should be mixed (if necessary, spin down) and incubated at room temperature for 15 min. The generated RNPs can be stored at 4°C up to 4 weeks or at -80°C for 6 months.

Table 3-2: Volumes of each reagent needed to produce the RNPs.

Reagent	Stock concentration (µM)	Volume (µL)
Cas9 stock solution	61	2
gRNA duplex	50	3
Sterile PBS	-	2

3.2.1 TRANSFECTION

Cells were cultivated as described in section 3.1. On the day of transfection, a 6 well plate was coated with the appropriated coating agent (**Table 2-16**). Cells at 80% confluency were washed with sterile PBS and detached as described in section 3.1.1 until cells were floating. Then 1 mL of medium was added to neutralize the detaching agent and the cells were collected in a 15 mL tube. Cells were centrifuged for 5 min at 300 x g and the supernatant was discarded. Then cells were resuspended in 2 mL of sterile PBS and counted as described in section 3.1.4. Cell solutions were diluted to have 10^6 cells per tube and centrifuged at 100 x g for 10 min. Meanwhile the transfection mix was prepared for F233del correction (**Table 3-3**) and for PURA KO (**Table 3-4**).

Table 3-3: List of reagents for transfection of iPSC and perform F233del mutation correction.

Reagent	Volume (uL) sample	Volume (uL) control
Nucleofector Solution	82	82
Supplement	18	18
RNP_3	7	-
100 µM HDR donor oligo (**Table** *2-14*)	1.2	-
100 µM Electroporation Enhancer	1.2	1.2
PBS	-	8.2

Table 3-4: List of reagents needed for transfection of HSNC and perform PURA KO.

Reagent	Volume (µL) sample	Volume (µL) control
Nucleofector solution	82	82
Supplement	18	18
RNP_1	6	-
RNP_2	6	-
Electroporation enhancer	4	4
PBS	-	12

After centrifugation, supernatant was discarded, and cells were resuspended in nucleofection mix and transferred to nucleocuvettes (Lonza). Nucleocuvettes

were placed in the Amaxa 4D device and program DN-100 was selected for nucleofection. After nucleofection 0.5 mL of prewarmed medium was added to the cuvette and mixed with the transfected cells. The cell suspension was plated on the pre-coated plate using the plastic Pasteur pipette (Lonza) and 1.5 mL of additional medium was added (iPS brew with RI for iPSC and HNSC proliferation medium for HSNCs). Cells were cultivated at 37°C and 5% CO_2 overnight, then medium was changed to remove the transfection reagents.

3.2.2 SINGLE CLONES GENERATION

One week after nucleofection, single cell clones were generated as follow:

- PURA KO HNSC line: In order to create HNSC clonal KO cell lines, a 96-well plate was coated with PDL and let it dry over night at room temperature. The day after, cells were washed with sterile PBS and detached as describe in paragraph 3.1.1 with the required detaching agent (**Table 2-16**). After resuspension in culture medium, cells were counted as described in section 3.1.4. Subsequently, a dilution series was made in a way that 100 µL medium were containing only one cell, then 100 uL per well were pipetted in the precoated 96-well plate. The plate was incubated at 37°C and 5% CO_2. Medium was changed every 3 days. After approximately two weeks, the colonies were analyzed under microscope and if the cells were confluent enough, the colonies were trypsinized, then 100 uL of medium was added and, without centrifugation (to prevent cell lost), cells were directly transferred to a 24-well plate. The process was repeated after around 2 weeks and the clones were transferred to a 12-well plate and subsequently to a 6-well plate for further expansion.
- F233del mutation correction iPSC line: in order to create clonal iPSC isogenic control (isoCTRL) cell lines, a 10cm dish was coated with GelTrex (GT). Cells were washed with sterile PBS and detached using the detaching agent (**Table 2-16**). After centrifugation cells were resuspended in 10 mL of iPS brew with RI and plated, on the next day, medium was changed. Cells were checked every day for single roundish colonies. Single colonies were picked with a 100 µL pipette tip and transferred to GT pre-coated 24-well plate. From there, when confluent, cells were transferred to a 12-well plate and then to a 6-well plate.

3.3 DOXYCYCLINE-INDUCIBLE CELL LINE

To produce a stable doxycycline-inducible cell line, the PiggyBac (PB) transposon system was used. The PB transposase, encoded by the helper vector, recognizes transposon-specific inverted terminal repeat sequences, located at both ends of the gene of interest. It cuts and paste into chromosomal TTAA sites. A tet-on/off system allows doxycycline (DOX) induce expression of the protein of interest. Hygromycin B resistance is conferred to successfully edited cells.

$4x10^5$ HNSC cells were plated in each well 2 days before lipotransfection. For lipotransfection, the Lipofefctamine 3000 transfection kit from Invitrogen was used. For each lipotransfection, three mixes were prepared as described in **Table 3-5** and table **Table 3-6.**

Table 3-5: List of reagents for Lipofectamine solution (mix1).

Reagent	Volume (μL)
optiMEM	125
Lipofectamine 3000	7.5
Tot vol	**132.5**

Table 3-6: List of reagents for vector containing solutions (mix2 and mix3). MP4, Flag-PURAwt-BirA. MP6, Flag-BirA. MP11, Helper vector.

Reagent	Volume (μL)
optiMEM	125
P3000	5
MP4 (mix2) or MP6 (mix3)	2.5 (ug)
MP11	2.5 (ug)
Tot vol	**133.88**

They were mixed thoroughly, then mix 1 was mixed with mix 2 and mix 3 in a 1:1 ratio. Meanwhile, cells were washed once with PBS and new medium was added (2 mL). 250 µL of reaction mixture were added dropwise to the cells and incubated in the CO_2 incubator at 37°C for 3 days. Afterwards medium was replaced by new medium containing 300 µg/mL of Hygromycin B. The medium was changed for 10 days every 2/3 days.

3.3.1 FLUORESCENCE-ACTIVATED CELL SORTING (FACS)

Cultured cells were doxycycline induced 24 h before FACS. Right before FACS, cells were washed once with PBS and trypsinized. After centrifugation at 300 x g for 5 min, they were resuspended in FACS buffer (0.5% BSA, 2mM EDTA, 25 mM HEPES in PBS), Trypan blue (1:100) was added and cell suspension was singularized by passing through a 35 µm cell strainer. Then Ejona Rusha (Head of Stem Cell Facility, Helmholtz) performed the FACS experiment. First, cells were gated for living cells, second, only single cells were taken from the control line (Flag-BirA) to create the gate channels based on GPF signal. During a first FACS experiment only mid GPF signal cells were collected. In a second FACS experiment, cells were sorted for low, intermediate, and high GFP signal. Sorted cells were centrifuged at 300 x g for 5 min and transferred to coated 12- or 6-well plate based on the number of sorted cells. Cells were kept in culture for 1-2 weeks. Then they were analyzed at fluorescence microscopy after 24h of DOX induction and collected for Western Blot experiment.

3.4 LINEAGE ASSAY

To test the pluripotency "ability" of isoCTRL and patient iPSC, cells were differentiated towards early progenitor cells (ectoderm, mesoderm and endoderm). To this purpose, cells were plated on a 12-well plate in 1:10 dilution. When cells reached 90% confluency, the differentiation started with three technical repeats per germ layer. Medium was changed every 24 h up to day 5, then cells were collected for RNA extraction.

For ectoderm differentiation, N2B27 medium was used (**Table 2-8**) using the B27 supplement with Vit. A instead of the one without Vit. A. Medium was supplemented with 0.5 µM Dorsomorphin, 10 µM SB-431542 and 5 µg/mL Insulin.

For mesoderm differentiation, DMEM/F12 medium was supplemented with 1% B27 with Vit. A and 10 µM CHIR99021.

For endoderm differentiation, RPMI 1640 medium was supplemented with 1% B27 with Vit. A, 1% Glutamax, 100 ng/mL Activin A, 1 µM CHIR99021 and sodium butyrate (0.250 mM on day 0; 0.125 mM on the other days).

3.5 NEURAL PROGENITOR CELL DIFFERENTIATION

Neural Progenitor Cells (NPC) are neural precursor cells derived from human Pluripotent Stem Cells (hPSC) or human induced pluripotent stem cells (iPSC). To differentiate NPCs (Reinhardt P, 2013) from isoCTRL and patient iPSCs, cells were plated in one well of a 6-well plate. After reaching 90% confluency they were detached by incubation at 37°C for 1 h with 1 mL of collagenase IV (1 mg/mL). After incubation, 1 mL of DMEM/F12 medium was added and pieces of colonies of cells were detached by pipetting up and down with a 5mL pipette. Colonies were transferred to a 15 mL falcon tube for 5 min sedimentation. Then DMEM/F12 was removed and substituted with 2 mL of Day 0 medium. Colonies were transferred to one well of a low attachment 6 well plate to form the embryonic bodies (EBs). Medium was changed every day, Day 0 and Day 1 medium was composed of KSR medium (**Table 2-8**) supplemented with 1 µM Dorsomorphin, 10 µM SB-431542, 3 µM CHIR 99021 and 0.5 µM PMA. Only for Day 0, RI (1:1,000) was added. Day 2 and 3 medium was composed of N2B27 (**Table 2-8**) with same supplemented molecule as for day 1. From day 4 on, medium was composed of N2B27 supplemented with 1 µM Dorsomophin, 10 µM SB-431542, and 150 µM Ascorbic Acid until day 7 and 20 ng/µL FGF2 from day 6 on. On day 7, the EBs, which showed intensive neuroepithelial outgrowth, were triturated with a 1,000 µL pipette tip into smaller pieces and plated on an entire GT coated 6-well plate per condition, medium was changed the day after and from that time every second day. Cells were incubated for one week at 37°C and 5% CO_2. After one week, cells were analyzed at bright-field microscope for neuronal rosettes structure. Presumptive positive wells were detached with accutase and plated on GT coated 6-well plate with 1:6 dilution. After one week of incubation at 37°C and 5% CO_2, while medium was changed every 2-3 days, cells were collected for differentiation process control via RNA extraction and neural marker analysis via qPCR. From this time point, cells are splitted every 6-7 days with 1:10 ratio in GT coated plates up to 10 passages. After a maximum of 5 splits, cultures were virtually free of contaminant non-NPCs.

3.6 MOLECULAR BIOLOGY

3.6.1 GENOMIC DNA EXTRACTION

Genomic DNA was extracted from cells using the DNeasy Blood & Tissue Kit by Qiagen. The extraction was performed according to the manufacturer´s protocol. Cells were harvested (section 3.1.5) and centrifuged at 300 x g for 5 minutes. The pellet was resuspended in 200 µL PBS. 20 µl of proteinase K was added

together with 200 µl buffer AL and the mixture was vortexed thoroughly. The sample was incubated at 56 °C for 10 minutes at 500 rpm. Then, 200 µL ethanol (96 % -100 %) was added and the samples were again mixed by vortexing. The mixture was transferred into a DNeasy Mini spin column, which was placed in a 2 mL collection tube. The column was centrifuged at 6.000 x g for 1 minute and the flow-through was discarded together with the collection tube. The spin column was placed in a new 2mL collection tube and 500 µL buffer AW1 was added. Another centrifugation step was performed at 6.000 x g for 1 minute, the collection tube with flow-through was discarded again and substituted with a new one. Subsequently, 500 µl of buffer AW2 was pipetted in the column and the sample was centrifuged at 20.000 x g for 3 minutes. For the elution of the DNA the column was placed into a 1.5 mL microcentrifugation tube and 50 µL buffer AE was added. After incubation for 1 minute at room temperature, samples were centrifuged at 6.000 x g for 1 minute. The flow-through contained the purified genomic DNA which was analyzed by UV spectroscopy at 260 nm with Nanodrop spectrometer (section 3.6.8).

3.6.2 POLYMERASE CHAIN REACTION

All polymerase chain reactions (PCR) were performed on a T100 Thermalcycler from Biorad Laboratories. For the amplification of template DNA CloneAmp HiFi PCR Premix (TaKaRa Bio Inc.) was used already containing polymerase, dNTPs and an optimized buffer. To perform the PCR, the samples were prepared according to manufacturer´s protocol. For each reaction, the reagents listed in **Table 3-7** were added to the premix.

Table 3-7: List of Reagents for a 25 µL volume PCR reaction.

Reagent	Volume in µL	Final concentration
CloneAmp HiFi PCR Premix	12.5	1x
Forward Primer	1	10 µM
Reverse Primer	1	10 µM
Template DNA	2	300 ng
Sterilized distilled water	Up tp 25	-
Total volume per reaction	**25.0**	**-**

The tubes were placed in the Thermocycler and the PCR reaction was performed with the program according to **Table 3-8**.

Table 3-8: PCR program.

Step	Temperature in °C	Time	
Initial Denaturation	98	30 sec	
Denaturation	98	10 sec	36 cycles
Annealing	59-71	15 sec	

Elongation	72	25 sec
Final extension	72	10 sec (20 min for TOPO cloning)
Hold	4	forever

3.6.3 AGAROSE GEL ELECTROPHORESIS

To analyze the PCR products, agarose gel electrophoresis was performed. To prepare the agarose gel, agarose powder was dissolved in TRIS Acetate EDTA (TAE)-buffer, the agarose concentration was dependent on the size of the amplicon (**Table 3-9**)

Table 3-9: Suggested agarose concentrations to separate different ranges of DNA molecules.

% agarose gel (m/v)	DNA size (kb = 1000 bp)
0,5 %	1 kb to 30 kb
1 %	50 bp to 10 kb
1,5%	200 bp to 3 kb
2,0 %	50 bp to 2 kb

The mixture was heated up in a microwave at maximum heat for approximately two minutes until the agarose was fully dissolved in the buffer. Before pouring the liquid gel solution into the gel tray, 5 µL of GelRed® (Biotium) were pipetted onto the surface of the tray. The gel was dried and hardened for 30 minutes until solidified. The agarose gel with tray was inserted into the agarose gel chamber, which was filled up with TAE-buffer to the filling line. Prior sample loading, the samples were mixed with 6x DNA loading dye and loaded into the wells. In addition, a suitable size marker (1 kb or 100 bp) was loaded. The gel electrophoresis was performed at 130 Volt for 30-40 minutes. Then, the gel was analyzed via ultraviolet fluorescence imaging by using a Fusion SL4 device and the software by Vilber Lourmat. To extract DNA from band, the desired band was cut and transferred to a 1.5 mL Eppendorf tube.

3.6.4 PCR PRODUCT COLUMN PURIFICATION

To purify the PCR product either after gel band but or directly after PCR, the NucleoSpin® Gel and PCR Clean-Up-Kit was used with the provided protocol from the manufacturer. Briefly, 200 µL of NTI buffer was added every 100 µL or 100 mg of PCR product or gel band, respectively (for gel containing >2% agarose, the buffer NTI was doubled). Only for gel extraction, the sample was incubated 5-10 min at 50 °C and 600 rpm, then vortexed until all the gel was dissolved. The samples were then transferred to a purification column placed into a 2 mL collection tube.

The column was centrifuged at 11.000 x g for 30 seconds, then the flow-through was discarded and the column was placed back into the collection tube. The silica membrane was washed twice by adding 650 µL of NT3 buffer and subsequent centrifugation at 11.000 x g for 30 seconds. For drying the membrane, the column was centrifuged at 11.000 x g for 1 minute. The flow-through and the collection tube were discarded, and the column was placed into a new 1.5 mL microcentrifugation tube. To elute the DNA, 20 µL of NE buffer was added to the column, which was then incubated for 1 minute at room temperature and centrifuged at 11.000 x g for 1 minute. Finally the amount of cleaned PCR product was analyzed by UV spectroscopy at 260 nm with Nanodrop spectrometer (section 3.6.8)

3.6.5 TOPO CLONING

To perform TOPO cloning (topoisomerase-based cloning), the Zero Blunt TOPO PCR cloning kit was used with the provided protocol from the manufacturer. Briefly, a PCR product was produced (section 3.6.2) being sure to perform the final extension step at 72°C for 20 min to produce blunt ends. Then a 6 µL TOPO cloning reaction was prepared according to **Table 3-10**. The rection solution was gently mixed and incubated for 5 min at room temperature, then it was put on ice until use.

Table 3-10: List of reagents for TOPO cloning reaction.

Reagent	Volume (for competent *E.coli*)
Fresh PCR product	4 uL
Salt Solution (provided with kit)	1 uL
pCR-Blunt II – TOPO (vector)	1 uL
Final Volume	6 uL

3.6.6 TRANSFORMATION INTO COMPETENT DH5α CELLS

Plasmid or TOPO vector were transformed into chemically competent *E.coli* DH5-α cells. To do so, competent cells, which were kept at -80°C were thawed on ice for at least 10 min. Then 1 µL of plasmid or TOPO vector was added to the cells and incubated on ice for 10 min. Then heat shock was performed by incubating cells for 45 sec at 42°C and then for 2 min on ice. 500 µL of room temperature sterile SOC medium was added and cells were incubated for 60 min at 37 °C and 900 rpm. Meanwhile Agar-plates containing the appropriate antibiotic, which are kept at 4°C, were wormed up to room temperature. After 1 h of incubation, 50 µL to all transformed cells are spread on the agar plate with sterile glass beads. Plated cells are left over night at 37°C. On the next day, several colonies together or one single colony were picked for plasmid and TOPO cloning analysis, respectively. The picked colonies are transferred to a 15 mL falcon tube containing 5 mL of LB medium with appropriate antibiotic and they were grown over night in a shaker at 37 °C and 250 rpm. Finally the amplified DNA was extracted using Nucleospin

Plasmid Mini kit (section 3.6.7) and the amount of plasmid DNA was analyzed by UV spectroscopy at 260 nm with Nanodrop spectrometer (section 3.6.8).

3.6.7 PLASMID DNA EXTRACTION

To purify plasmid DNA the Nucleospin Plasmid Mini kit was used. Briefly, the 15 mL falcon tubes were centrifuged at 4,500 rpm for 10 min. The supernatant was discarded and the pellet was resuspended in 250 µL of buffer A1 and then transferred to a 1.5 mL Eppendorf tube. 250 µL of buffer A2 was added to the sample which was then shacked by inverting slowly and incubated at room temperature for 5 min. Subsequently, 300 µL of buffer A3 was added and the sample was centrifuged at 11.000 x g for 5 to 10 min. After centrifugation the supernatant was loaded onto column placed in a 2 mL collection tube and centrifuged again at 11,000 x g for 1 min. The flow-through was discarded and the column was placed back into the collection tube. 400 µL of buffer A4 was added and another centrifugation at 11.000 x g for 1 min was performed. The flow-through was discarded again and the column placed back into the collection tube. The membrane was dried by centrifugation at 11.000 x g for 2 min. Then, flow-through and collection tube were discarded, and the column was placed into a new 1.5 mL microcentrifugation tube. To elute the plasmid DNA, 50 µl of AE buffer was added to the column, which was then incubated for 1 minute at room temperature and centrifuged at 11.000 x g for 1 minute. Finally, the purified plasmids was analyzed by UV spectroscopy at 260 nm with Nanodrop spectrometer (section 3.6.8).

3.6.8 MEASURING RNA/DNA CONCENTRATION

DNA or RNA concentrations were measured using NanoDrop 2000 by ThermoFisher Scientific. After starting the Nanodrop operating software, 1.5 µL of DNase/RNase free water were used to perform an auto wavelength verification. Since the Nanodrop measures the absorbance of all molecules in the sample, 1.5 µL of the appropriate elution buffer was used as a blank, which was subtracted automatically by the program. The software settings were adjusted depending on the type of nucleic acid that was measured. Then, 1.5 µL of the samples were pipetted on the NanoDrop measuring unit and analysis was performed. After each measurement, the Nanodrop was cleaned with a dry, lint free laboratory wipe.

3.6.9 SEQUENCING DNA

A sample was sent to Eurofins genomic where they performed Sanger sequencing with the respective sequencing primer (**Table 2-13**) or the primer M13rev-29 furnished by Eurofins genomic for TOPO vector sequencing. The sample was diluted to 10 ng/µL into 15 µL final volume. Sanger sequencing was performed with a maximum output of approximately 1000 nucleotides in one direction. The resulting sequences were aligned to the expected plasmid or PCR sample sequence using the BENCHLING software (Benchling, 2023).

3.6.10 QUANTITATIVE REAL-TIME PCR (qPCR)

During the whole qPCR experiment RNase free tubes and equipment was used to avoid any RNA contamination and therefore falsification of the results.

3.6.10.1 ISOLATION OF TOTAL RNA

Total RNA was isolated from cultured cells by using the TRIzol/Chloroform protocol. For a sufficient amount of RNA, cells were cultivated in 6-well plates until a confluency of 100 % was reached. Then cells were harvested (3.1.5) and centrifuged at 16.000 x g for 10 minutes. Cell pellet was re-suspended in 1 mL of TRIzol and incubated at 55°C for 10 min, then it was transferred into ice. 200 µL of Chloroform was added and the tube was vigorously shacked, then it was centrifuged for 15 min at 12.000 x g and 4°C. The obtained product had three phases:

1. Top layer: clear, aqueous (RNA)
2. Middle layer: white precipitated (DNA)
3. Bottom layer: pink organic phase

The top layer was transferred to another tube and 100% isopropanol in a 1:1 ratio was added. Optionally, glycogen can be added (0.5 µL) to better see the pellet in further step. The solution was vortexed and stored over night at -20 °C.

On the day after, the solution was centrifuged for 30 min at 12.000 x g and 4°C. The supernatant was discarded, and the pellet of RNA was washed twice with 70% Ethanol (without pipetting up and down to avoid RNA destruction) and centrifugated at 12.000 for 10 min at 4°C. After the second centrifugation, all the ethanol should be removed with 10 µL pipette tip and quick spin down. The RNA pellet was let dry for a 10-20 min with open tube at room temperature, then RNA was resuspended with 50 µL of RNAse free water.

3.6.10.2 DNase DIGEST

To remove the whole remaining DNA in the sample, a DNase digest was performed according to the protocol provided by Turbo DNA-free Kit by ThermoFisher Scientific. The reagents were mixed like reported in **Table 3-11** and incubated at 37 °C for 30 minutes.

Table 3-11: List of Reagents for DNase digest.

Reagent	Amount in µL
10x DNase buffer	5
DNAse	1
RNA Elution	50
Total Vlume	56

The reaction was inactivated by adding 5.6 µL of inactivation beads to the solution and incubating at room temperature for 5 minutes. Afterwards, it was centrifuged at 10.000 x g for 1.5 minutes and the supernatant was transferred to a new microcentrifugation tube. The purified RNA can be stored at -20°C for short term

or at -80°C for long term.

3.6.10.3 GENERATION OF COMPLEMENTARY DNA (cDNA) LIBRARY

To generate the cDNA library, the RNA concentrations of the samples were measured in advance with NanoDrop (section 3.6.8) and diluted to the required concentration with RNase free water. Then the reagents for cDNA generation were mixed (**Table 3-12**) and incubated at 37 °C for 15 minutes. Then sample wase heat-shocked for 5 seconds at 85 °C. The cDNA can be stored at 4°C.

Table 3-12: List of reagents for cDNA generation.

Reagent	Amount for 10 uL	Amount for 60 uL
5x primescript RT master mix	2uL	12uL
Total RNA	500 ng	3000ng
RNAse free water (DEPC)	Up to 10 uL	Up to 60uL

3.6.10.4 PERFORMING qPCR

To perform the quantitative PCR (qPCR) reaction, the Light Cycler® 480 Instrument II (Roche Molecular Systems) was used. The samples were prepared with a 2x Power SYBR Green Master Mix (ThermoFisher Scientific) already containing the SYBR green dye, Taq DNA Polymerase, dNTPS, a reference dye and optimized buffers. The volume per well is in **Table 3-13**.

Table 3-13: List of reagents for qPCR.

Reagent	Per sample in µL
Buffer(2x) SYBR Green	10
Forward Primer	2
Reverse Primer	2
Water	4
Total Volume	18 + 2µL cDNA

The prepared primer pair master mixed (18 µL/well) and the cDNA (2 µL) were pipetted into a 96-well plate. Subsequently, the plate was covered with a plastic film and spined down at 500 x g for 5 minutes. The plate was then transferred in the Light Cycler System and the qPCR was performed with the program shown in **Table 3-14**.

Table 3-14: qPCR program.

Step	Temperature in °C	Time	
Initial denaturation	95	10 sec	
Denaturation	95	10 sec	60 cycles
Annealing, extension, reading fluorescence	60	5 sec	
Elongation	72	10 sec	
Melting Curve	-	-	
Hold	4	forever	

3.7 BIOCHEMICAL METHODS

3.7.1 WESTERN BLOT

Western Blot was performed using Invitrogen provided 4-12% Bis-tris gel and Buffers. Chamber was assembly according to manufacturer's instructions.

3.7.1.1 PROTEIN EXTRACTION

To extract proteins, cells were harvested (section 3.1.5) and centrifuged at 300-500 x g. The pellet was resuspended in 50-100 µL of RIPA buffer (**Table 2-6**) with 1:100 protease inhibitor. The sample was sonicated for 1 minute and then put on ice for 20 min. After centrifugation for 10-40 min at 16.000 x g and 4°C, the supernatant was transferred to a new tube.

3.7.1.2 BCA PROTEIN ASSAY

To measure concentration of total protein, the BCA Protein assay was performed. Briefly, the purified protein was diluted 1:10 in 50 µL water in dark tubes. BCA reagent A and BCA reagent B were mixed in a 50:1 ratio. Then 1 mL of the A-B solution was added to the sample and incubated at 37°C for 30 min and 700 rpm. Afterwards, the total protein concentration was measured using the BioPhotometer.

3.7.1.3 SAMPLE PREPARATION AND SDS PAGE

Samples were diluted to a final protein concentration of 1,500 µg/mL and 2,500 µg/mL for HNSC and iPSC, respectively. Then, the 4x SDS loading dye and 1:100 reducing agent were added and sample was incubated for 10 min at 70°C and 700 rpm. Meanwhile, the Invitrogen chamber was assembled according to manufacturer's instructions and filled with 1x Nupage Running buffer (**Table 2-6**). 500 µL of antioxidant were added in the front part of the chamber. 18 µL of the samples were loaded onto the 4-12% Bis-Tris gradient gel, as well as 5 µL of protein marker. The gel was run at 180 V for 50 min.

3.7.1.4 BLOTTING

The SDS gel was extracted from the pre-cast set up and the blotting module was assembled as instructed by manufacturer (bottom-sponge-Whatman-gel-blotting membrane-Whatman-sponge-top). The PVDF blotting membrane was first activated in 100% methanol for at least 30s. All other components were soaked in 1 x transfer buffer, prior to blotting module assembly. The blotting module was transferred to the chamber and the chamber was filled with MQ water. The blot was performed for 90 min at 30 V.

3.7.1.5 DETECTION OF PROTEIN OF INTEREST

The blotting module was disassembled, and successful blotting was tested by Ponceau stain of the blotting membrane. The Ponceau solution was washed off with water and the membrane was blocked in 15 or 50 mL tube with 1% casein solution in PBST for 30 min at room temperature while rotating. Then, blocking solution was discarded and the primary antibody (**Table 2-9**) in 0.5% casein in PBST was added. The membrane with primary antibody was incubated over night at 4°C on a rotating device. On the next day, the primary antibody was removed (it can be used again if kept at 4°C up to one week) and blot was washed 3 timed for 5 min each in PBST. Meanwhile the secondary antibody was diluted in PBST. Blot was incubated with secondary antibody for 1 h at room temperature in the rotating device. Finally secondary antibody was discarded, and blot was washed 3 times for 5 min each in PBST. The membrane was then placed onto a clear plastic film and 1:1 mix solution A and solution B of ECL kit was distributed on the membrane. Two types of ECL solution were used based on the expected signal intensity. For standard applications, “low” ECL was used, whereas for high-sensitivity detection like PURA, the “high” ECL was applied. The membrane was analyzed using the Fusion SL4 device and – software. Analysis and quantification of the protein bands were done with ImageJ/Fiji software.

3.7.2 IMMUNOFLUORESCENCE STAINING

Cells were cultured on coated cover slides in 24 wells (section 3.1). After reaching the desired confluency, cells were washed with PBS and fixed with 2% formaldehyde for 15 min at room temperature. Then the fixed cells were washed three times with PBS, cells can be used right away or stored up to one week in the third washing. Cells were permeabilized with 0.5% Triton-X in PBS for 5 min and then washed two times with PBS leaving the second wash. Afterwards the cover slides were transferred to a Parafilm/Whatman paper set-up and blocking was initiated with blocking solution (1% donkey serum in PBST) for 10 min. Then cells were incubated for 1h at room temperature with primary antibody (**Table 2-9**) diluted in blocking solution, except for PURA which was used undiluted. Afterwards, cells were washed three times for 5 min each with PBST and secondary antibody (**Table 2-10**) diluted in blocking solution was added. After 1 h of incubation of secondary antibody in dark at room temperature, cells were washed 3 times for 5 min each with PBST. To stain the nucleus, DAPI was added diluted 1:2,000 in PBS for 5 min at room temperature. Then cells were washed two times with PBS and the second wash was left. The edge of the cover slide was dried on a paper and then they were glued upside down in ProLong mountaing “medium” on a slide. The

slides were let dry overnight at room temperature in the dark. Imaging was performed with Axio Observer.Z1 inverted fluorescence microscope. Exposure time was kept the same to allow quantification of intensity. Analysis was performed using ImageJ/Fiji software.

3.7.2.1 ANALYSIS OF IMMUNOFLUORESCE IMAGES - CELL COUNTING

Cell counting was performed with ImageJ software (version 2.14.0/1). Channels were split and DAPI channel was used. First, the background signal was removed (process-subtract background, with a rolling ball radius of 100 pixels) and a binary image was created (image-color-Stack to RGB). In the binary image, the holes in the cells were filled (process-binary-fill holes) and overlapping cells were separated using the watershed tool (process-binary-watershed). The separated cells were counted (analyze-analyze particles) setting a particle size of 100-infinity to avoid counting cell debris.

3.7.2.2 ANALYSIS OF IMMUNOFLUORESCE IMAGES - INTENSITY QUANTIFICATION

Quantification of the intensity was performed with ImageJ software (version 2.14.0/1). For this purpose, the channels were separated, and background signal was removed (subtract background command with a rolling ball radius of 100 pixels), then the signal intensity for whole image was measure (analyze-measure command). To obtain the signal intensity per cell, the number of cells was counted (section 3.7.2.1).

3.7.2.3 ANALYSIS OF IMMUNOFLUORESCENCE IMAGES - COLOCALIZATION

Colocalization was performed using ImageJ software (version 2.14.0/1) and JACoP plugin. Briefly, channels were separated and chosen in JACoP window as for image A and image B. Then the analysis was started being sure that the wanted types of analysis were checked on the “analysis to perform” section.

4 RESULTS

4.1 GENERATION OF ISOGENIC CONTROL iPSC

To better understand PURA's role in PURA syndrome, fibroblasts from three independent PURA syndrome patients (#1, #2, #3) were collected. The three patients presented the very same heterozygous mutation, namely the deletion of phenylalanine at position 233 (F233del) in the third PUR repeat (PURIII). Cells were reprogrammed to clonal induced Pluripotent Stem Cell (iPSC) cell lines (Ejona Rusha) using a non-integrative mRNA-based method. To have a proper control with the same genetic background an isogenic control (isoCTRL) was generated by correcting the mutation using the CRISPR/Cas9 genome editing technology. Two gRNAs were tested to guide the Cas9 towards the target mutated DNA sequence and one showed consistent mutation correction (unpublished data, Carolin Ketteler). After Double-Stranded DNA Breaks (DSB), the missing base pairs were inserted at the specific genomic locus via homology-directed repair (HDR, **Figure 4.1-A, B**). The isoCTRL cell line was created by Carolin Ketteler for patient #3, whereas patients #1 and #2 were part of this project. Due to a restricted number of pages, only results related to patient #1 are presented.

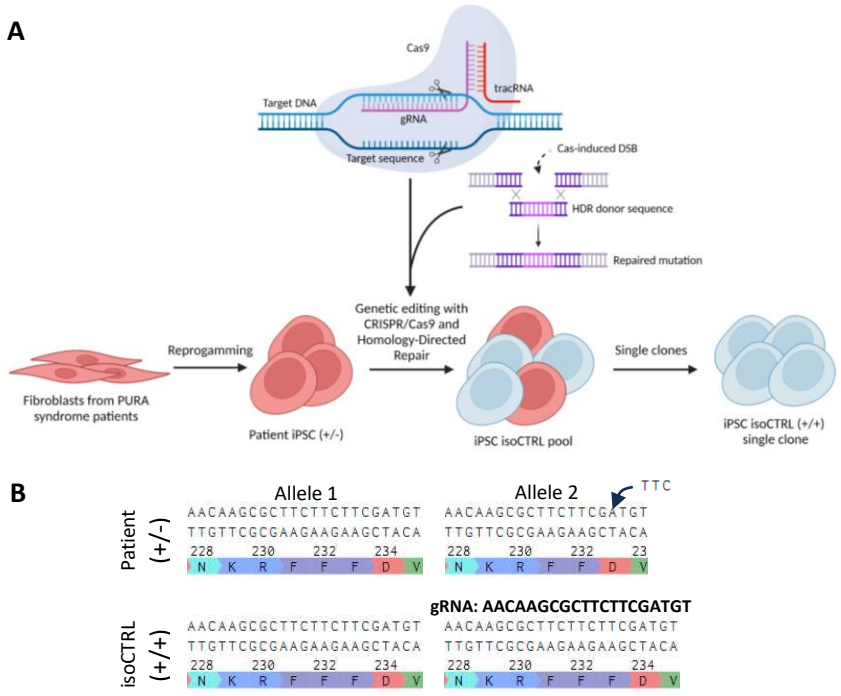

Figure 4.1: isoCTRL generation. (A) Schematic overview of experimental procedure to generate the isoCTRL starting from patient derived fibroblasts. **(B)** Representative alleles of isoCTRL with corrected mutation and of patient with heterozygous F233del mutation.

4.1.1 isoCTRL VALIDATION

The success of the mutation correction was validated via cell pool sequencing (section 3.6.9, **appendix Figure 6.1**), which presented a mixed sequences since

the mutation correction has not 100% efficiency. Sequencing of independent clones confirmed the success of the mutation correction (data not shown). One positive clone was chosen for further validation, sequencing of the chosen clones in **Figure 4.2-A**.

isoCTRL and patient chosen single clones iPSCs were first checked for morphology changes and no abnormalities were observed (**Figure 4.2-B**). Subsequently, the genomic PURA PCR amplicons of both isoCTRL and Patient, were cloned into a TOPO cloning vector (section 3.6.5) to test the homozygosity of the isoCTRL, assuming that each colony represents one PCR amplicon. The PCR amplicon used here, was shorter than the one used for single cell clones screening, to facilitate the

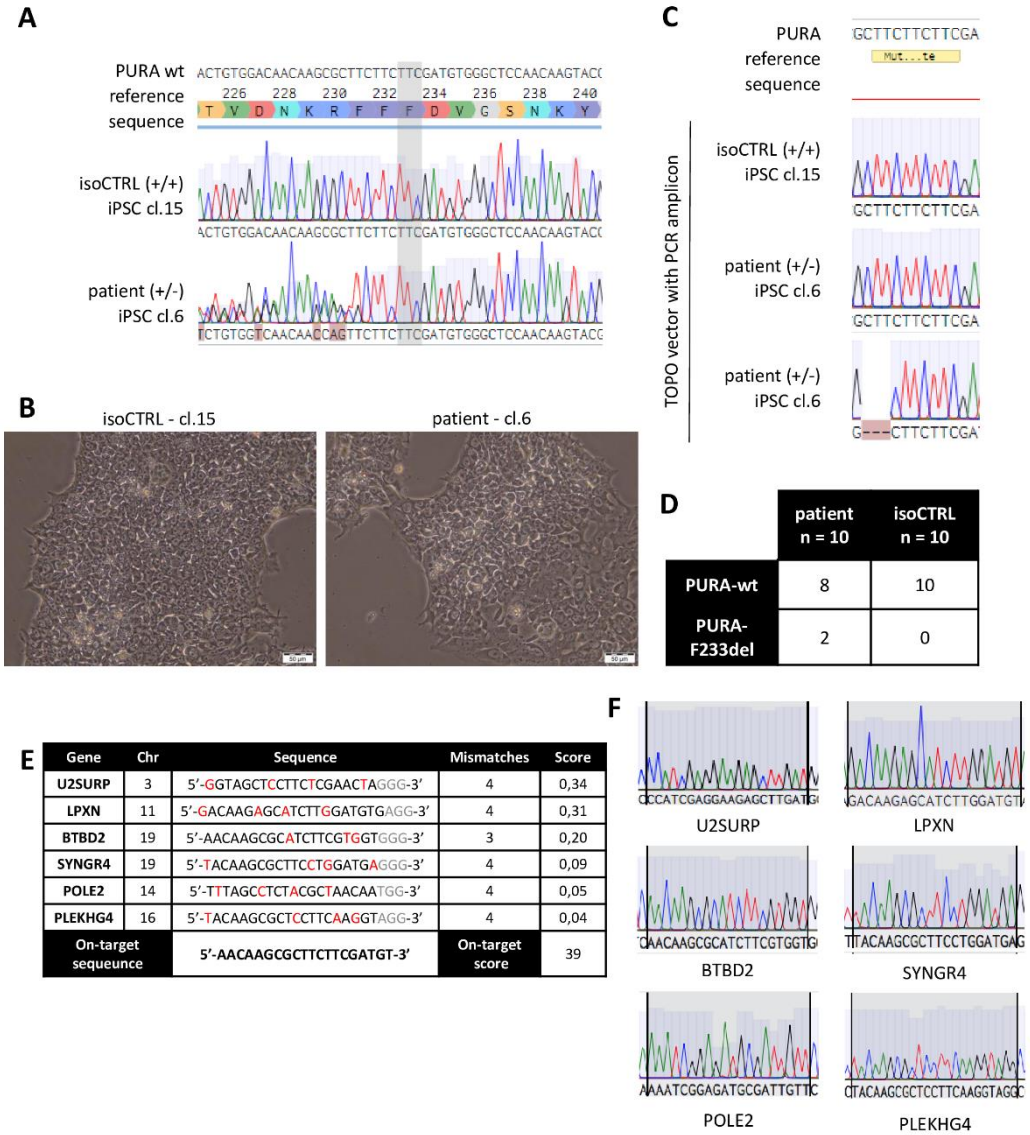

Figure 4.2: Morphology and genetical validation of isoCTRL iPSC. (A) single clones PURA PCR amplicon reverse sequencing. A mutation rescue was observed. **(B)** AS isoCTRL and patient iPSC bright-field images. Scale bras, 50 µm. **(C)** TOPO cloning of PURA PCR amplicon zoomed in the mutation site from both isoCTRL and patient. **(D) S**ummary of identified sequences from TOPO clones (n=10), observing a homozygous wt PURA sequence from isoCTRL and mixed wt and F233del sequences from patient TOPO clones. **(E)** Selected potential off-target based on datasets from Benchling and Crispor websites and based on off-target score. In red the mismatches, in grey the PAM sequence. **(F)** Sequences results of potential off-target showing no altered sequences.

integration in the TOPO vector. After *E. coli* transformation, plasmids from 10 single isolated colonies (section 3.6.7) were isolated and sent for sequencing (section 3.6.9). A representative sequencing result is in **Figure 4.2-C, D**. 10/10 isoCTRL TOPO clones had a wt sequence, while in the patient TOPO clones there were 8/10 of wt and 2/10 of mutated sequence, confirming the heterozygosity of the patient derived iPSC as well as a complete rescue of the mutation in the isoCTRL.

CRISPOR (Concordet J. P., 2018) and BENCHLING (Benchling, 2023) were used to predict the off-target regions. The datasets from the two websites were overlapped. Potential off-targets sequences lying on encoding genes having the highest score were chosen for screening via PCR amplification and sequencing (for BTB2, PLEKH4, POLE2, SYNGR4 and U2SURP), while POLE2 PCR amplicon was inserted into a TOPO vector, as neither one of POLE2 PCR primers was giving suitable results when used for sequencing. No unwanted genetic changes on those genes were observed (**Figure 4.2-E, F**).

4.1.2 isoCTRL AND patient iPSCs ARE PLURIPOTENT

To test the pluripotency of the generated cell lines IF was performed (section 3.7.2) using three pluripotency markers: OCT4, SOX2, and NANOG. Since all markers were detected, the cells were considered pluripotent (**Figure 4.3-A**).

In addition, pluripotency cells should be able to differentiate towards all three germ layers, therefore, a linage assay was performed (section 3.4 (Grosch M, 2020)) differentiating the iPSC towards the three germ layers, namely ectoderm, mesoderm and endoderm. During the differentiation process, no evident morphological differences were noted when comparing isoCTRL and patient (**Figure 4.3-B**). After 5 days of differentiation, a qPCR was performed (section 3.6.10) to validate specific differentiation markers. Both isoCTRL and patient in ectoderm and mesoderm showed downregulation of pluripotency markers (Oct4 and Nanog) and upregulation of lineage markers, except for MESP. In endoderm the pluripotency markers were not consistently downregulated, however, the upregulation of endoderm specific marker was much higher than the pluripotency markers (**Figure 4.3-C**)

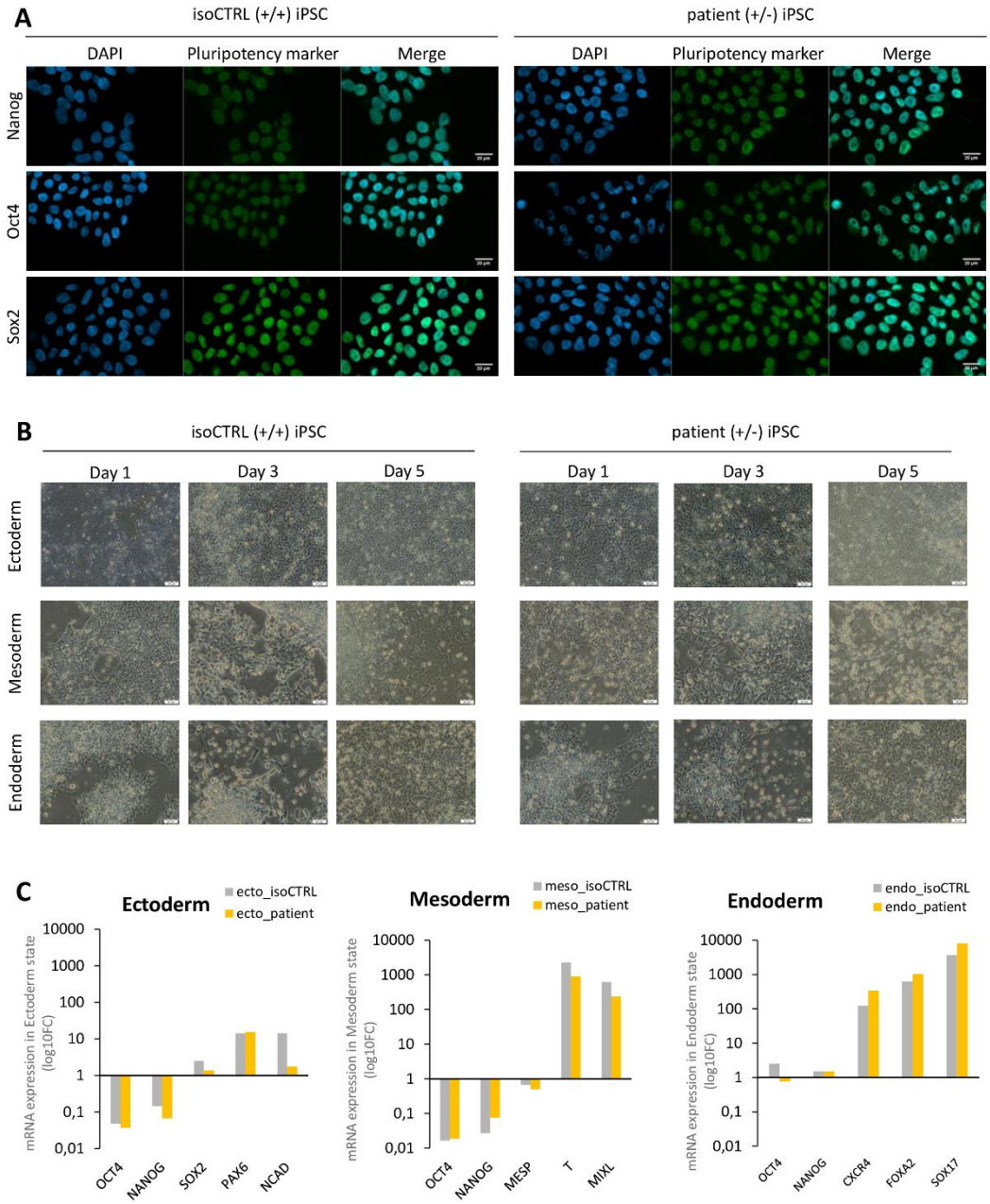

Figure 4.3: Pluripotency ability of isoCTRL and patient iPSC. (A) Immunofluorescence staining of Pluripotency Marker (green) together with DAPI (blue) as nuclear stain in isoCTRL (left) and patient (right) iPSC. Scale bars, 20 µm. **(B)** Bright-field images of three germ layers differentiation (ectoderm, mesoderm, endoderm) from isoCTRL (left) and Patient (right) iPSC on days 1, 3 and 5. Scale bars, 50 µm. **(C)** Expression of RNAs marking differentiation from iPSC to the three germ layers (ectoderm, mesoderm, endoderm) measured by qPCR on day 5. Expression of all RNAs is normalized to RPL32 and TUBA. Expression in germ layers is given relative to expression in iPSC.

4.1.3 qPCR PRIMERS TO VALIDATE isoCTRL AT mRNA LEVEL

To validate the mutation correction at mRNA level, a qPCR was performed. Primer were designed using BENCHLING (Benchling, 2023) such that they specifically bind at the mutation site in either its wild type sequence (PURA_wt, primer CK67) or in its mutant sequence lacking the third TTC codon repeat (PURA_del, primer CK70). Primers binding downstream the mutation site were also designed (PURA, primer CK76/CK77).

The primers were first tested for specificity and efficiency. Primers' specificity was validated by counting the number of peaks within the melting curves. A clear single peak indicates a single qPCR product whereas multiple peaks denote for low primer specificity. Additionally, the specificity of the primers was validated by gel electrophoresis of the qPCR product. A single band indicates a unique qPCR product, while band absence or multiple bands indicate the incapacity of the primer to bind to the target sequence or an unspecific primer binding, respectively. Lastly, a serial dilution of cDNA concentration together with the respective Ct values was used to generate a standard curve. The standard curve was used to calculate the coefficient of determination (R^2) which should be ideally > 0.99 indicating a strong linear relationship between the values of each sample. The standard curve was also used to calculate the amplification efficiency:

$$E = (10^{\frac{-1}{slope}}) - 1$$

The efficiency gives an insight of how far the experiment is from the ideal situation of doubling the DNA concentration in each cycle, acceptable values range between 90% and 110%.

To perform the tests on the newly designed primers, we used the patient cDNA which presents both the wild type and the mutant sequences (we used cells derived from patient #3 because the experiment was performed before generating the isoCTRL for patient #1). All identified primers showed single peaks from the melting curves and a single band in the gel electrophoresis of the qPCR product (**Figure 4.4-A, B**). Nevertheless, the standard curve showed a R^2 higher than 0.99 only from PURA primers, whereas PURA_del and PURA_wt had R^2 of 0.9869 and 0.9511, respectively. Moreover, the efficiency of all primers was higher than 110%. (**Figure 4.4-C, D**).

Although the efficiency calculated was higher than expected and R^2 was not consistently > 0.99, mutation correction validation was performed for patient #3, comparing the isoCTRL and the WT relative to the patient mRNA level. A strongly significant lower level of PURA_del was observed in both isoCTRL and wt iPSC and a significant higher level of PURA_wt was detected in isoCTRL compared to patient. Differently from expected, a slightly significant higher level of PURA was observed in isoCTRL compared to patient. Lastly, non-significant difference was observed when comparing PURA_wt and PURA between patient and WT iPSC (**Figure 4.4-E**).

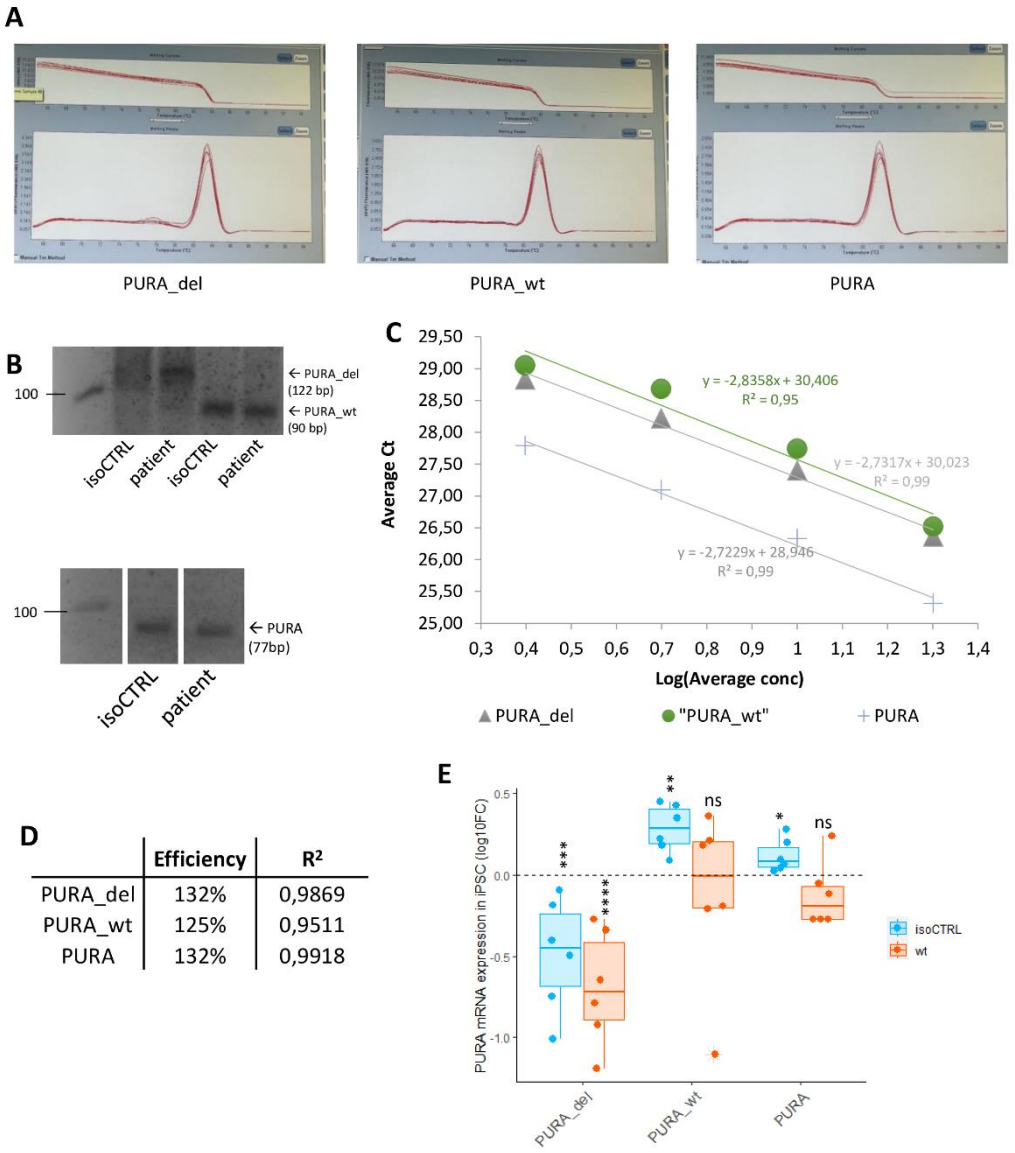

Figure 4.4: isoCTRL validation at mRNA level. (A-B) Specificity test. Melting curves of PURA_del (left), PURA_wt (middle) and PURA primers (right) (A). Gel electrophoresis of qPCR product in isoCTRL and Patient (MT) of PURA_del, PURA_wt and PURA (B). **(C-D)** Standard curve of PURA_del, PURA_wt and PURA in Patient MT iPSC. Standard Curve (four dilutions and relative Ct values) (A). R^2 and Efficiency calculated from Standard Curve (D). **(E)** Expression of PURA mRNAs when carrying the mutation (PURA_del), when wt (PURA_wt) or when primers bind outside the mutant area (PURA) in isoCTRL, WT and Patient iPSC. Expression of all RNAs is normalized to RPL32 and TUBA. Expression in isoCTRL and WT is relative to expression in patient. Dots show three biological replicates each repeated twice. *, P value < 0.05; **, P value < 0.01; ***, P value < 0.001; ****, P value < 0.0001.

4.2 F233DEL EFFECT ON PURA PROTEIN IN iPSC

To study the effect of the F233del mutation on PURA protein levels, iPSCs cells were collected for WB analysis and IF (section 3.7.1.5 and 3.7.2), showing a reduced, although not significant, protein level in patient cell line compared to isoCTRL (**Figure 4.5-A, B**). Similarly, also IF showed lower but not significant PURA signal per cell in patient when compared to isoCTRL iPSCs (**Figure 4.5-C, D**).

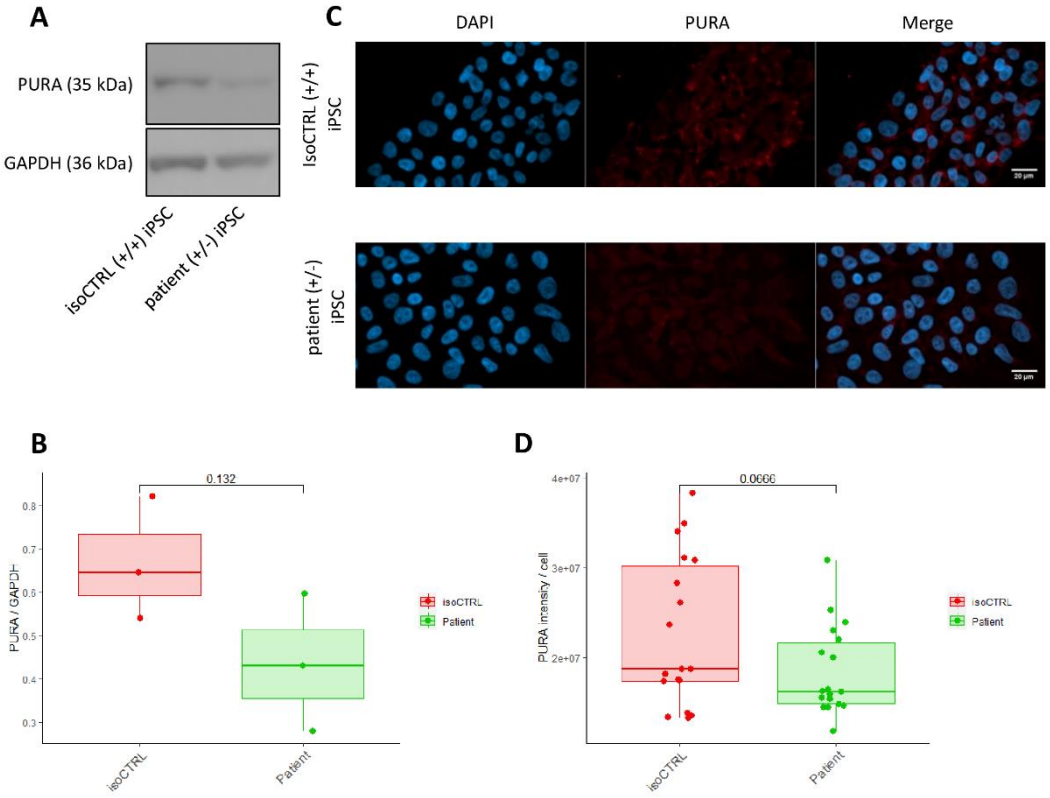

Figure 4.5: PURA protein levels in patient. (A-B) PURA level is not significantly reduced in patient iPSC. Representative Western Blots (A) and quantification of replicates (B). PURA was detected with anti-PURA^{12D11}. GAPDH was used as control (n=3, unpaired two-sided Student's *t*-test). **(C)** Immunofluorescence staining of PURA (red) together with DAPI (blue) as nuclear stain in isoCTRL (top) and patient (bottom) iPSC. Scale bars, 20 µm. **(D)** Quantification (ImageJ) of PURA intensity of approximately 40 cells per replicate and condition (three biological replicates with six technical replicates each), each dot is a technical repeat, unpaired two-sided Student's *t*-test.

4.3 NEURAL PROGENITOR CELL DIFFERENTIATION IS NOT IMPAIRED BY F233DEL

To study the impact of the heterozygous F233del mutation during neural differentiation, cells were differentiated in 2D towards neural progenitor cells (NPC, section 3.5, **Figure 4.6-A** (Reinhardt P, 2013)). After 7 days of differentiation in 3D forming the so-called embryonic bodies (EBs), cells were plated on GT-coated plates for 7 days. After that (day 14 of differentiation), cells were analyzed for neural rosette structures and stained for Pax6. One technical repeat was maintained for 7 days more. Presumptive positive well with identified neural rosettes were expanded. On day 21 (passage 1), cells were collected to analyze specific NPC expression markers: *paired box 6* (*PAX6), microtubule associated protein 2* (*MAP2*), and *forkhead box G1* (*FOXG1*).

During the differentiation, no morphological differences were observed between isoCTRL and patients, indeed they both showed gradual EBs' size enlargement until day 7 and they both had neural rosettes structures. In addition, they both had PAX6 positive neural rosettes (**Figure 4.6-B, C)**.

A qPCR was performed to test the expression of NPC markers (PAX6, MAP2 and FOXG1). Both isoCTRL and patient showed significant upregulation of the three NPC makers, except for MAP2, and significant downregulation of pluripotency markers when compared to their respective iPSCs (**Figure 4.6-D**). In addition, the neural markers were compared between isoCTRL and Patient in their NPC state, no significant difference was revealed (**Figure 4.6-E**).

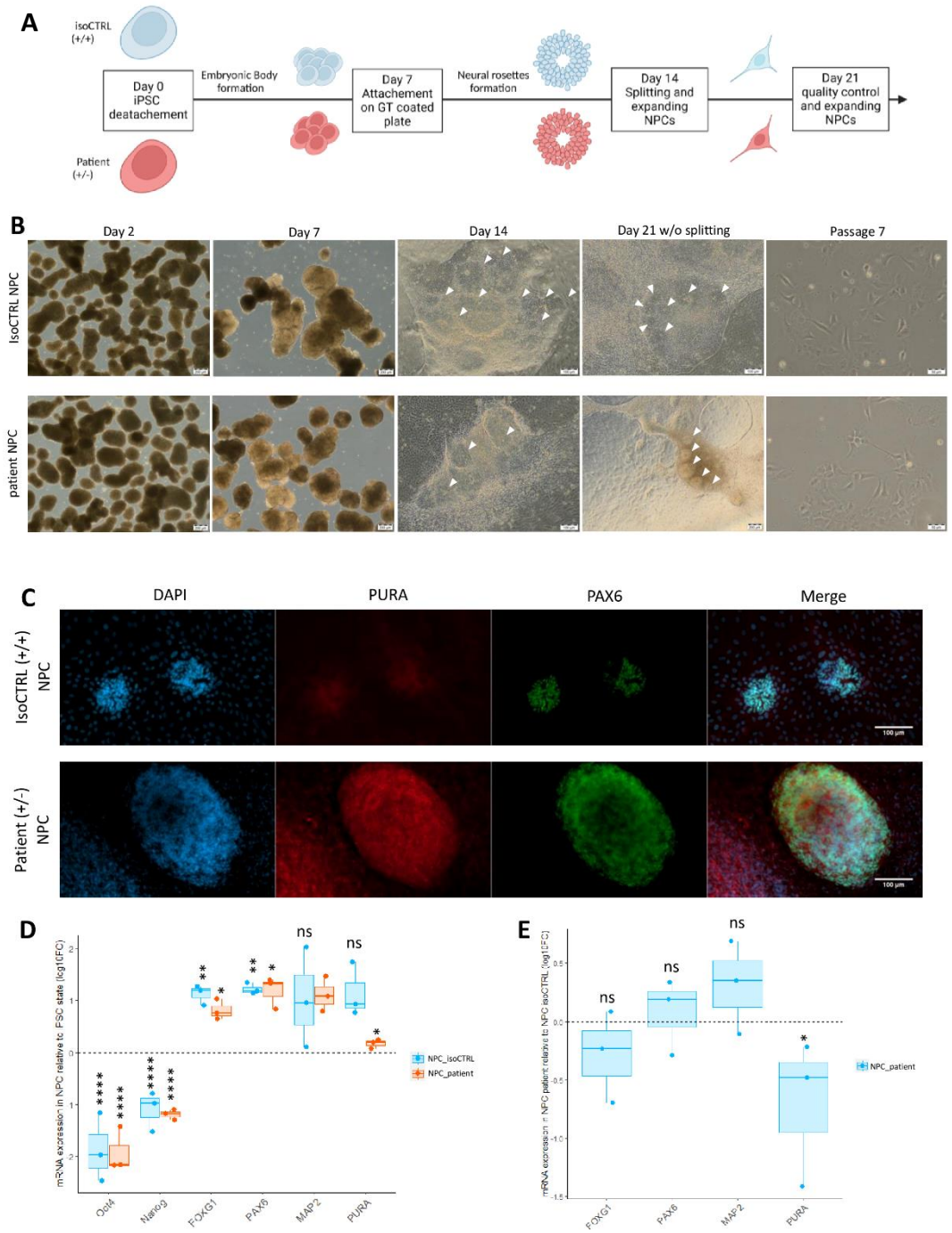

Figure 4.6: **isoCTRL and patient NPC differentiation from iPSC. (A)** Schematic overview of iPSCs differentiation towards NPCs with embryonic bodies and neural rosettes formation. **(B)** Bright-field images of iPSCs to NPC differentiation of isoCTRL (top) and patient (bottom) at day 2 and day 7 (3D embryonic bodies), day 14 and day 21 without splitting (2D, white arrows indicate neural rosettes) and mature NPCs at passage 6. Scale bars, 200 µm, 100 µm and 50 µm **(C)** Immunofluorescence staining of PURA (anti-PURA^{12D11}, red) together with PAX6 (green) and DAPI (blue) to stain nuclei in isoCTRL (top) and patient (bottom) NPCs on day 21 without splitting, showing PAX6 positive cells at neural rosette structures. Scale bars, 100 µm. **(D)** Expression of RNAs marking transition from iPSCs to NPCs at day 21 (Passage 1) of isoCTRL and patient. Expression in NPCs is given relative to iPSCs. Dots show three biological replicates. PURA expression was measured with primers recognizing the wt sequence at the mutation site. *, P value < 0.05; **, P value < 0.01; ***, P value < 0.001; ****, P value < 0.0001, unpaired Student's *t*-test. **(E)** Comparison of neural marker and PURA-wt mRNA expression between isoCTRL and patient NPC. Expression in patient is given relative to isoCTRL. PURA expression was measured with primers recognizing the wt sequence at the mutation site. *, P value < 0.05; **, P value < 0.01; ***, P value < 0.001; ****, P value < 0.0001, unpaired Student's *t*-test.

4.3.1 PURA wt mRNA and PROTEIN LEVEL IN NPCs

To test if PURA mRNA level changes in NPCs, a qPCR (section 3.6.10) comparing PURA wt mRNA level in isoCTRL and Patient NPCs relative to their iPSCs state was performed. Primer specifically binding to the mutation site in its wt form was used, meaning that it recognizes only half of the total PURA mRNA level in patient (assuming that patient cells equally expressed both PURA alleles) and the complete PURA mRNA level in the isoCTRL. PURA wt mRNA level was higher in both isoCTRL and Patient NPCs when compared to their respective iPSC state, although it was not significant in isoCTRL (**Figure 4.6-D**). We also compared PURA wt mRNA level between isoCTRL and Patient NPCs, detecting a significant lower expression in patient relative to isoCTRL. Precisely, around one-third of wt PURA mRNA was quantify in patient relative to isoCTRL ($log_{10}FC = -0.5$).

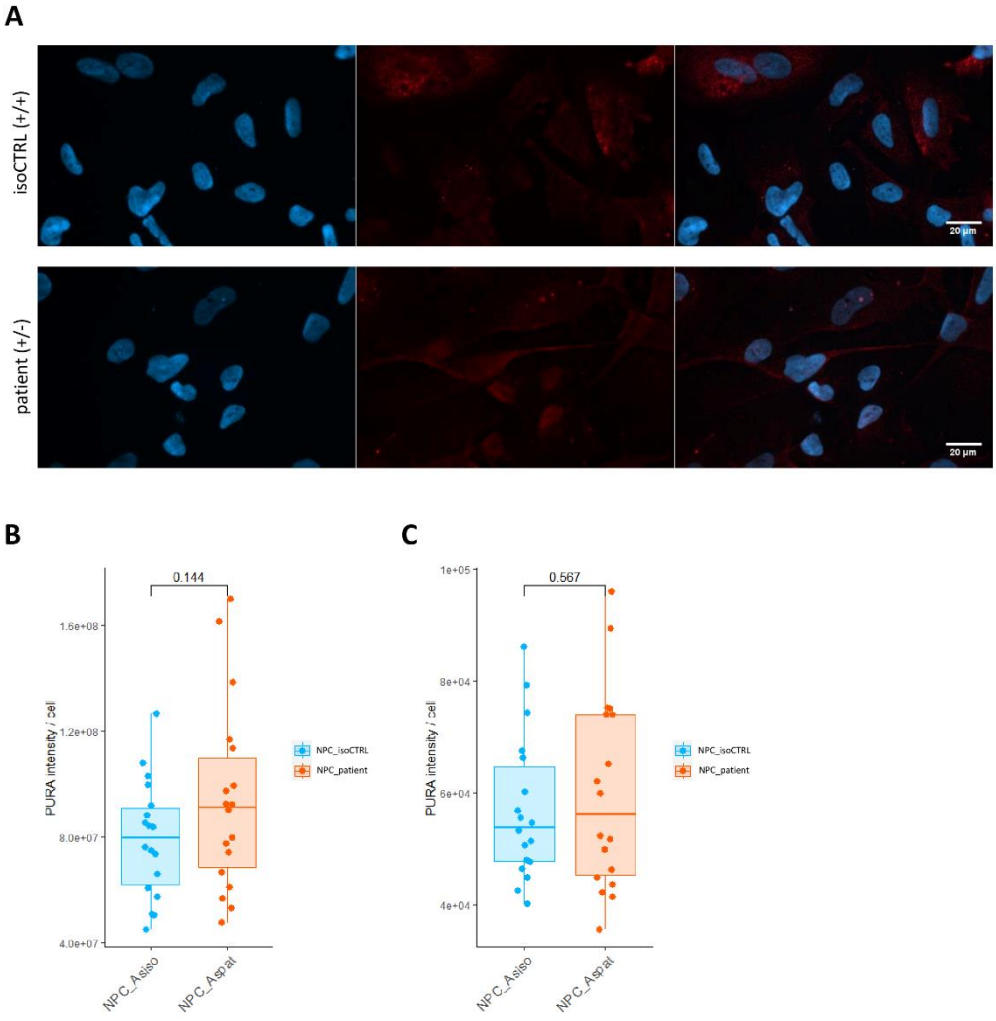

Figure 4.7: PURA protein level after NPC differentiation. (A) Immunofluorescence of PURA (anti-PURA^{12D11}, red) with DAPI (blue) in isoCTRL and patient NPCs (passage 6). Scale bars, 20 µm. **(B)** Quantification (ImageJ) of PURA intensity when using AlexaFluor 647 (left) and AlexaFluor 488 (right) of approximately 20 cells per replicate and condition (three biological replicates with six technical replicates each), dots indicate technical repeats, unpaired two-sided Student's *t*-test.

To test if the protein level changes during NPC differentiation, WB should be performed, however, due to the impossibility to get all the biological repeat to a high enough passage, IF was performed (section 3.7.2). A high PURA signal variability was observed from both isoCTRL and patient NPCs. Differently from what was observed in iPSC, the protein level is similar between isoCTRL and Patient NPCs. This result was consistent when using two different secondary antibodies. (**Figure 4.7-A, B, C**).

4.3.2 PURA and FMRP COLOCALIZATION

It is known that PURA co-localizes with neuronal RNA-binding proteins PURB, Staufen, hnRNPU, and fragile X mental retardation protein (FMRP) in neuronal transport granules (Mitsumori K., 2017; Ohashi S, 2002; Johnson E. M., 2006). A Proximity-dependent biotin identification assay (BioID) experiment in HeLa cells (unpublished data, Proske M.) confirmed FMRP (or FMR1) and its paralogues FXR1 and FXR2, as PURAwt interacting partner. These proteins were not identified in F233del-PURA interactome, which had YBX1 as one of the best hits. Lastly, an enrichment analysis comparing PURAwt and F233del-PURA interacting

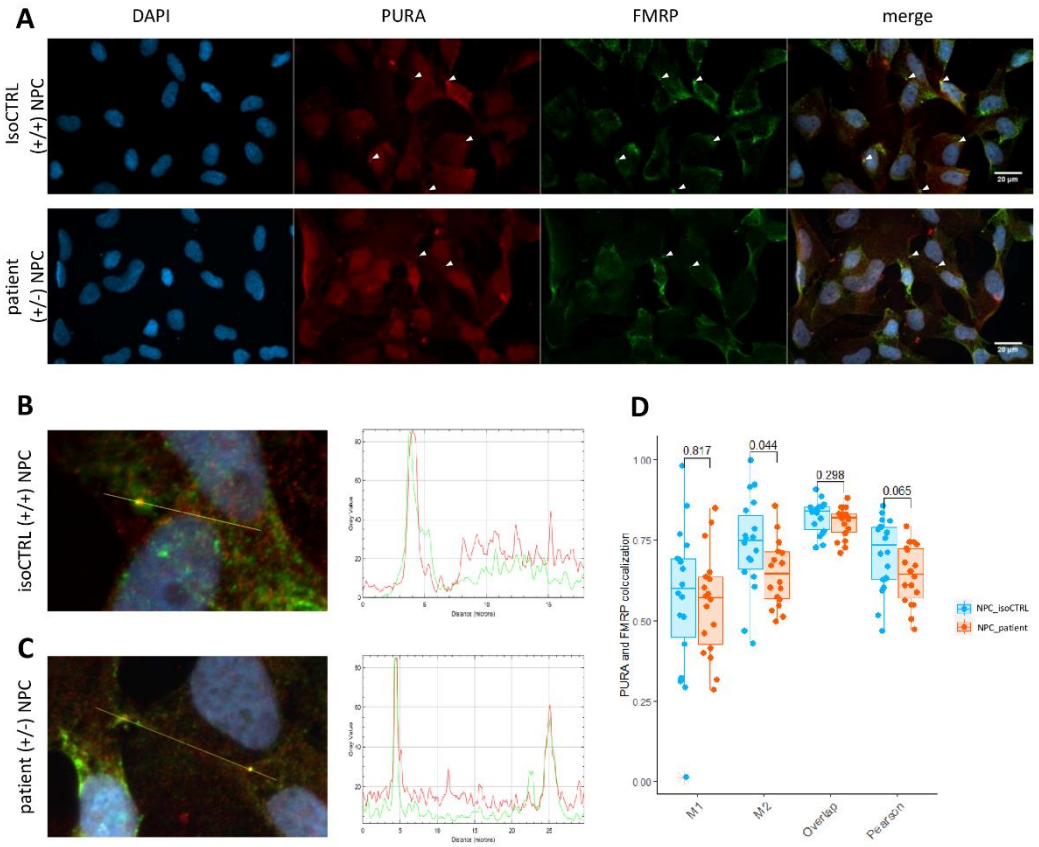

Figure 4.8: PURA and FMRP colocalize in NPCs. (A) Immunofluorescence staining of PURA (anti-PURA^{12D11}, red) together with FMRP (green) and DAPI (blue) in isoCTRL (top) and patient (bottom) NPCs. Arrowheads indicate PURA and FMRP colocalization spots. Scale bars, 20µm. **(B-C)** Histogram plots along yellow line drawn through FMRP granules (green) with enriched PURA co-staining (PURA^{12D11}, red) in isoCTRL (B) and patient (C). **(D)** Quantification (ImageJ, JACoP plugin) of PURA-FMRP co-colocalization in isoCTRL and patient NPCs. Three biological replicates, six technical replicates each. Four parameters were measured: Mander's Coefficients (M1 and M2), Overlap coefficient (overlap) and Person's Coefficient (Pearson). Unpaired two-sided Student's *t*-test.

proteins, revealed FMR1, FXR1 and FXR2 decreased interaction with F233del-PURA.

To study the colocalization, IF staining was performed on isoCTRL and patient NPC (section 3.7.2). Representative images can be seen in **Figure 4.8-A**. A zoomed in image was used to create and overlap the plot profile of each channel. The plot profiles showed peaks of intensity throughout a line drown on the image, confirming overlapped signals (**Figure 4.8-B, C**). To quantify the colocalization, JACoP Plugin of ImageJ was used. It computes the Pearson's Coefficient (R^2), which describes the correlation between intensity distribution, ignoring the signal intensity, ranging between -1 and 1; the Overlap Coefficient according to Manders (overlap), which indicates the overlap signal, ranging between 0 and 1; and the Manders' Coefficients using automatic threshold value (M1 and M2), which indicates the contribution of each one from two selected channels to the pixels of interest (Zinchuk V., 2007). An Overlap Coefficient of around 0.8 and R^2 of around 0.7 in both isoCTRL and patient were calculated. A stronger contribution from the FMRP channel can be deduced as the M2 is generally higher than M1 in both isoCTRL and patient. Despite the validated colocalization, non-significant difference was observed if isoCTRL and patient are compared (**Figure 4.8-D**).

4.4 GENERATION OF PURA OVEREXPRESSING HNSC CELL LINE FOR BIOID ASSAY

Previous studies on HeLa cells revealed several potential RNAs and proteins interacting with PURA (section 1.2.3). However, a more physiological cell model to perform these studies should be used to eventually detect neural progenitor markers, hence Human Neural Stem Cell (HNSC) were used. HNSCs are monoclonal, immortalized and nestin-positive cell line with neural morphology and neurite outgrowth. They also have differentiation capability towards astrocytes, oligodendrocytes and neurons allowing cell-type specific analysis (Villa A., 2000). An HNSC line was generated to perform BioID assay, a tool to identify protein-protein interactions in living cells (Sears R. M., 2019). This method utilizes a promiscuous biotin ligase, called BirA, fused to a protein-of-interest that when expressed in cells can be induced to biotinylate interacting and proximate proteins over a period of hours, thus generating a history of protein associations. To generate the HNSC line for BioID, PiggyBac vector system (PB, section 3.3) was used. The PB transposase (encoded by the helper vector, MP11), recognizes transposon-specific inverted terminal repeat sequences, which are located at both ends of the gene of interest in the vector and “cut and paste” it into chromosomal TTAA sites. The included Tet-On/Off System allows doxycycline (DOX) induced expression of the protein of interest. In addition, the vector confers Hygromycin B resistance, which was used to select transfected cells.

The concentration of Hygromycin B to use for selection in HNSCs was not known, hence, an overtime experiment with different concentration of Hygromycin B, namely 100 µg/mL, 300 µg/mL, 500 µg/mL, 700 µg/mL, and 900 µg/mL, was performed (**appendix Figure 6.2**). Cells growth was observed under Evos FL fluorescent microscope and compared to the non-treated cells. After 5 days of treatment, cells exposed to all Hygromycin B concentration, except 100 µg/mL, were dead. After 7 days of treatment, the non-treated control cells were dead due to an overcrowded environment. After 10 days, cells treated with 100 µg/mL were still

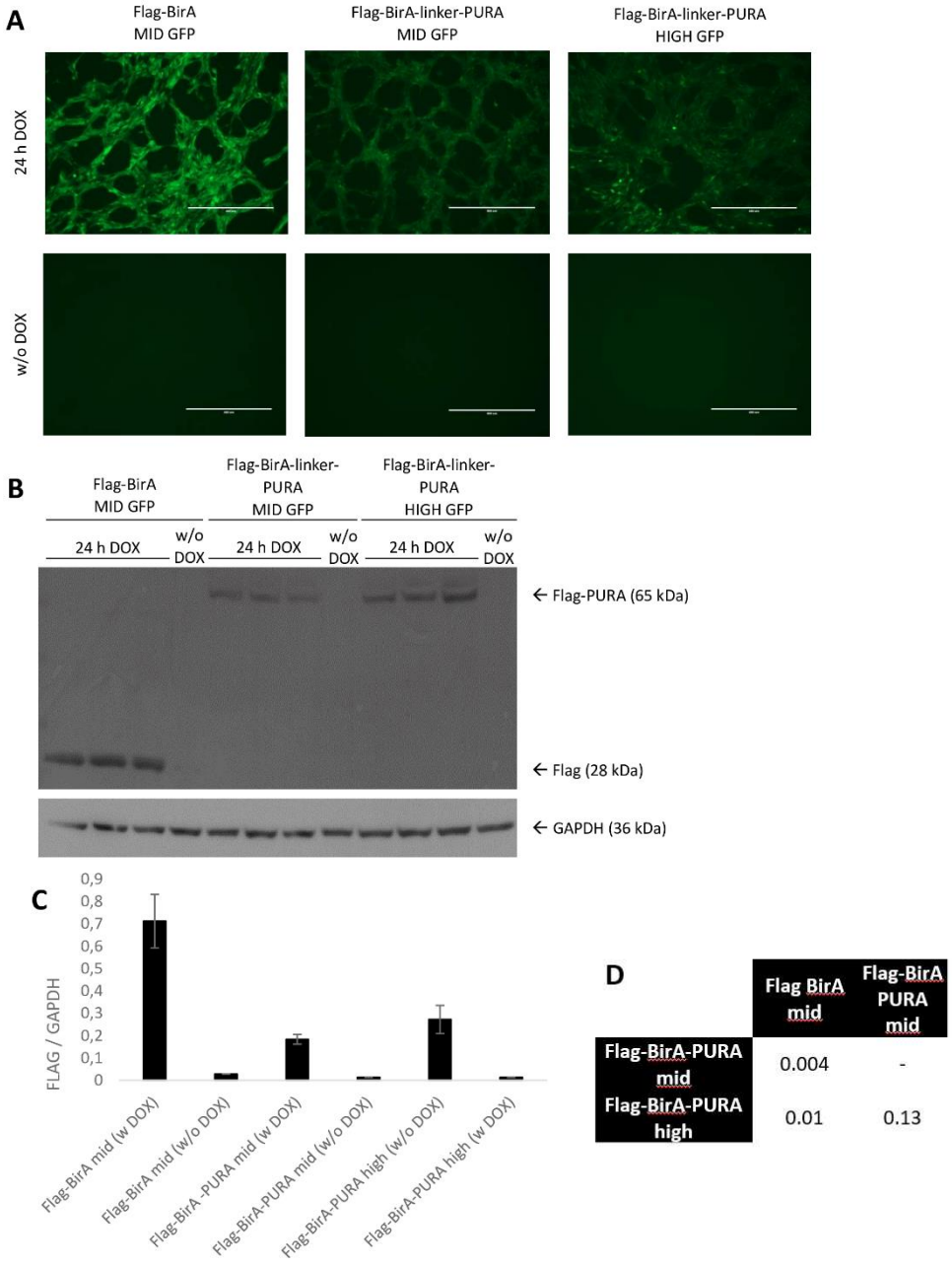

Figure 4.9: PURA overexpressing cell line generation for BioID. (A) Evos FL Fluorescent microscope images of sorted Flag-BirA (mid GPF signal) and Flag-PURA-BirA (mid and high GPF signal) cells after 24h of DOX induction (top) or without DOX induction (bottom). Scale bars, 400 µm. **(B)** Western Blot of sorted Flag-BirA and Flag-PURA-BirA after 24h of DOX induction. For detection, commercial Flag and GAPDH antibodies was used. GAPDH was used as housekeeping marker to quantify the amount of protein. **(C)** Quantification of the Western Blot (n=3). **(D)** Two-sided pairwise Student's *t*-test.

alive, and after 12 days, one single cells treated with 100 µg/mL was alive. Given these results, we decided to perform selection with 300 µg/ml to maximize the selection efficiency minimizing the amount of Hygromycin B to use to avoid side effects. Two different cell lines were generated with two different vectors, one carrying PURA (MP4) and one without (MP6, **appendix Figure 6.3**), the latter will be needed as a "background" control when analyzing the BioID data.

A first lipotransfection approach was performed and cells were selected for 10 days with 300 µg/ml Hygromycin B. To achieve a similar level of expression a fluorescence-activated cell sorting (FACS) was performed after 24 hours of DOX (1:1000) induction (section 3.3.1). To exclude debris, a first gating was set based on Forward Scattering Area (FSC-A) and Side Scattering (SSC-A) which are directly proportional to cell size and cell granularity, respectively. The doublet discrimination was done by setting the gate on Forward scattering width (FSC-W) and FSC-A. Finally, a gating based on GFP signal was set selecting cells with a mid GFP intensity. Interestingly, a GFP signal was detectable already in the non-induced cells meaning that a high background was present (**appendix Figure 6.4**). After expansion of sorted cells, a time course analysis of GFP signal at Evos FL fluorescent microscope was performed revealing a gradual increase of signal intensity (**appendix Figure 6.5**). The signal reached the maximum after 24h to be stable until 48h, but a difference between the two cell lines was visible. The signal was further analyzed via WB (section 3.7.1.5) after 24 hours of DOX induction showing a persistent difference of signal intensity (beside the FACS) but also a second unexpected band at the Flag-BirA size from the Flag-BirA-PURA sample (appendix fig), suggesting a potential contamination between cells, therefore, a new approach was performed. After the second approach of lipotransfection and hygromycin B selection, cells were sorted again collecting a "low-intensity", a "mid-intensity" and "high-intensity" GFP signal population (data not shown) for both cell lines, however the low-GFP-intensity Flag-BirA didn't survive. Protein expression after 24h of DOX induction was checked again at Evos FL fluorescent microscope (**Figure 4.9-A**) and via WB. The latter revealed a non-significant difference between the "high-intensity" and the "mid-intensity" Flag-BirA-PURA cell lines, while they both had a significantly lower GFP signal than the Flag-BirA (**Figure 4.9-B, C, D**).

4.5 PURA KO HNSCs CELL LINE GENERATION

To study PURA's molecular role, a PURA Knock out (KO) HNSC cell line was generated using the CRISPR/Cas9 technology (section 3.2). Of note, another PURA KO HNSC cell line was previously generated, but the morphology was strongly altered (flatten and shorter cells as well as bigger nuclei than WT, Isabella Bienek Master thesis). For this reason, the experiment was reproduced to assess whether the morphology alteration was a PURA KO phenotype, or a technical problem occurred during the procedure. To this aim, two different previously validated gRNAs (Lena Molitor, PhD thesis) were used: the first gRNA cuts before the start codon and the second one cuts approximately 600 ahead which results in the complete loss of the PURA protein (**Figure 4.10-A**).

The editing efficiency was validated using SYNTHEGO (Synthego, 2023) online software, which estimates the frequency of occurred insertions and deletions after a CRISPR/Cas9 induced editing of cells. To perform the analysis, the cleaned PCR product of the cell pool was sent for sequencing with the primer LM22 (section

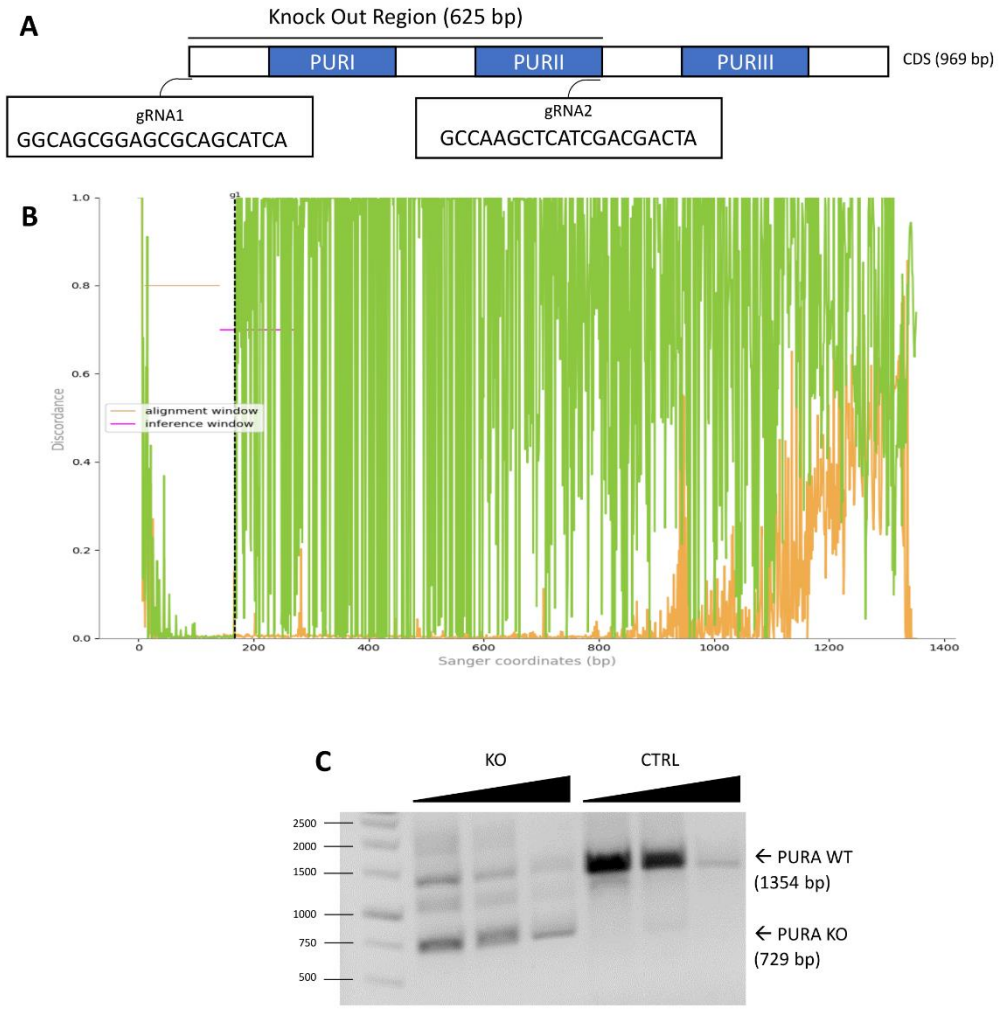

Figure 4.10: PURA KO HNSC cell line generation. (A) Schematic overview of PURA gene with the three PUR repeats (blue), the used gRNAs and the knocked out region. **(B)** Synthego discordance plot between the control sample (orange) and the KO sample (green). The vertical dotted line indicates the inferred cut site. **(C)** PURA PCR (with temperature gradient) amplicon size analysis of KO and CTRL.

3.6.2, 3.6.4 and 3.6.9). Then, the resulted .ab1 files were uploaded together with the gRNA_2 to the online software. The gRNA_1 was not used for this analysis because it binds too far from the sequencing starting point, leading to sequencing mistakes.

SYNTHEGO calculated an indel percentage of 43%, meaning that almost half of the sample sequences were different from the control sequence but not necessarily all of them result in the correct KO sequence. It also calculated a KO score of 38 assessing the contributing indels which likely result in a functional knockout. However, the R^2 parameter (an indicator of how well the proposed indel distribution model fits to the sanger sequence data) was of 0.43. The discordance plot (**Figure 4.10-B**) details the level of alignment per base between the control and the edited sample before and after the cut site (dotted line). Typically, the control and the sample sequences before the cutting site are aligned, however in this case they are both closed to zero. At the cutting site, a high jump of the discordance between sample and control was calculated. The discordance remained high in the sample after the cut site.

Lastly, a PCR amplicon size analysis with gel electrophoresis of control and KO pool was performed (**Figure 4.10-C**). A single band in the control at the right amplicon size was detected while three different bands in the KO pool were visible. One band from the KO pool was at the same height as the WT sequence, one was at 1000 bp and one at around 700 bp.

To generate single cell clones, both the KO and the CTRL pool were diluted to have one cell per well of a 96-well plate. After expansion, single cell clones were harvested for PCR amplicon size analysis. Within the single cell clones, there were some with only a WT band (1300 bp), some with only a KO band (700 bp) and some with both bands (1300 and 700 bp) which can either be the result of a non-single cell clones or a heterozygous KO. A predicted homozygous KO clone (#7) and a CTRL clone (#2) were chosen to further proceed with validation via sequencing, Off-target, WB, and IF.

A single band of the expected size for both KO and CTRL was observed when a PCR amplicon size analysis was performed (**Figure 4.11-A**). Sequencing of the cleaned PCR product showed the KO at the expected region and a zoom in the gRNAs binding sites confirmed the cut at the expected regions (**Figure 4.11-B**). Cellular morphology of both CTRL and KO was observed with a bright-field microscope. Both cell lines showed typical HNSC morphology, meaning unipolar shape and cross-interaction (**Figure 4.11-C**). CRISPOR (Concordet J. P., 2018) and Benchling (Benchling, 2023) were used to predict the off-targets. Four off-targets per gRNA with highest score from the overlapped datasets and laying on coding genes were chosen, no unwanted genetic changes were visualized from sequencing screening (**Figure 4.11-D, E**). Screening of all off-target, except DNAH1 (whose PCR amplicon was sequenced with the reverse PCR primer) was performed by inserting the PCR amplicon in TOPO vector and sequencing the isolated plasmid as none of their PCR primer, when used for sequencing, gave an utilizable result.

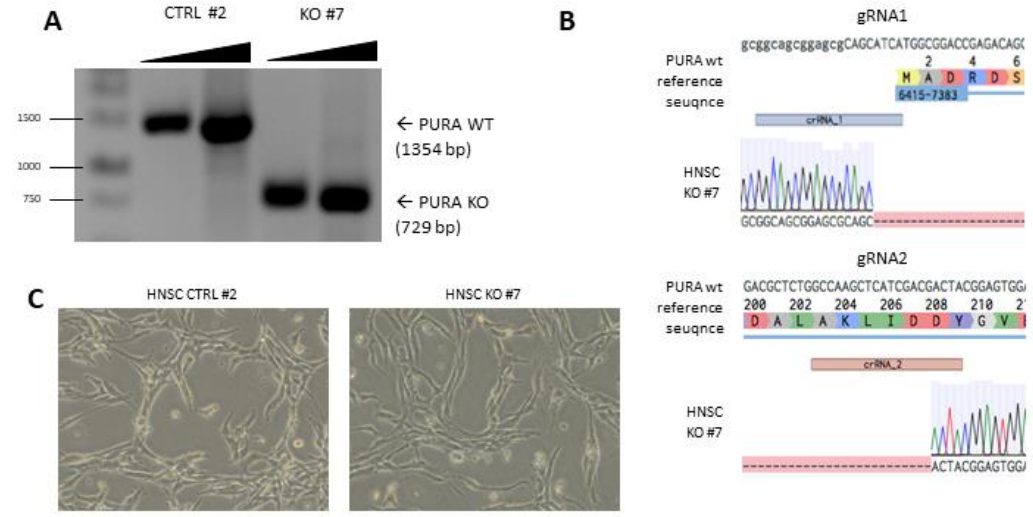

D

Gene	Chr	Sequence	Mismatches	Score
FAM43A	3	5'-GGCGTGGCAGCGCAGCATCACGG-3'	3	0,83
STRIP1	1	5'-GGCTGAGAAGCGCAGCATCCTGG-3'	4	0,49
LAMB3	1	5'-GTCCGCTGAGCGCAGCATGATGG-3'	4	0,43
DNAH1	3	5'-GGAGGTGGAGCGCAGCATGAAGG-3'	4	0,36
On-target sequnce		5'-GGCAGCGGAGCGCAGCATCATGG-3'	Score	15

Gene	Chr	Sequence	Mismatches	Score
PURB	7	5'-GCGAAGCTCATAGACGACTACGG-3'	2	3,91
C8A	1	5'-GCCAAGTTCATCAATGACTATGG-3'	3	0,20
SON	21	5'-GCCAAGCACATCAACAACAATGG-3'	4	0,04
MINDY3	10	5'-GCCAAGCTCTTCGACAGCCAAGG-3'	4	0,03
On-target seqeunce		5'-GCCAAGCTCATCGACGACTACGG-3'	Score	52

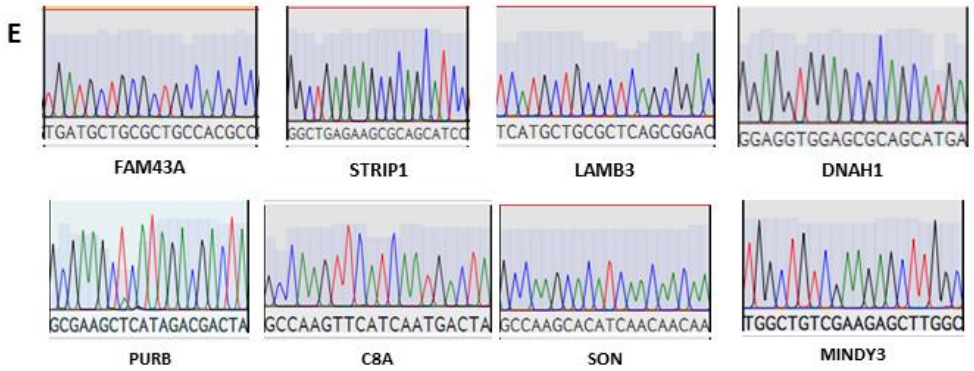

Figure 4.11: HNSC PURA KO genomic validation. (A) Temperature gradient PCR amplicon size analysis of generated single clones, KO #7 and CTRL #2. **(B)** PURA KO HNSC single clones sequencing results at gRNAs binding sites. **(C)** Bright-field microscopy images of HNSC CTRL #2 (left) and KO #7 (right). **(D)** Selected potential off-target based on datasets from Benchling and Crispor websites and based on off-target score for gRNA_1 (top) and gRNA_2 (bottom). In red the mismatches, in grey the PAM sequence. **(E)** Off-target sequencing results.

To complete the validation of the cell line, PURA protein level in HNSCs CTRL and KO was measured via WB (section 3.7.13.7.1) and IF (section 3.7.2).

Both methods displayed a significant reduction of PURA signal in HNSC KO compared to the control (**Figure 4.12-A to D**).

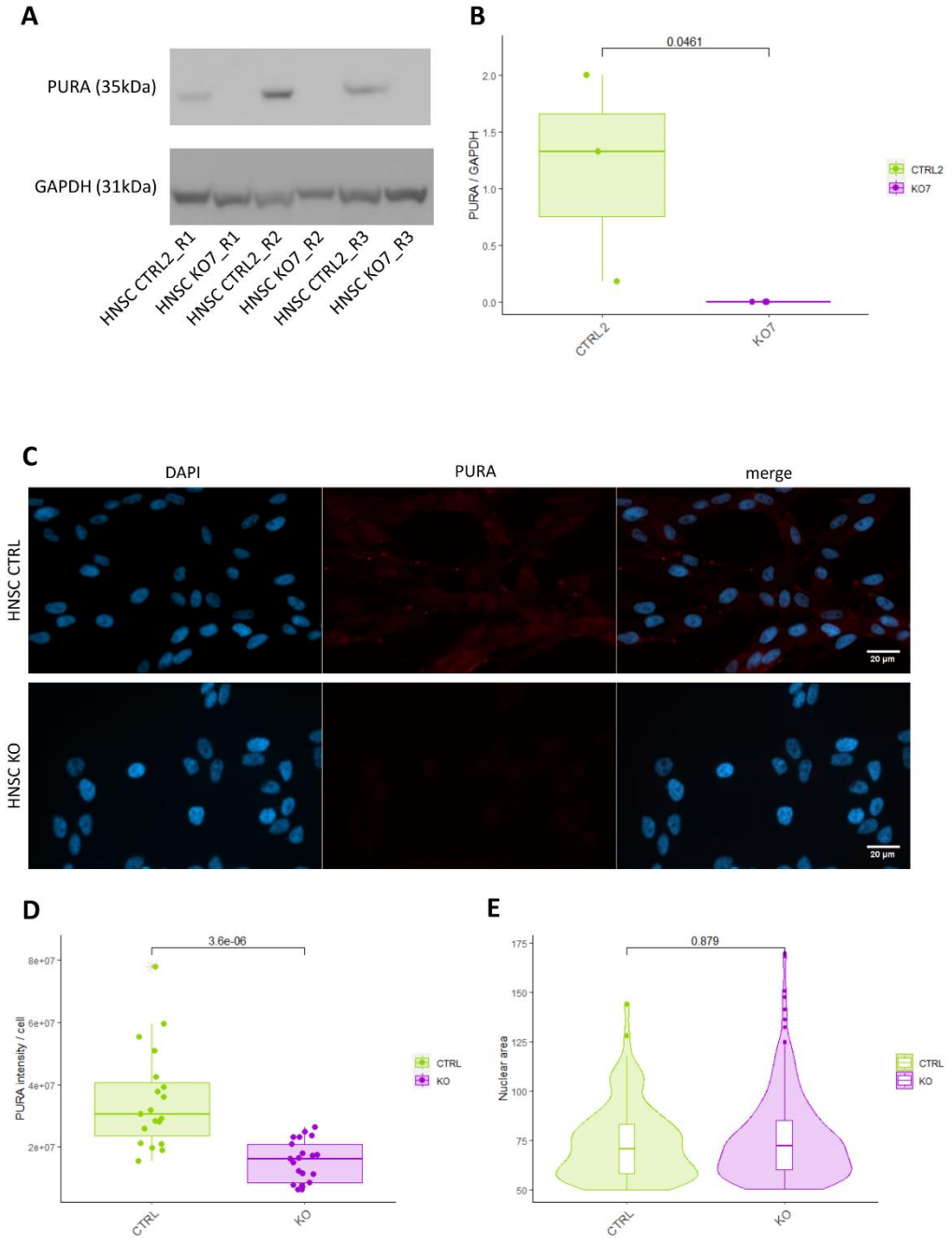

Figure 4.12: PURA protein in HNSC KO. (A) Western Blot of HNSC PURA KO and CTRL. PURA was detected with anti-PURA^{12D11} and GAPDH was used housekeeping marker to quantify the amount of PURA protein. **(B)** Quantification of Western Blot between CTRL and KO. Dots indicate the three biological replicates. Unpaired one-sided Student *t*-test. **(C)** Immunofluorescence of PURA (anti-PURA^{12D11}, red) and DAPI (blue) in HNSC CTRL (top) and HNSC KO (bottom). Scale bars, 20 µm. **(D)** Quantification (ImageJ) of PURA signal of approximately 20 cells per replicate per condition (three biological replicates with six technical replicates each). Dots indicate technical repeats, unpaired one-sided Student's *t*-test. **(E)** Nuclear area analysis (ImageJ) using DAPI staining in approximately 20 cells per replicate per condition (three biological replicates with six technical replicates each). Unpaired two-sided Student's *t*-test.

Lastly, as the first attempt to generate a PURA KO HSNC cell line resulted in PURA KO cells with bigger nuclei than wt, the nuclear size was measured in the newly produced cell line using the same IF images used to compare PURA level between CTRL and KO HNSCs. No significant difference between HNSC PURA KO and control nuclear size was observed (**Figure 4.12-E**).

4.5.1 P62 and DDX6 are NOT ALTERED IN HNSC KO

A recent multi-omic study on HeLa cell upon PURA KD, revealed the autophagy receptor Sequestome 1 (SQSTM1, also known as P62) and of the P-body marker, DEAD Box Protein 6 (DDX6) as potential PURA regulated targets (Molitor L. K. M.-P.-P., 2023). The generated PURA KO HNSC cell line was used to validate such findings, hence, a western blot was performed comparing both P62 and DDX6 protein level between HNSC CTRL and KO. Both tested targets displayed slightly reduced protein level in HNSC PURA KO, although not significant, compared to the control (**Figure 4.13-E to G**).

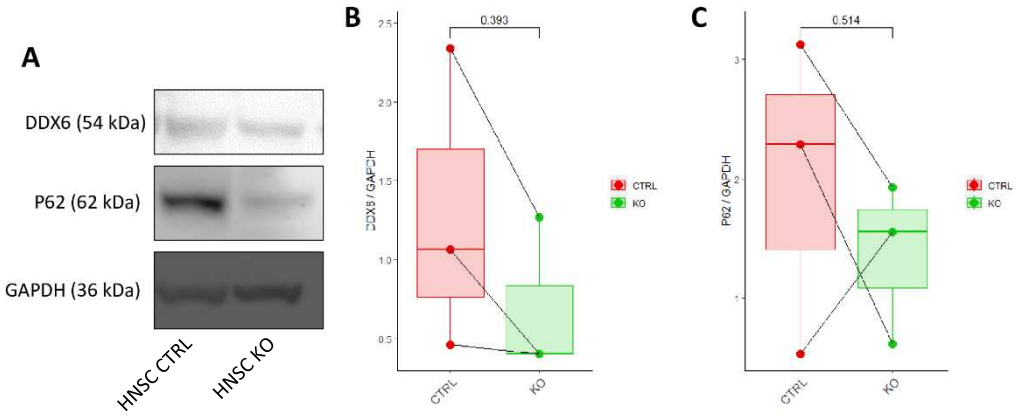

Figure 4.13: PURA KO in HNSC has no effect on P62 and DDX6 protein level. (A-C) Representative Western Blot (A) and quantification of DDX6 (B) and P62 (C) using GAPDH as housekeeper in HNSCs CTRL and KO. Dots represent biological replicates (n=3). Unpaired two-sided Student's t-test.

5 DISCUSSION

5.1 GENERATION OF ISOCTRL IPSC CELL LINE

PURA syndrome patient derived iPSCs are fundamental to investigate PURA mutations and their effect on the neurodevelopmental disorder. For this purpose, a proper isogenic control with corrected mutation but same genetic background as the patient iPSC is needed. Three isoCTRL iPSC cell lines from three independent patients carrying the same heterozygous F233del mutation were successfully generated, two of them were part of this project (section 4.1.1). To confirm the mutation correction, sequencing of PCR amplicon which includes the mutation site, was performed on cell pool, however as the CRISPR/Cas9 technology has not a 100% gene editing efficiency, the isoCTRL sequences results were still showing mixed alignment, therefore, single clones were generated by picking isolated colonies and expanding them. Although the chosen clone validation (see below) confirmed a complete rescue of the mutation in the isoCTRL, to increase the probability of a single clone derived population a second cycle of single cell cloning using the first one can be performed.

Besides PCR amplicon sequencing of single clone, another confirmation of the complete mutation rescue was done via TOPO cloning, which also allows to check heterozygosity on patient iPSC. For this purpose, competent *E.* coli, were transformed with TOPO vector containing the PCR amplicon with the mutation site. Plasmid from single colonies was isolated and sequenced assuming that each colony represents one single PCR amplicon. As all the sequenced plasmid from the isoCTRL contained the wt PURA allele, the complete rescue of F233del mutation in isoCTRL was confirmed. On the other hand, since the patient iPSCs are heterozygous, wt and mutant sequences were expected to be in a 1:1 ratio from patient TOPO cloning, however only 2/10 sequences were mutant, and 8/10 sequences were wt. Of note, when TOPO cloning was performed on patient #2 and #3 (data not shown), the number of mutant sequences was always lower than the number of the wt sequenced in patient TOPO clones. Such difference might be consequence of low number of picked and analyzed colonies, or a lower insertion rate of the mutant sequence in the TOPO clone or else a lower survival of bacteria carrying the mutant TOPO vector.

When performing CRISPR/Cas9 gene editing, a major concern is about the so-called off-target effect, namely the deposition of unexpected, unwanted, or even adverse alterations in the genome (Guo C., 2023). Different *in silico* tools predict off-target sites and calculate the likelihood of an off-target editing (Guo C., 2023). Here, CRISPOR (Concordet J. P., 2018) and BENCHLING (Benchling, 2023) have been used. BENCHLING scoring system integrates and quantify the contribution of mismatched location, density and identity of sequences close to NAG and NGG (Hsu PD, 2013). CRISPOR searches for off-targets up to 4 mismatches and next to a PAM sequence (NGG, NAG, NGA). In this work, six predicted off-targets with highest score and lying on coding genes were tested, and none of them presented any mutation, indicating that the gRNA used is highly specific for targeting PURA with F233del mutation. Alternative algorithms to predict off-targets are available,

which compute the scoring not only based on the gRNA sequence but also on epigenetic features such as chromatin opening and DNA methylation (Guo C., 2023).

To complete the genomic validation of iPSC generated cell lines, a karyotyping is missing. Such test would give insights about big chromosome regions alteration which might have occurred during reprograming, genetic editing, nucleofection and expanding of the iPSCs.

iPSCs are pluripotent cells generated by reprogramming mature cells. iPSCs have self-renewal ability, and differentiation potential. They have a flat-shaped morphology in 2D culture (cobblestone-like) and grow in tightly packed colonies with clear borders. They express surface markers like stage-specific embryonic antigen 4 (SSEA49), tumor related antigen 1-81 (TRA 1-81), TRA 1-60, and cluster of differentiation (CD30). Lastly, they express intracellular markers like Nanog, Oct4, Sox2 and c-myc (Brouwer M., 2016; Zahumenska R., 2020). To test whether the generated isoCTRL and patient cell lines are pluripotent, IF and lineage assay were performed. Pluripotency markers (namely Nanog, Sox2 and Oct4) expression was observed in both isoCTRL and patient via IF staining. Besides that, functional evaluation of the generated iPSC was performed by assessing the *in vitro* differentiation potential towards the three germ layers, namely ectoderm, mesoderm and endoderm (lineage assay (Grosch M, 2020)). Both isoCTRL and patient iPSCs differentiated into each of the three germ layers as upregulation of lineage specific markers, except for MESP2, was observed from qPCR data (section 4.1.2). Together with the lineage specific markers, pluripotency markers (Oct4 and Nanog) were also quantified which were expected to be downregulated after differentiation. In isoCTRL and patient ectoderm and mesoderm, but not endoderm, a downregulation of pluripotency mRNAs was observed. Even though the segmentation gene MESP2, a mesodermal marker, was not upregulated after mesoderm differentiation and both Oct4 and Nanog markers had an expression level in endodermal cells similar to the one in iPSCs, the strong upregulation of the other lineage markers in endoderm and mesoderm suggest that the iPSC are able to differentiate towards all three germ layers but the 5 days protocol of differentiation might be not sufficient to upregulate MESP2 in mesoderm and downregulate pluripotency markers in endoderm.

PURA mRNA quantification via qPCR was performed only in patient #3 (section 4.1.3). This experiment aims to assess whether the total PURA mRNA level remains consistent between isoCTRL and patient. As well as to compare PURA expression in isoCTRL, after mutation correction with that in wt iPSC. Finally, it can be distinguished between wt-PURA and F233del-PURA mRNAs, providing a further confirm of the heterozygosity of patient and a confirm of the complete mutation rescue in isoCTRL. Even though such qPCR analysis offers strong advantages, the designed primers had too high efficiency and low R^2 (most likely due to primer hairpins) to be suitable to further conduct the experiment, hence, new primers should be tested.

Since the F233del is located on the dimerization repeat PURIII, PURA dimerization is likely impaired (Proske M., 2024). On the other hand, since the mutation is heterozygous, the PURA-wt allele is still expressed and functional, indeed haploinsufficiency has been hypothesized (Brown N., 2013). To answer this

question, PURA protein was quantified via WB and IF in iPSCs (section 4.2). A non-significant lower PURA signal in patient iPSCs compared to isoCTRL was observed, probably due to the high standard deviation of the data. Indeed, such experiment was performed also in sample #2 and #3 iPSCs (data not shown) in which PURA was consistently and significantly reduced in patients compared to isoCTRL. To clarify the uncertainty observed in patient #1, conducting additional replicates could provide further insight into whether there is a difference in PURA protein levels among these different cell lines.

5.2 F233DEL DOES NOT AFFECT NPC DIFFERENTIATION

Patient #1 derived iPSC and its relative isoCTRL were differentiated to the 2D neural model NPCs (Reinhardt P, 2013), demonstrating that F233del-PURA is not affecting early neural differentiation as both isoCTRL and patient NPC reached the same differentiation state in the same time and with the same morphology. Three genes were tested via qPCR, namely *PAX6* (a *neuronal progenitor marker*), *MAP2* (a *dendritic marker*), and *FOXG1* (a *cerebral cortex marker*). The first two were significantly higher in both isoCTRL and patient NPCs relative to iPSC, whereas MAP2 was higher but not significantly, due to the high variance the marker had within the biological replicates. When the three markers were compared between isoCTRL and patient NPCs, none of them was differently expressed. Together these results suggest that F233del-PURA is not affecting the mRNA level of PAX6, FOXG1 and MAP2, however it is not known whether mutant PURA may affect these markers at the protein level, of particular interest is MAP2 as a reduced protein signal has been reported in *PURA*-/- mice (Khalili K., 2003; Hokkanen S., 2012). Expression of the three markers (MAP2, PAX6 and FOXG1) can give a general indication whether the differentiation is correctly occurring, however a high throughput technique, like RNA sequencing, could offer a more comprehensive assessment and could also reveal differentially expressed genes between isoCTRL and patients.

A qPCR experiment revealed increased PURA mRNA, in its wt sequence, from iPSCs to NPCs, which suggests that PURA might have a to-be-defined role in this differentiation process. Furthermore, PURA wt mRNA was significantly lower in patient than in isoCTRL, confirming the mutation correction also at the mRNA level.

Differently from what was observed in iPSC (i.e: a reduction of protein level in patient than in isoCTRL), PURA protein level was similar between isoCTRL and patient NPCs. However, the latter was concluded only from IF experiments and at low passages, not from WB which is a more suitable technique to quantify specific proteins, hence it needs to be verified whether PURA haploinsufficiency observed in iPSC occurs also in NPCs.

Overall, as PURA syndrome is caused by heterozygous mutation in the *PURA* gene (Lalani S. R., 2014; Reijnders M. R. F., 2018), it seems like that the mutated protein cannot fulfil the normal function, and the still available wild type protein cannot fully rescue the phenotype, supporting the hypothesis of a dominant-negative effect because of haploinsufficiency (Brown N., 2013). No experimental evidence is available to support the non-functional mutant PURA hypothesis and

the haploinsufficiency hypothesis. The patient derived iPSC and the relative isoCTRL are of fundamental importance to understand the effect of PURA syndrome causing mutations on both the mutated and the unmutated PURA protein in a more or less differentiated cellular context.

In addition, differentiation towards 3D models like the neural organoid or neural spheroid (for a more specific brain area) with the generated cell lines can be performed. Such differentiation can get a general overview of PURA mutation effect during brain development but also a deeper understanding of potential blocked or deviated deeper differentiation processes (*e.g.* neurons and neuron subtypes, astrocytes, oligodendrocytes, etc.).

5.3 PURA AND FMRP COLOCALIZATION IN NPC

The Fragile X mental retardation protein (FMRP) has been shown to colocalize with PURA in granular structures of neuron body and dendrites (Johnson E. M., 2006). Additionally, FMRP has been identified in PURA-wt interactome but not in PURA-F233del interactome in HeLa cells. A colocalization experiment of FMRP and PURA was performed in NPCs carrying the F233del mutation to test whether such impaired interaction occurs in the patient cellular model. PURA-FMRP colocalization in cytoplasmic granules was observed in both isoCTRL and Patient NPCs, without any difference between the two cell lines. Together these data support PURAwt-FMRP interaction found in HeLa but not the disruption of such interaction when F233del mutation is present. However, in IF experiments, we cannot distinguish between PURAwt and F233del-PURA with the anti-PURA^{12D11} antibody as it binds to the linker region between PURI and PURII repeats, plus, no experiment confirmed the total absence of a folded F233del-PURA protein in NPC cells, thus, we cannot state that the colocalization observed is NPC is solely with PURA-wt.

A first confirm of FMRP and PURA interaction would be FMRP presence in the BioID dataset from HNSC PURA overexpressing cell line, as well as FMRP presence from Coimmunoprecipitation or Pull-down assay, if performed. To specifically validate FMRP and PURA interaction, nanoBRET or Yeast two-hybrid assays can be performed, which can also be executed with mutant PURA, allowing to understand whether mutant PURA is affecting PURA-FMRP interaction.

The type of granules in which the two proteins localize, and the function of their interaction, remain open questions. Since PURA has been found to localize in stress granules (Daigle J. G., 2016) and P-bodies (Molitor L. K. M.-P.-P., 2023), co-staining of PURA and FMRP, together with granule markers, like G3BP stress granule assembly factor 1 (G3BP1) for stress granules, DDX6 or Decapping mRNA 1A (DCP1A) for P-bodies allows to identify the type of granules in which PURA-FMRP are colocalizing. In addition, as both PURA and FMRP are RNA binding proteins found in the RNA transport granules, the iCLIP datasets can be used to test whether PURA and FMRP are binding the same RNAs via Electrophoretic Mobility Shift Assay (EMSA) or RNA pull-down assay. The TRIBE-STRAP approach can be performed to simultaneously detect all the molecular RNA targets of two different RBPs in cells (Flamand M. N., 2022).

5.4 HNSC CELL LINES

Although PURA interacting partners and regulated targets (protein and RNA) have been deeply studied in HeLa cells, potential neural markers might have been missed which can be essential to understand PURA's role in a more physiological environment linked to the neurodevelopmental disorder. For these reasons the immortalized, nestin-positive, high proliferative neural stem cell (HNSC) were used here to generate an overexpressing cell line to study PURA interactome via BioID and to generate a PURA KO cell line to perform transcriptomic and proteomic studies.

5.4.1 PURA OVEREXPRESSING HNSC FOR BioID

The BioID assay allows to identify the surrounding proteins of the protein of interest in the cellular context (Sears R. M., 2019). For this purpose, HNSC were transfected with either a vector containing only BirA (as a background control) or a vector containing PURA linked to BirA which (upon biotin addition) biotinylates the surrounding proteins in a ~10 nm radius, lately identifiable via Mass Spectrometry. The vector confers hygromycin B resistance, which was used to perform a selection of successfully transfected cells. Lastly, a tet on/off promotor allows the expression of the protein of interest as well as of GFP. Cells were visualized at the Evos FL fluorescent microscope after 24 of DOX induction, successfully transfected cells were GFP positive, however an expression difference between control and sample was observed. To avoid biases caused by different levels of BirA in the control and in the BirA-PURA cell lines, cells were sorted via FACS based on GFP signal, colleting those with a mid-GFP intensity. The FACS sorting analysis and WB analysis after the first transfection attempt, revealed a higher protein expression in Flag-BirA than in Flag-BirA-PURA samples. Such difference was thought to be addressed by collecting three different FACS sorted cell populations (low, mid and high GFP signal) from a second lipotransfection approach. Nevertheless, Flag-BirA construct expression in mid-sorted control cell line was still higher than Flag-BirA-PURA expression in mid and high sorted sample cell lines. We hypothesized that such difference is due to the bigger construct that the PURA-BirA cell line is expressing compared to the control cell line. Keeping this in mind, once the BioID is performed, the background interacting protein may be higher than expected, meaning that weakly PURA interacting proteins might not be significant, whereas highly significant interacting proteins are strongly interacting with PURA.

5.4.2 PURA KO HNSC

The self-renew capability and neural characteristics of HNSCs render them a powerful cell model for investigating PURA's molecular function within a more physiologically relevant context compared to HeLa cells. In the recent years, a PURA KO HNSC line was generated, however, cell morphology was strongly altered with shorter extension and bigger nuclei than wt HNSCs (Sabrina Bacher, Master thesis; Isabella Bienek, Master thesis). It was unknown whether such difference was due to PURA KO or the treatment itself, hence, a new PURA KO HNSC

line was successfully generated, validated and used to test PURA targets previously identified from HeLa PURA KD multi omics study (Molitor L. K. M.-P.-P., 2023).

To knock out PURA with CRISPR/Cas9, two gRNAs were used. The first gRNA cuts before the start codon blocking protein translation, while the other gRNA cuts approximately 600 bases ahead, thus, a complete loss of PURA protein is expected. PCR amplicon size analysis and sequencing were performed on the cell pool. As the used PCR primes binds before and after the KO region, the expected KO PCR amplicon size was of around 729 bp while the WT PCR amplicon size is of 1354 bp. The expected bands were observed in wt and in KO cell pool. The latter had an additional unexpected band of 1000 bp and the WT band as the CRISPR/Cas9 has not 100% efficiency. The 1000 bp band was not observed when PCR amplicon from single clones was analyzed. The sequenced PCR products of control and KO cell pool was used to compute the indel percentage together with the KO efficiency using SYNTHEGO online tool (Synthego, 2023). Both values were lower than 50, suggesting an overall low KO efficiency which can be increased with another nucleofection program specifically optimized for HNSCs.

Single cell cloning was performed, and a potential homozygous PURA KO clone, based on PCR amplicon size analysis, was further validated. Within the tested single clones, potential heterozygous PURA KO clones were observed. It could be interesting to test whether transcriptomic and proteomic changes in the homozygous PURA KO are the same in the heterozygous cell line. Perhaps, a heterozygous PURA expression can in part rescue the homozygous KO effect, narrowing potential differentially expressed mRNAs and proteins.

As CRISPR/Cas9 was used to perform the KO, off-targets effects should be validated (Guo C., 2023). Interestingly, within the identified off-targets of the gRNA2, PURA paralog, PURB, was present with a score of 3.91, at least 20 times higher than the other listed off-targets. Instead PURG, the other PURA paralog, was not part of the list, indeed, PURA and PURB share 70% of their sequence (Graebsch A. R. S., 2009; Molitor L. B. S., 2021), while PURA and PURG are only sharing 48% of their sequence. Nevertheless, sequencing of all off-targets, PURB of particular interest, revealed no unwanted mutations, suggesting a high specificity of the used gRNAs. However, using other algorithms which also take into consideration epigenetic feature when performing the prediction (Guo C., 2023) could expand the off-target list.

Since the gRNA1 is guiding the Cas9 to cut before the start codon, no PURA protein should be present in HNSC KO. To test the hypothesis WB and IF of PURA protein were performed which showed strong PURA signal reduction in KO, concluding that PURA translation in HNSC KO is impaired. In line with PURA cytoplasmic localization in HeLa (Molitor L. K. M.-P.-P., 2023), IF in HNSC CTRL, showed PURA to locate in cytoplasm granules, however their nature remains undefined. Considering that PURA localizes in stress granules (Daigle J. G., 2016) and in P-bodies (Molitor L. K. M.-P.-P., 2023), co-staining of PURA and granule markers, like G3BP for stress granules, DDX6 or DCP1A for P-bodies, might identify these granules. Alternatively, given the colocalization of PURA with FMRP (Johnson E. M., 2006), as confirmed in NPCs by this study, the presence of PURA-

FMRP complexes (by costaining) in HNSCs might not only support such finding, but also facilitate the identification of the observed PURA granules in HNSCs.

As previously mentioned, a PURA KO HNSC cell line was already generated (Sabrina Bacher, Master thesis; Isabella Bienek, Master thesis), which presented altered morphology as they were less elongated and also had bigger nuclei than HNSC WT, the latter was also observed in astrocytes, differentiated from HNSCs. The successfully newly generated PURA KO HNSCs maintained the flattened unipolar morphology like the control HNSCs. In addition, the nuclear size, measured with DAPI staining, was similar between HNSCs KO and CTRL, suggesting that PURA depletion has no effect on cellular morphology and nuclear size. However, such findings should be validated also in a more differentiate state of HNSCs such as astrocytes or neurons together with synapses formation studies and MAP2 dendritic localization since it is known that neurogenesis, synapse formation and MAP2 localization are impaired in *PURA*-/- mice (Khalili K., 2003; Hokkanen S., 2012).

The newly generated PURA KO HNSC line was used to validate previously identified downregulated targets upon PURA KD in HeLa cells (section 5.4.3). Concurrently, a transcriptomic experiment is ongoing, with the potential to reveal neural targets not previously identified.

5.4.3 P62 AND DDX6 ARE NOT ALTERED BY PURA KO IN HNSC

A recent publication showed downregulation of P62 and DDX6 mRNA and protein upon PURA KD in HeLa cells (Molitor L. K. M.-P.-P., 2023), suggesting PURA's potential role in autophagy regulation and in P-body formation, respectively. The effect of homozygous PURA KO on P62 and DDX6 protein level was tested via WB and a small but not significant reduction was observed. We concluded that the non-consistent downregulation of P62 and DDX6 between HeLa PURA KD and HNSC PURA KO is due to different cellular types, confirming the importance of transcriptomic and proteomic studies with the newly generated HNSC PURA KO cell line to identify more physiological markers.

6 CONCLUSIONS AND OUTLOOK

In conclusion, this thesis has provided valuable insights into the molecular mechanisms underlaying the neurodevelopmental disorder PURA syndrome and the effects of the F233del mutation on various cellular processes.

Firstly, our experiments have demonstrated successful generation and validation of an isoCTRL iPSC cell line, providing a tool for investigating the impact of one of the most common PURA syndrome causing mutations. Through genomic validation, the complete rescue of F233del mutation in isoCTRL, was confirmed, while functional lineage assay and pluripotency markers staining confirmed the pluripotency capability of iPSCs.

Secondly, the investigation about F233del mutation effect during NPC differentiation revealed that such mutation does not impair the possibility of early neural differentiation as both isoCTRL and patient iPSC reached NPC state. qPCR experiments did not reveal significant differences of the three neural markers studied (PAX6, MAP2 and FOXG1) between isoCTRL and patient, however future studies should explore mRNA expression of other markers as well as neural markers at protein level, in particular MAP2.

Additionally, we confirmed PURA haploinsufficiency in iPSC as PURA protein level was consistently reduced in patient than in isoCTRL. We also showed PURA mRNA increasing during differentiation to NPCs, suggesting a to-be-defined PURA's role in neural differentiation. PURA staining alone in NPCs did not confirm the haploinsufficiency in the neural progenitors, however other more precise experiments are advised to verify PURA haploinsufficiency in NPCs.

The colocalization studies between PURA and FMRP in NPCs provided insights into their interaction dynamics revealing that it is not impaired by F233del mutation. However, further experiment using advanced techniques are recommended to validate this interaction, while other colocalization studies are advised to identify the nature of FMRP-PURA colocalizing granules.

Lastly, BirA-PURA overexpression cell line and a PURA KO cell line were generated from HNSCs, providing two cellular models with self-renewal and differentiation capabilities as well as access to neural marker not available in HeLa cell model. The BirA-PURA overexpressing HNSC line can be used for BioID whereas PURA KO HNSC line is suitable for transcriptomics and proteomics experiments. Two PURA targets previously demonstrated to be downregulated upon PURA KD, were not validated in PURA KO HNSCs, remarking the advantages of repeating these omics studies in a more physiological cell model.

In summary, this thesis contributes to advancing our understanding of PURA syndrome and remark the importance of continued research efforts in unraveling its complexities, towards improving patient care and ultimately enhancing the quality of life for individuals affected by this disorder.

BIBLIOGRAPHY

Barbe M. F., K. J. (2016). Memory deficits, gait ataxia and neuronal loss in the hippocampus and cerebellum in mice that are heterozygous for Pur-alpha. *Neuroscience*, 337:177-190. doi:10.1016/j.neuroscience.2016.09.018

Benchling. (2023). Tratto da https://www.benchling.com/

Bergemann A. D., M. Z. (1992). Sequence of cDNA Comprising the Human pur Gene and Sequence-Specific Single-Stranded-DNA-Binding Properties of the Encoded Protein. *Molecular and Cellular Biology*, 5673-5682. doi:10.1128/mcb.12.12.5673-5682.1992

Bergemann A. D., M. Z. (1992). Sequence of cDNA comprising the human pur gene and sequence-specific single-stranded-DNA-binding properties of the encoded protein. *Mol Cell Biol*, 5673-82. doi:10.1128/mcb.12.12.5673-5682.1992

Brinkman EK, C. T. (2014). Easy quantitative assessment of genome editing by sequence trace decomposition. *Nucleic Acids Research, Volume 42, Issue 22*, e168. doi:https://doi.org/10.1093/nar/gku936

Brown N., B. T. (2013). 5q31.3 Microdeletion syndrome: Clinical and molecular characterization of two further cases. *J Med Genet Part A*, 161A:2604–2608. doi:DOI 10.1002/ajmg.a.3610

Concordet J. P., H. M. (2018). CRISPOR: intuitive guide selection for CRISPR/Cas9 genome editing experiments and screens. *Nucleic Acids Research*, W242–W245. doi:https://doi.org/10.1093/nar/gky354

Daigle J. G., K. K. (2016). Pur-alpha regulates cytoplasmic stress granule dynamics and ameliorates FUS toxicity. *Acta Neuropathol*, 605-20. doi:10.1007/s00401-015-1530-0

Darbinian N., G. G. (2001). Helix-destabilizing properties of the human single-stranded DNA- and RNA-binding protein Puralpha. *J Cell Biochem*, 80(4):589-95.

Du Q., T. A. (1997). Transcriptional regulation of neuronal nicotinic acetylcholine receptor genes. A possible role for the DNA-binding protein Puralpha. *J Biol Chem*, 272(23):14990-5. doi:10.1074/jbc.272.23.14990

Gallia G. L., D. N. (1999). Self-association of Puralpha is mediated by RNA. *J Cell Biochem*, 334-48.

Graebsch A., R. S. (2009). X-ray structure of Pur-alpha reveals a Whirly-like fold and an unusual nucleic-acid binding surface. *Proc Natl Acad Sci U S A*, 106(44):18521-6. doi:10.1073/pnas.0907990106

Graebsch A., R. S. (2010). Of bits and bugs--on the use of bioinformatics and a bacterial crystal structure to solve a eukaryotic repeat-protein structure. *PLoS One 5:e13402*. doi:10.1371/journal.pone.0013402

Grosch M, I. S. (2020). Nucleus size and DNA accessibility are linked to the regulation of paraspeckle formation in cellular differentiation. *BMC Biol*, 18(1):42. doi:10.1186/s12915-020-00770-y

Gupta M., S. V. (2003). Single-stranded DNA-binding proteins PURalpha and PURbeta bind to a purine-rich negative regulatory element of the alpha-myosin heavy chain gene and control transcriptional and translational regulation of the gene

expression. Implications in the repressi. *J Biol Chem*, 44935-48. doi:10.1074/jbc.M307696200

Haas S., T. P. (1995). A 39-kD DNA-binding protein from mouse brain stimulates transcription of myelin basic protein gene in oligodendrocytic cells. *J Cell Biol*, 130(5):1171-9. doi:10.1083/jcb.130.5.1171

Hariharan S., K. R. (2014). Purα/Purβ single-strand DNA-binding proteins attenuate smooth-muscle actin gene transactivation in myofibroblasts. *J Cell Physiol*, 1256-71. doi:10.1002/jcp.24564

Herault Y., C. G. (1995). RNA-dependent DNA binding activity of the Pur factor, potentially involved in DNA replication and gene transcription. *Gene Expr*, 85-93.

Hokkanen S., F. H.-M. (2012). Lack of Pur-alpha alters postnatal brain development and causes megalencephaly. *Hum Mol Genet*, 21(3):473-84. doi:https://doi.org/10.1093/hmg/ddr476

Hosoki K., O. T. (2012). Clinical Phenotype and Candidate Genes for the 5q31.3 Microdeletion Syndrome. *Am J Med Genet Part A*, 158A:1891–1896. doi:10.1002/ajmg.a.35439

Hunt D., L. R. (2014). Whole exome sequencing in family trios reveals de novo mutations in PURA as a cause of severe neurodevelopmental delay and learning disability. *Journal of Medical Genetics*, 51:806-813. doi:10.1136/jmedgenet-2014-102798

Janowski R., N. D. (2020). The large family of PC4-like domains - similar folds and functions throughout all kingdoms of life. *RNA Biol*, 1228-1238. doi:10.1080/15476286.2020.1761639

Johannesen K. M., G. E. (2021). PURA-Related Developmental and Epileptic Encephalopathy. *Neurol Genet*, 7(6):e613. doi:10.1212/NXG.0000000000000613

Johnson E. M., K. Y. (2006). Role of Pur alpha in targeting mRNA to sites of translation in hippocampal neuronal dendrites. *J Neurosci Res*, 83(6):929-43. doi:10.1002/jnr.20806

Khalili K., D. V. (2003). Purα Is Essential for Postnatal Brain Development and Developmentally Coupled Cellular Proliferation As Revealed by Genetic Inactivation in the Mouse. *Mol Cell Biol*, 6857-75. doi:10.1128/MCB.23.19.6857-6875.2003

Lalani S. R., Z. J.-G. (2014). Mutations in PURA cause profound neonatal hypotonia, seizures, and encephalopathy in 5q31.3 microdeletion syndrome. *Am J Hum Genet.*, 95(5):579-83. doi:10.1016/j.ajhg.2014.09.014

Lee B. H., R. M. (2018). Expanding the neurodevelopmental phenotype ofPURAsyndrome. *Am J Med Genet Part A.*, 176A:56–67. doi:DOI: 10.1002/ajmg.a.38521

Mitsumori K., T. Y. (2017). Components of RNA granules affect their localization and dynamics in neuronal dendrites. *Mol Biol Cell*, 1412-1217. doi:10.1091/mbc.E16-07-0497

Molitor L., B. S. (2021). The Molecular Function of PURA and Its Implications in Neurological Diseases. *Front. Genet.*, 12:638217. doi:10.3389/fgene.2021.638217

Molitor L., K. M.-P.-P. (2023). Depletion of the RNA-binding protein PURA triggers changes in posttranscriptional gene regulation and loss of P-bodies. *Nucleic Acids Res*, 1297-1316. doi:10.1093/nar/gkac1237

Mroczek M., I. S. (2023). Neuromuscular and Neuromuscular Junction Manifestations of the PURA-NDD: A Systematic Review of the Reported Symptoms and Potential Treatment Options. *Int J Mol Sci.*, ;24(3):2260. doi:10.3390/ijms24032260

Ohashi S., K. K. (2002). Identification of mRNA/protein (mRNP) complexes containing Puralpha, mStaufen, fragile X protein, and myosin Va and their association with rough endoplasmic reticulum equipped with a kinesin motor. *Biol Chem*, 37804-10. doi:10.1074/jbc.M203608200

Pandey P. R., Y. J. (2020). circSamd4 represses myogenic transcriptional activity of PUR proteins. *Nucleic Acids Res*, 3789-3805. doi:10.1093/nar/gkaa035

Proske M., J. R.-R. (2024). PURA Syndrome-causing mutations impair PUR-domain integrity and affect P-body association. *Elife*, 13:RP93561. doi:10.7554/eLife.93561.1.sa1

Reijnders M. R. F., J. R. (2018). PURA syndrome: clinical delineation and genotype-phenotype study in 32 individuals with review of published literature. *J Med Genet*, 55:104–113. doi:10.1136/jmedgenet-2017-104946

Reinhardt P, G. M. (2013). Derivation and expansion using only small molecules of human neural progenitors for neurodegenerative disease modeling. *PLoS One*. doi:10.1371/journal.pone.0059252

Shimojima K., I. B. (2011). A new microdeletion syndrome of 5q31.3 characterized by severe developmental delays, distinctive facial features, and delayed myelination. *Am J Med Genet Part A*, 155:732–736. doi:10.1002/ajmg.a.33891

Synthego. (2023). Tratto da https://ice.synthego.com/#/

Weber J., B. H. (2016). Structural basis of nucleic-acid recognition and double-strand unwinding by the essential neuronal protein Pur-alpha. *Elife*, 5:e11297. doi:10.7554/eLife.11297

West J. A., D. C. (2014). The long noncoding RNAs NEAT1 and MALAT1 bind active chromatin sites. *Mol Cell*, 791-802. doi:0.1016/j.molcel.2014.07.012

Zambrano N., D. R. (1997). DNA-binding protein Pur alpha and transcription factor YY1 function as transcription activators of the neuron-specific FE65 gene promoter. *Biochem J*, 328 (Pt 1)(Pt 1):293-300. doi:10.1042/bj3280293

APPENDIX

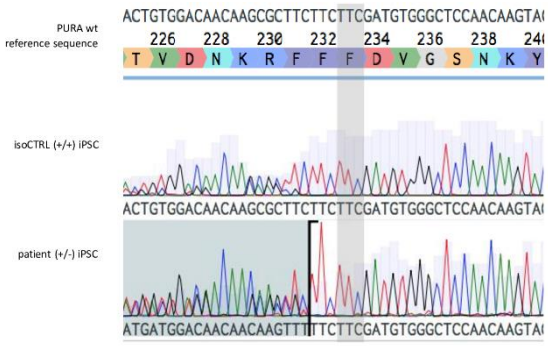

Figure 6.1: Sequencing of isoCTRL and patient cell pool. A mixed sequencing is still visible in the isoCTRL because the mutation correction efficiency is not 100%.

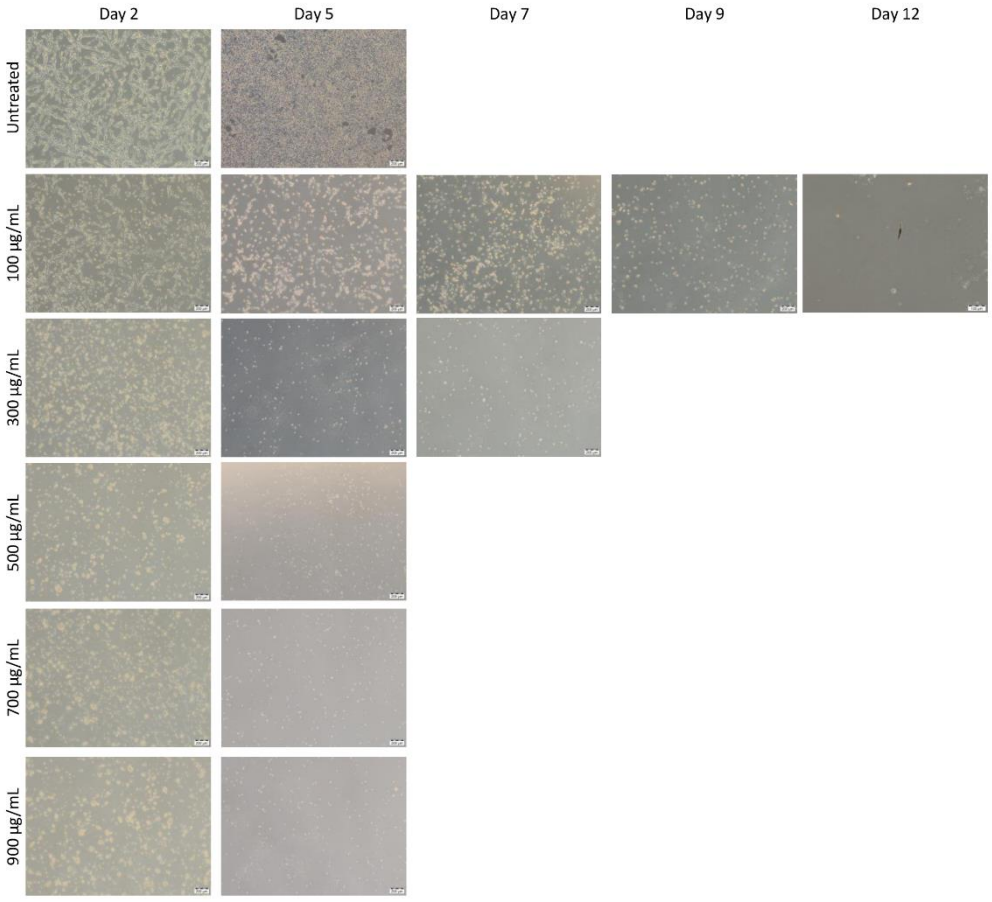

Figure 6.2: Over-time HNSC wt treatment with different concentration of Hygromycin B.

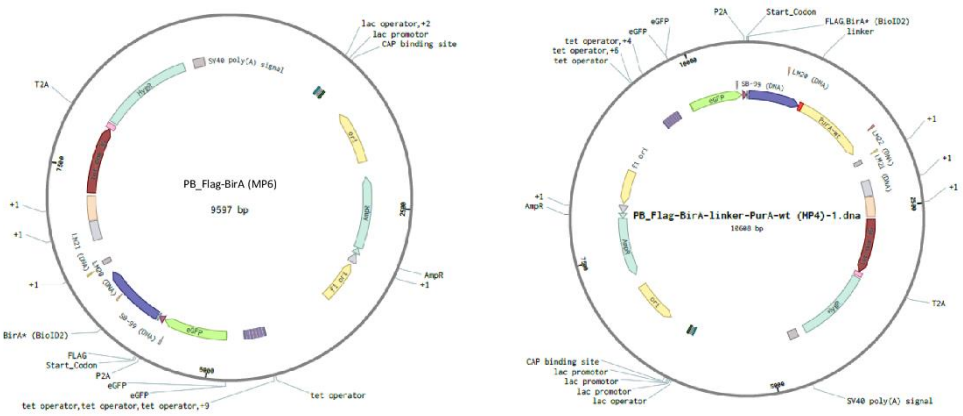

Figure 6.3: Vectors for HNSC cell line generation for BioID. Flag-BirA vector (left) and Flag-BirA-PURA vector (right).

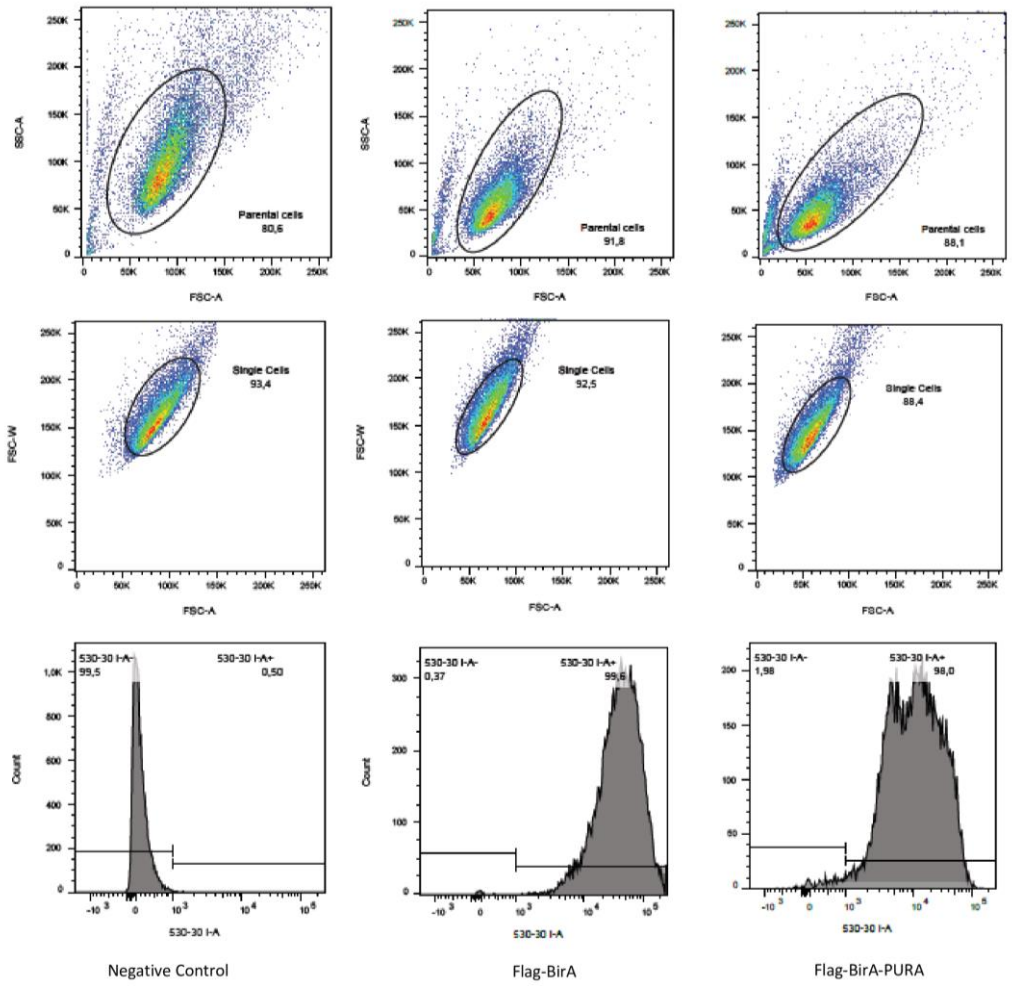

Figure 6.4: FACS sorting analysis from Ejona R. Negative control (left), Flag-BirA (middle) and Flag-BirA-PURA (right). Cellular debris gating (top), cell duplet gating (middle) and GFP signal gating (bottom).

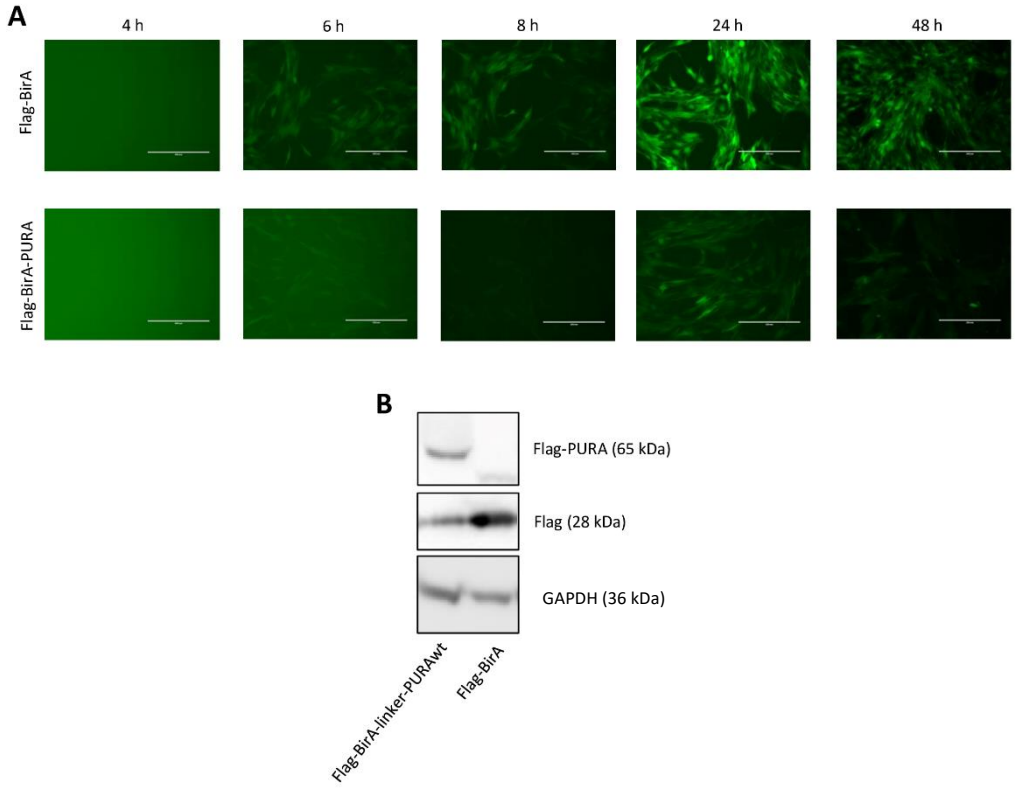

Figure 6.5: Unsuccessful first attempt of HNSC cell line generation for BioID. (A) Over time DOX induction of FACS sorted HNSCs Flag-BirA (top) and of Flag-BirA-PURA (bottom). (B) Western Blot after 24h of DOX induction in HNSC Flag-BirA and HNSC Flag-BirA-PURA. Anti-Flag antibody was used to detect the two constructs. An unexpected band is detected in HSNC Flag-BirA-PURA sample of the control vector size (Flag, 28 kDa).